CREB3/LUMAN AS A NOVEL REGULATOR OF ENERGY METABOLISM

by

Brandon S. Smith

A Thesis

presented to

The University of Guelph

In partial fulfillment of requirements

for the degree of

Doctor of Philosophy

in

Molecular and Cellular Biology

Guelph, Ontario, Canada

ABSTRACT

CREB3/LUMAN AS A NOVEL REGULATOR OF ENERGY METABOLISM

Brandon Smith

University of Guelph, 2022

Advisors:

Professor Ray Lu

Professor Marica Bakovic

CREB3 is a cellular stress-associated protein with much of its physiological and cellular functions remain to be elucidated. Stress-associated proteins have been previously well established as metabolic regulators and protect cells from toxic levels of reactive oxygen species (ROS). This thesis investigated a novel role of CREB3 in regulating energy metabolism by utilizing *Creb3*-deficient mice and mouse embryonic fibroblast (MEF) cells. It was found that *Creb3*-deficient mice had an increase in energy expenditure with no differences in energy intake. This resulted in the protection from high-fat diet-induced weight gain, hyperglycemia, and sex-specific tissue lipid accumulation in *Creb3*-deficient mice. *Creb3*-deficient males in particular were protected from hepatic accumulation of lipids and resisted high-fat diet-induced glucose intolerance while *Creb3*-deficient females were protected from lipid accumulation in skeletal muscle. These results suggest CREB3 acts as a metabolic brake, presumably under stressed conditions such as feeding on a high-fat diet. CREB3 has previously been linked to the regulation of endoplasmic reticulum (ER)-Ca^{2+} release which can stimulate ATP production as it enters the mitochondria. ER and mitochondrial Ca^{2+} homeostasis was investigated in *Creb3*-deficient MEF cells as a potential mechanism in which CREB3 controls energy metabolism. It was found that CREB3 did indeed inhibit ER-Ca^{2+} release although the exact mechanism of this remains unknown.

Subsequently, *Creb3*-deficient MEFs had increased mitochondrial Ca^{2+} levels and thus drastically elevated basal mitochondrial respiration and ATP production along with an increase in basal ROS levels. Since Ca^{2+}, ATP, and ROS have an intricate mutual interplay with one another, when one is dysregulated, often the others are as well. This thesis established a novel role of CREB3 as a potent regulator of energy metabolism homeostasis both at the organism and cellular levels.

ACKNOWLEDGMENTS

I would first like to thank my advisor, Dr. Ray Lu, for accepting me into his lab and giving me the opportunity to pursue my dream. I am very grateful for your wonderful insights, guidance, and understanding throughout my studies with you. Secondly, I want to thank my co-advisor, Dr. Marica Bakovic, for your unwavering confidence in me and your unparalleled wisdom in metabolism. Thank you to Dr. Jim Uniacke, my committee member, for your valuable feedback and comments. I would also like to thank all past and current Lu Lab members. Jenna Penney, Tiegh Taylor, and Shayla Larson accepted me into the lab with open arms and made me feel so welcome. My project would not have made it this far without Jenna and Tiegh's mentoring and assistance with mouse work, and other experiments. Thanks to Briana Locke, for all your support, help with managing the lab together, and for bouncing ideas off of. I'd also like to thank Lalonde Lab members Aly Walczyk – Mooradally, Tristen Hewitt, and my lovely girlfriend Jennifer Holborn. Your friendship and support through the years have meant so much to me and couldn't thank you enough. Jennifer, your constant love and support has kept me going and driven me to keep pushing and achieve better in all aspects of my life. To my parents, Karen and Stephen Smith, words can't even begin to describe the kind of unconditional love and support you've given me which has allowed me to accomplish my dream and cannot thank you two enough. This achievement is all of ours to share.

DECLARATION OF WORK PERFORMED

All work reported in this thesis was performed by myself under the supervision of Dr. Ray Lu and my advisory committee with the following exceptions: High-fat diet mouse metabolic cages completed and analyzed by Dr. Robin E. Duncan, Kalsha Diaguarachchige De Silva, and Ashkan Hashemi at the University of Waterloo, Department of Kinesiology and Health Sciences. Live ER-Ca^{2+} release imaging was performed and analyzed by Tristen Hewitt, University of Guelph, Department of Molecular and Cellular Biology, Lalonde Lab. High-fat diet liver western blots completed by Sophie Grapentine of the Marica Bakovic Lab, Department of Human Health and Nutrition Sciences, University of Guelph.

TABLE OF CONTENTS

LIST OF FIGURES

LIST OF ABBREVIATIONS

ATF4 Activating Transcription Factor 4

ATF6α Activating Transcription Factor 6 alpha

ATP Adenosine triphosphate

BfA Brefeldin A

BiP Binding immunoglobulin protein

bZIP Basic Leucine Zipper Domain

cAMP Cyclic Adenosine Monophosphate

CD Control diet

CHOP C/EBP homologous protein

CRE Creb Response Element

CREB3 CAMP Responsive Element Binding Protein 3

DAG Diacylglyceride

DNA Deoxyribonucleic acid

ER Endoplasmic Reticulum

ERAD Endoplasmic Reticulum Associated Degradation

ERSE ER stress response element

ETC Electron transport chain

FA Fatty acid

GAPDH Glyceraldehyde-3-Phosphate Dehydrogenase

GRE Glucocorticoid Response Element

GR Glucocorticoid Receptor

GRP78 Glucose Regulated Protein 78

GTT Glucose tolerance test

HCF-1 Host Cell Factor 1

HDL High-density lipoprotein

Herp Homocysteine-induced endoplasmic reticulum protein

Het Heterozygous

HFD High-fat diet

HSV Herpes Simplex Virus

I.P intraperitoneal injection

IRE1α Inositol-requiring Enzyme 1α

KO Knock Out

LDL Low-density lipoprotein

LPL Lipoprotein lipase

LRF Luman Recruiting Factor

MAG Monoacylglceride

MEF Mouse embryonic fibroblast

NR Nuclear Receptor

OCR Oxygen consumption rate

PBS Phosphate Buffered Saline

PCR Polymerase Chain Reaction

PERK protein kinase RNA-like endoplasmic reticulum kinase

PPRE Peroxisome Proliferator-Activated Receptor Response Element

RER Respiratory exchange ratio

RIP Regulated Intramembrane Proteolysis

RNA Ribonucleic acid

ROS Reactive oxygen species

RT PCR Reverse Transcription Polymerase Chain Reaction

S1P/S2P Sphingosine-1/2-phosphate

SDS Sodium dodecyl sulfate

Tg Thapsigargin

TG Triglyceride

TM Transmembrane

UPR Unfolded Protein Response

VLDL Very low-density lipoprotein

WT Wild Type

XBP1 Immature/inactive X-Box Binding Protein 1

XBP1s Mature/active X-Box Binding Protein 1

Chapter 1: Literature Review

1.0 Metabolism

Metabolism is the balance of anabolic and catabolic chemical reactions, typically converting one molecule to another in order to maintain homeostasis and provide energy for a cell or whole organism. There are four basic types of biological macromolecules: nucleic acids, proteins, lipids, and carbohydrates. While nucleic acids hold genetic codes in the form of DNA and RNA, the other three macromolecules may be used to generate energy through dietary intake or from catabolic reactions within the cell or organism. Protein/amino acids contribute to energy production by being converted to glucose, the main form of carbohydrate used for energy, through a process called gluconeogenesis. Glucose and lipids (fat) however, are the predominant two substrates used for the production of adenosine triphosphate (ATP), the main molecule used for energy by cells

1.1 Glucose Metabolism

Glucose is largely accumulated through diet and used as a substrate for cells to perform glycolysis. Glycolysis is an anaerobic reaction that occurs in the cytosol that converts one molecule of glucose a net gain of 2 ATP, 2 Pyruvate, and 2 NADH (Figure 1) (Chaudhry & Varacallo, 2021). The 2 pyruvates are later oxidized into 2 more NADH and 2 Acetyl-CoAs which fuel the aerobic Krebs cycle (Citric acid cycle) within mitochondria (Figure 1) (Chaudhry & Varacallo, 2021). The NADH, go on to supply power to the electron transport chain (ETC) and oxidative phosphorylation within the

inner mitochondrial membrane and produce around 2.5 ATP each (Figure 1) (Chaudhry & Varacallo, 2021). The Krebs cycle, through a series of enzymatic reactions of the 2 Acetyl-CoAs produced from glycolysis, generates a net gain of 2 ATP, 6 more NADH, and 2 FADH2 (Figure 1) (Salway, 2018). FADH2, similarly to NADH is used to supply power (electrons) to the ETC and produces about 1.5 ATP per FADH. (Zhao et al., 2019). This brings the total theoretical ATP output of a single glucose molecule to 30-38, depending on NADH -> ETC -> ATP efficiency (Chaudhry & Varacallo, 2021; Salway, 2018).

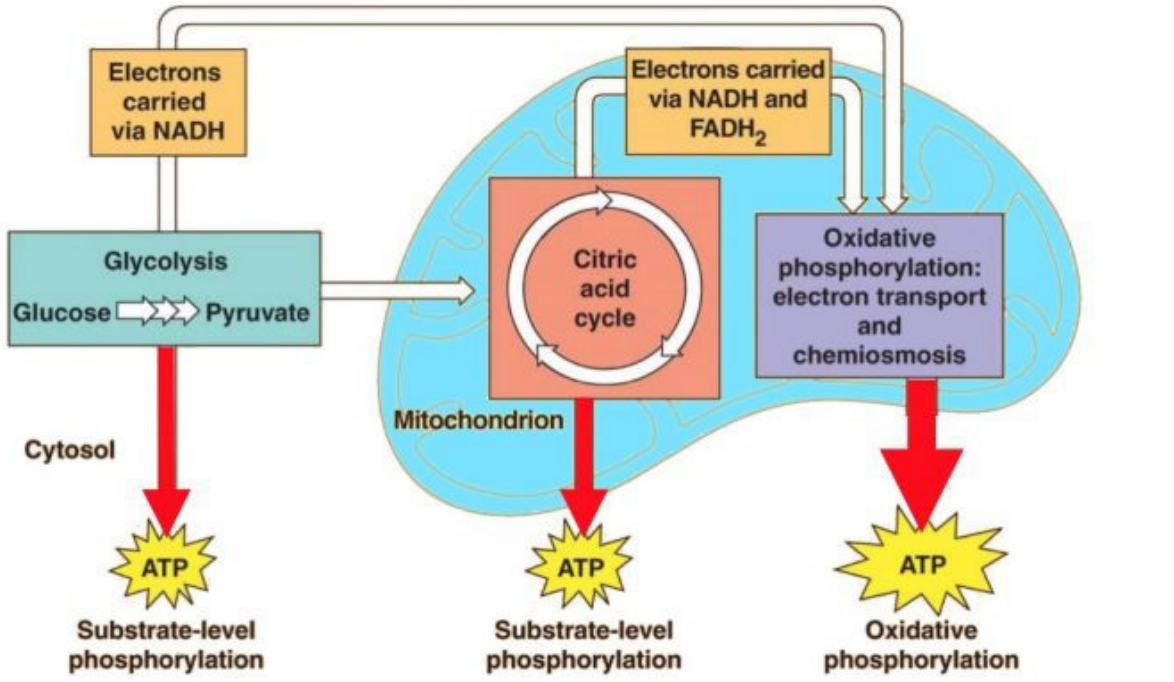

Figure 1: Summary of cellular respiration processes. Glucose feeds into the glycolysis reaction producing 2 pyruvates. These pyruvates are oxidized into 2 acetyl-CoAs and 2 NADH. Acetyl-CoA enters the mitochondria and enters the Krebs cycle (Citric acid cycle) to generate 2 more ATP, 6 NADH, and 2 FADH2. The NADH and

FADH2 molecules carry electrons to the electron transport chain to further produce more ATP. (Retrieved from: https://quizlet.com/263384632/cellular-respiration-diagram/)

Carbohydrates are consumed through diet and broken down into simple sugars (monosaccharides) such as glucose and fructose. Glucose is actively absorbed through intestinal epithelial cells of an organism and then transported into the blood via a glucose uniporter (GLUT2) (Schmitt et al., 2017.). Once in the blood, glucose is accessible by the organs and can be used for ATP production. However, too low, or too high levels of glucose in the blood can lead to homeostatic alterations and damage to the organism. In order to maintain proper blood glucose levels, mammals possess pancreas-derived endocrine hormones insulin and glucagon. When high glucose concentrations cause cellular stress to pancreatic beta cells, they produce and secrete insulin into the bloodstream. Insulin primarily acts upon the liver, muscle, and adipose cells to take up the excess blood glucose by binding to Insulin Receptors (IR) located on the plasma membrane beginning an intracellular signaling cascade. IRs are receptor tyrosine kinases (RTK) that when activated, autophosphorylate allowing it to bind, phosphorylate, and activate other proteins such as Insulin Receptor Substrate (IRS) (Haar et al., 2007; Ozes et al., 2001). Activated IRS propagates the insulin signal down to metabolic regulators such as Protein Kinase B (AKT). AKT stimulates the translocation of Glucose Transporter 4 (GLUT4) to the plasma membrane, allowing the influx of glucose from the blood into the cell, lowering the glucose concentrations in the plasma (Haar et al., 2007; Ozes et al., 2001). This influx of glucose is then converted into the glucose storage molecule, glycogen. AKT also stimulates the main cellular survival and growth regulator, mammalian target of rapamycin (mTOR) which induces

lipid synthesis while inhibiting the breakdown of lipids (lipolysis) at the same time, as well as many other genes required for growth (Haar et al., 2007; Ozes et al., 2001). In times of low blood glucose, alpha cells in the pancreas produce and secrete glucagon into the bloodstream which has the opposite effect as insulin. Glucagon primarily acts upon liver cells by binding to the Glucagon Receptor, a G-protein-coupled receptor (GPCR) on the surface membrane. The Glucagon GPCR transduces its signal into the cell inhibiting glycolysis and stimulating gluconeogenesis in order to create more glucose from other sources within the organism to reestablish blood glucose homeostasis (Hayashi, 2021; Janah et al., 2019).

1.2 Lipid Metabolism

Lipids are the main form of energy storage while also serving as signaling molecules and structural components of plasma and organelle membranes. They take many forms, though 4 main types include fatty acids (e.g. Palmitate), glycerolipids (e.g. Triglyceride), glycerophospholipids (e.g. Phosphatidylcholine), and sterols (e.g. Cholesterol). The major site of lipid metabolism takes place in the liver. Dietary lipids are absorbed in the intestines and transported to the liver and other tissues through lipid transport vesicles called chylomicrons (Trujillo-Viera et al., 2021). Adipose tissue can also undergo lipolysis and transport lipids back to the liver in high-density lipoproteins (HDLs) in times of low glucose to use as energy (T. Zhang et al., 2019). The liver can also send lipids out to peripheral tissue packaged in very-low-density lipoproteins (VLDLs). VLDLs are susceptible to degradation by extracellular enzyme, lipoprotein

lipase (LPL), attached to vascular endothelial cell surfaces (He et al., 2018; Young et al., 2019). LPL breaks down the triglycerides (TGs) located in the VLDL membrane into free fatty acids (FAs) which are transported into adjacent cells by FA transporters such as fatty acid translocase (CD36), fatty acid-binding protein (FABP), and fatty acid transport proteins (FATPs) (He et al., 2018; Young et al., 2019). FAs that enter the cell can then be used to produce ATP through beta-oxidation (FA oxidation or FAO) in the mitochondria or be synthesized into TGs and stored. FAs can also be synthesized from Acetyl-CoAs that are produced from the pyruvates derived from glycolysis in response to insulin by enzymes such as Fatty Acid Synthase (FASN) (Paiva et al., 2018).

The major sites of TG synthesis in an organism are in adipose and liver tissue. Within these cells and the ER membrane through a series of enzymatic reactions, 3 FA chains are esterified to a glycerol molecule to form a TG. TGs synthesized in the liver are then packaged into VLDL vesicles and excreted into the blood. The main transcription factor family responsible for lipid synthesis downstream of the IR-PI3K-AKT-mTOR pathway are the Sterol Regulatory-Element Binding Proteins, or SREBPs (Eberlé et al., 2004; Porstmann et al., 2008; X. Wang et al., 1994). There are two types of SREBPs, SREBP1 and SREBP2. SREBP2 is ubiquitously expressed while SREBP1 contains two isoforms, SREBP1a which is mostly expressed in intestinal, heart, macrophage, and dendritic cells, and the also ubiquitously expressed SREBP1c (Eberlé et al., 2004; Porstmann et al., 2008; X. Wang et al., 1994). All SREBPs are retained within the ER membrane in complex with SREBP Cleavage Activating Protein (SCAP), which is anchored in the ER by the Insulin Induced Gene 1 (INSIG) protein. In low cholesterol environments, INSIG undergoes a conformational change releasing the

SREBP1a/2-SCAP complex. SCAP escorts SREBP1a/2 to the Golgi apparatus where it is cleaved off by site-1 and site-2 proteases (S1P and S2P) (Eberlé et al., 2004; X. Wang et al., 1994). Cleaving of SCAP releases the active SREBP1a or SREBP2 transcription factors to translocate to the nucleus and stimulate lipogenic gene expression such as cholesterol synthesis genes. SREBP2 is particularly activated by low cholesterol levels within the ER (C. Guo et al., 2018). SREBP1c however, is not cleaved in response to low cholesterol, but instead activated by insulin (Kohjima et al., 2008). SREBP1c is largely considered a major lipogenic regulator by inducing FA and TG synthesis in metabolic tissues such as liver and adipose (Eberlé et al., 2004; Kohjima et al., 2008; Porstmann et al., 2008; X. Wang et al., 1994). Overactivation of SREBP1 is known to contribute to cellular stress through lipotoxicity and is significantly connected with various metabolic diseases such as obesity, diabetes, hepatic steatosis (liver lipid accumulation), and atherosclerosis (Eberlé et al., 2004; Kohjima et al., 2008; Porstmann et al., 2008).

TGs stored in adipose tissue accumulates as lipid droplets within the cytosol of adipocytes. During times of energy demand such as exercising or fasting, lipolysis may begin to occur (Duncan et al., 2007; Greenberg et al., 1991). Lipids must be broken down into FA chains in order to be used as an energy substrate in mitochondrial FA oxidation. TG is first hydrolyzed by adipose triglyceride lipase (ATGL) into diacylglycerol (DAG). Next, hormone-sensitive lipase (HSL) then hydrolyzes DAG into monoacylglycerol (MAG), finally followed by monoacylglycerol lipase (MGL) hydrolysis into glycerol, with each step releasing a single FA chain off the glycerol (Duncan et al., 2007). In order for FAs in the cytosol to enter the mitochondria, they must be esterified

to fatty acyl-CoA by the enzyme Fatty-acyl-CoA Synthase (FACS) (Purdom et al., 2018). Fatty acyl-CoA is then converted to acylcarnitine by Carnitine Palmitoyltransferase 1 (CPT1) allowing it to enter the mitochondria (Purdom et al., 2018). Once inside, Carnitine Palmitoyltransferase 2 (CPT2) replaces the carnitine with CoA reverting the molecule back to fatty acyl-CoA which then enters the FA β-oxidation reaction (Purdom et al., 2018).

FA β-oxidation occurs over a 4-step dehydration/hydration reaction process by enzymes Acyl-CoA Dehydrogenase, Enoyl-CoA Hydratase, 3-hydroxy acyl-CoA Dehydrogenase, and finally Beta-ketoacyl-CoA Thiolase (Adeva-Andany et al., 2019; Purdom et al., 2018). The products resulting from these reactions per 2 fatty acyl-CoA carbon atoms of the FA chain are 1 NADH, 1 FADH2, and 1 acetyl-CoA (Figure 2). Acetyl-CoA then feeds into the Krebs Cycle previously discussed to generate ATP (Figure 2). The NADH and FADH2 go on to support ETC function in ATP production (oxidative phosphorylation) (Figure 2). A single 16 carbon palmitate can generate 7 NADH, 7 FADH2, and 8 acetyl-CoA providing up to 129 ATP molecules compared to 30-38 ATP per glucose molecule (Adeva-Andany et al., 2019; Purdom et al., 2018).

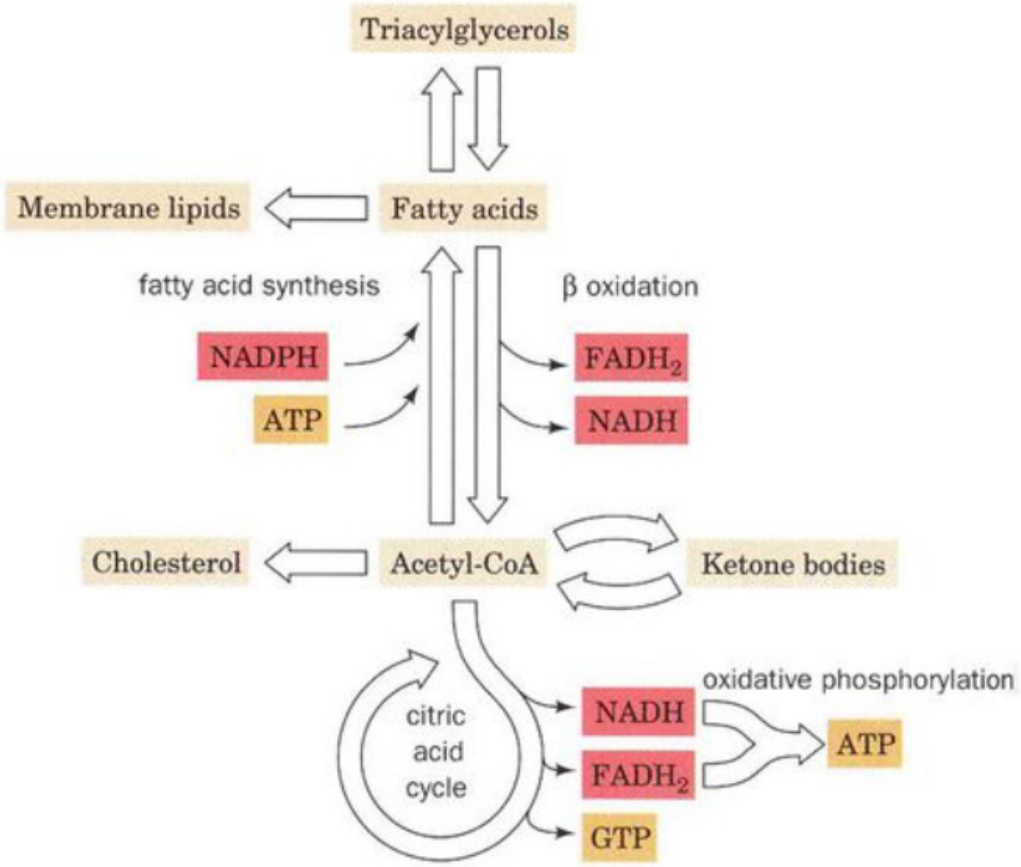

Figure 2: Fatty Acid Metabolism Overview. Fatty acid chains can enter the β oxidation pathway in mitochondria which produces 1 NADH, 1 $FADH_2$, and 1 Acetyl-CoA per 2 carbons of a fatty acid chain and repeated until only 2 carbons remain. The Acetyl-CoA then is either used for cholesterol synthesis or moves on to the Citric acid cycle (Krebs cycle) and generates 1 ATP, 3 more NADH, and 1 more FADH2. NADH and FADH2 then go on to supply the ETC chain with electrons to generate even more ATP. In the anabolic direction, fatty acids can be synthesized from Acetyl-CoAs which can then be used for membrane phospholipid synthesis or stored in the form of triglycerides. (Retrieved from: https://slideplayer.com/slide/13329485/).

The ETC is a series of electron-powered proton pumps called complexes I-IV that are located within the inner mitochondrial membrane (Figure 3). The objective of the ETC is to generate an H^+ proton gradient across the mitochondrial membrane by pumping H^+ protons from the mitochondrial matrix to the intermembrane space. It does this by accepting donated electrons from NADH and FADH2 which then pass through each of the ETC complexes, supercharging them (Figure 3). Once the H^+ gradient is established, ATP Synthase allows H^+ back inside, using this driving force as an energy substrate for adenosine diphosphate (ADP) to ATP conversion within the mitochondria (Figure 3).

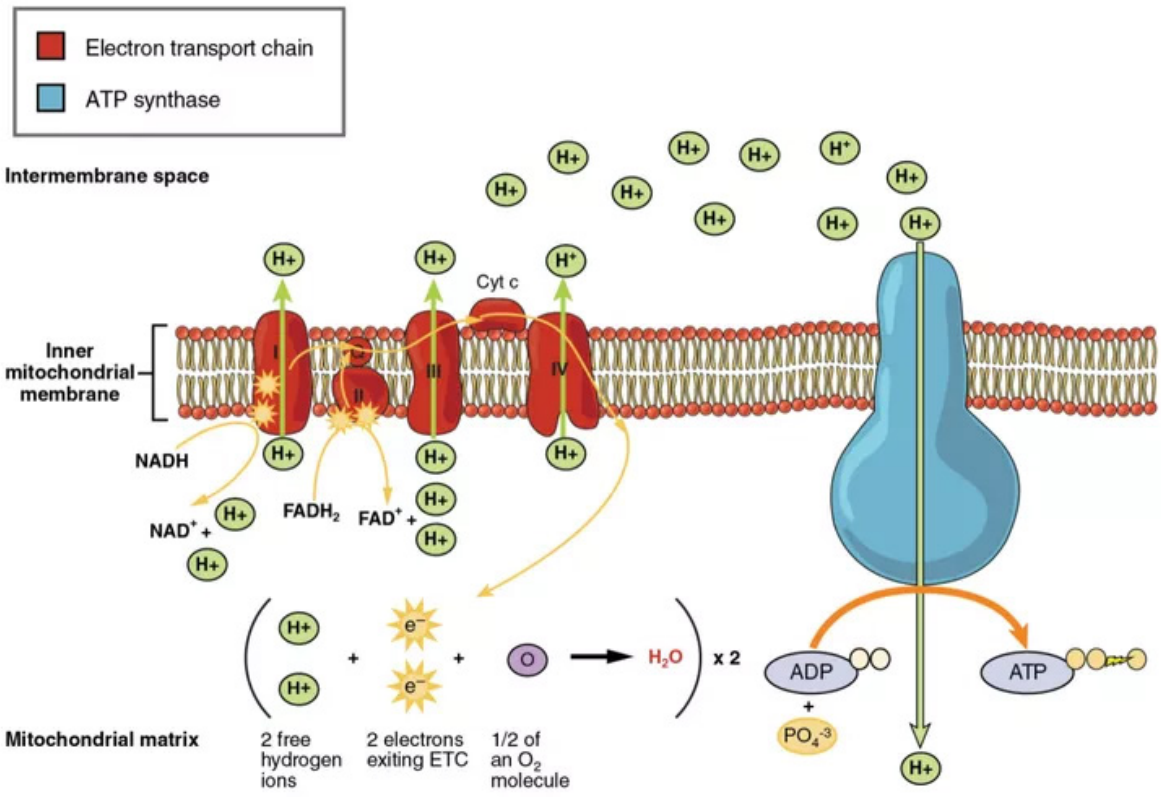

Figure 3: Electron Transport Chain Diagram. NADH donates its electron to complex I (red) while $FADH_2$ donates to complex II (red), driving the H^+ protons out of the mitochondrial matrix creating the proton motive force. H^+ then return to the

mitochondrial matrix through ATP synthase (blue) (Retrieved from: https://www.thoughtco.com/electron-transport-chain-and-energy-production-4136143)

Transcriptional stimulation of FA oxidation and energy expenditure genes are largely regulated by two nuclear proteins, scaffold protein Peroxisome Proliferator-Activated Receptor Gamma Coactivator 1-alpha (PGC-1α), and TF Peroxisome Proliferator-Activated Receptor Alpha (PPARα) (Gasparotto et al., 2021; J. Kim et al., 2018). PGC-1α is a nuclear receptor that is widely considered the master regulator of energy metabolism in metabolic tissues and is typically upregulated during states such as fasting, exercise, or cold exposure (Gasparotto et al., 2021; J. Kim et al., 2018). PGC-1α itself cannot bind DNA but rather acts as a scaffold protein forming various complexes with TFs to activate genes involved in energy metabolism (Cheng et al., 2018; Puigserver & Spiegelman, 2003). PPARα is one protein known to interact with PGC-1α and stimulate FA oxidation, gluconeogenic, and thermogenic genes through a promoter Peroxisome Proliferator-Activated Receptor Response Element (PPRE) (Cheng et al., 2018; Puigserver & Spiegelman, 2003). For example, it is known that PGC-1α aids in the transcription of mitochondrial and ETC genes supporting mitochondria activity, but also in tandem with PPARα can stimulate Uncoupling Protein 1 (UCP1) gene expression through a PPRE (Barberá et al., 2001; Wu et al., 1999). UCP1 is a proton channel membrane protein that embeds into the mitochondrial membrane (Golozoubova et al., 2006; Larrarte et al., 2002; Nedergaard et al., 2001). UCP1 allows H^+ to re-enter the mitochondrial matrix without production of ATP, uncoupling respiration from ATP production, and giving off heat as a by-product (Golozoubova et al., 2006; Larrarte et al., 2002; Nedergaard et al., 2001). PGC-1α-

PPARα-UCP1 is a non-shivering adaptive thermogenic pathway predominantly found in brown adipose tissue (BAT) or burning/browning white adipose tissue (WAT) (Barberá et al., 2001; J. Y. Lee et al., 2011; Wu et al., 1999). BAT is the main thermogenic tissue in humans while WAT is used for energy storage. Interestingly in contrast to its FA oxidation and thermogenic induction, PGC-1α was also found to have a role in adipocyte differentiation (adipogenesis) by coregulating another PPAR protein, Peroxisome Proliferator-Activated Receptor Gamma (PPARγ) (Berger, 2005; Spiegelman et al., 2000). PPARγ has the highest expression in adipose tissue and oppositely of PPARα, strongly induces lipid uptake and synthesis cellular processes thus being essential for adipogenesis (Berger, 2005; Spiegelman et al., 2000).

1.3 Cellular Stress and Unfolded Protein Response

The endoplasmic reticulum (ER) is the main homeostatic sensing organelle in eukaryotic cells. The ER is also the main site of folding newly synthesized peptides into their final tertiary structures. Maintaining optimal protein folding conditions within the ER is required for the efficient productivity of nascent protein folding. Deviation from homeostasis within the cell or ER can reduce protein processing efficiency which results in the accumulation of unfolded proteins in the ER, termed ER stress. Alterations to homeostasis can be caused by factors such as too high or low levels of ions or nutrients, increased energy demand, temperature changes, exposure to toxins, inflammatory cytokines, cell division/differentiation (Badiola et al., 2011; Barrera et al., 2016; Elvira et al., 2020; Farrukh et al., 2014; S. U. Kang et al., 2018; D. Lee et al.,

2019; Tanis et al., 2015; Walter & Ron, 2011; Z. Yu et al., 2018). In response to the particular cellular stress, the ER responds by activating three main pathways that make up the Unfolded Protein Response (UPR). The purpose of the UPR is to alleviate the specific stress through downstream activation of various genes and pathways. The UPR pathways begin with three ER transmembrane proteins PKR-like ER kinase (PERK), Inositol-Requiring Enzyme 1 (IRE1), and Activating Transcription Factor 6 alpha (ATF6α) (Scheuner et al., 2001; Yoshida et al., 1998, 2001). Each is activated in a similar manner in which protein folding chaperone proteins called Binding immunoglobulin protein (BiP), also known as Glucose Regulated Protein 78 (GRP78), detach from each receptor in the presence of accumulated unfolded proteins within the lumen of the ER (Back et al., 2005; Scheuner et al., 2001; Yoshida et al., 1998, 2000, 2001). The unbinding of basally bound BiP/GRP78 from each UPR transmembrane receptor in the ER lumen under stress relieves each UPR receptor's inhibition and thus activating them.

Upon PERK activation it oligomerizes with itself and autophosphorylates, becoming an active kinase which then phosphorylates eukaryotic initiation factor 2 (eIF2α), an essential mRNA translation initiation factor (Scheuner et al., 2001). Phosphorylation of eIF2α disrupts the formation of the ribosomal initiation complex (RIC) resulting in halted general protein synthesis within the cell (Scheuner et al., 2001). This attenuation of protein synthesis allows the ER to reduce its unfolded protein load and restore homeostasis (Scheuner et al., 2001). However, various gene mRNAs have the ability to bypass this effect where eIF2α phosphorylation induces translation such as Activating Transcription Factor 4 (ATF4) (Elvira et al., 2020; Scheuner et al., 2001;

Walter & Ron, 2011). ATF4 is the main transcription factor responsible for the induction of pro-apoptotic gene, C/EBP Homologous Protein (CHOP) (Scheuner et al., 2001; Walter & Ron, 2011). CHOP is ubiquitously expressed at low levels while prolonged significant upregulation of CHOP expression induces apoptosis through the mitochondrial death receptor pathway (Averous et al., 2004).

IRE1, similarly to PERK, also activates in response to ER stress through oligomerization and autophosphorylation upon removal of inhibitory GRP78 binding (Back et al., 2005; Yoshida et al., 2001). Activated IRE1 is an endoribonuclease that actively splices immature XBP1 mRNA into an active mature form XBP1s, that when translated is a potent transcription factor (TF) that targets various genes that aid in relieving the ER stress (Back et al., 2005; Yoshida et al., 2001).

Once relieved from GRP78 binding, ATF6α activates in a different manner than the aforementioned PERK and IRE-1 ER receptors. Removal of GRP78 from ATF6α releases it from the ER membrane and is shuttled to the Golgi apparatus where it is then cleaved by enzymes site-1 and site-2 proteases (S1P and S2P) to release the cytosolic N-terminus (Yoshida et al., 2000; C. Zhang et al., 2012). The N-terminus of ATF6α is an active TF that localizes to the nucleus and stimulates transcription of genes that aid in relieving ER stress such as the *Grp78* gene(Yoshida et al., 2000; C. Zhang et al., 2012).

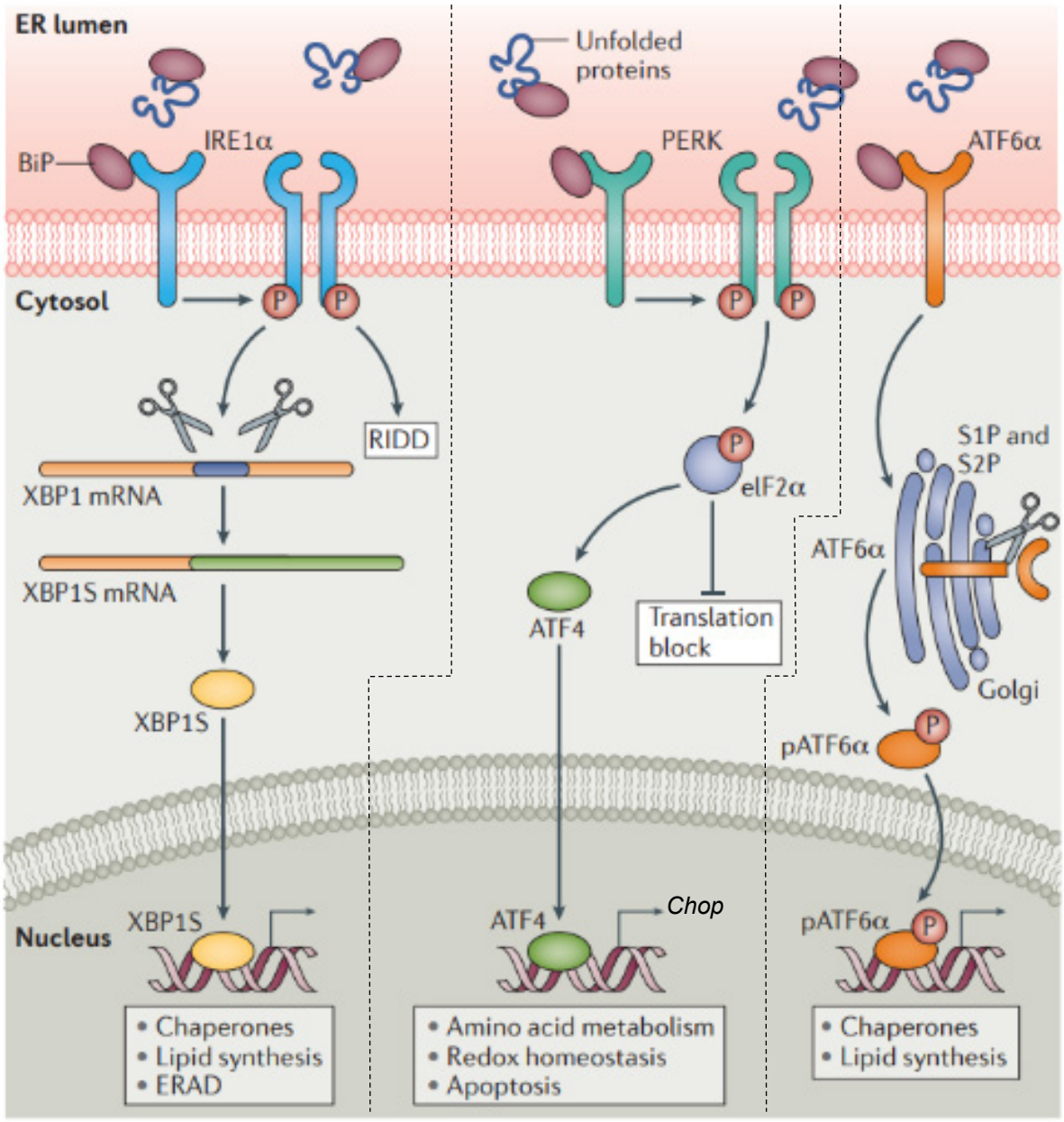

Figure 4: Three arms of the Unfolded Protein Response. As unfolded proteins accumulate within the ER lumen, BiP/GRP78 release from ER-membrane receptors IRE1α (left), PERK (middle), and ATF6α (right) of the UPR, activating them. Activated IRE1α alternatively splices XBP1 mRNA into XBP1s which produces an active XBP1s transcription factor stimulating ER chaperone, lipid metabolism, and ER-associated degradation (ERAD) genes. Once PERK is activated it phosphorylates eIF2α blocking

the majority of protein translation but inducing ATF4 TF expression which stimulates amino acid metabolism, redox homeostasis, and apoptosis genes such as *Chop*. When ATF6α is relieved from BiP/GRP78 binding it translocates to the Golgi where the active N-terminus is cleaved off by S1P and S2P, which then translocates to the nucleus and activates ER chaperones and lipid metabolism genes. (Modified from: Navid & Colbert, 2017).

1.4 UPR and Metabolism

It is well known that ER stress and thus the three UPR arms possess the capabilities to regulate metabolism (Moncan et al., 2021). In fact, overexpression of ER chaperone GRP78, which reduces ER stress and UPR activation, in obese *ob*/*ob* (leptin knockout) mice significantly decreased obesity-induced hepatic ER stress and SREBP-1c cleavage (Kammoun et al., 2009). One of the three UPR arms, PERK, has been reported to activate and phosphorylate eIF2α in mouse livers by fasting for 4 hours then refeeding on a control diet, with an even greater effect fed a high-fat diet (HFD) (Oyadomari et al., 2008). INSIG1, the SCAP-SREBP ER retainer, is especially affected by PERKs global translational inhibition leading to an upregulation of SREBP dependent lipogenesis in response to PERK activation (J. N. Lee & Ye, 2004; Y. Yu et al., 2013). Indeed, *Perk*-KO mouse embryonic fibroblasts (MEFs) depict reduced expression of SREBP lipogenic targets such as FASN and SCD1 (Bobrovnikova-Marjon et al., 2008). A mouse model with chronic dephosphorylation of hepatic eIF2α showed higher susceptibility to fasting hypoglycemia, reduced glycogen stores, and increased insulin

sensitivity on a normal diet compared to WT (Oyadomari et al., 2008). On HFD, these mice showed protection from hepatic steatosis with greater insulin sensitivity and reduced expression of lipogenic genes in the liver (Oyadomari et al., 2008). Major lipogenic regulator PPARγ as well as its lipogenic target genes were decreased, as well as lipogenic/adipogenic transcription factors CCAAT Enhancer-Binding Protein Alpha and Beta (C/EBPα and β) (Oyadomari et al., 2008). PERKs translational attenuation of most proteins actually stimulates ATF4 translation through an upstream open reading frame (P. D. Lu et al., 2004). *Atf4*-KO mice fed a high-carbohydrate diet (HCD) had reduced glucose and insulin tolerance, with decreased hepatic and serum TG levels compared to WT (Yoshizawa et al., 2009). *Atf4*-KO mice also showed a reduction in hepatic lipogenic gene expression (*Scd1*, *Fasn*) which contributed to the protection from hepatic lipid accumulation (C. Wang et al., 2010).

IRE-1 also has strong connections to metabolic regulation. Hepatocyte-specific *Ire1α* deletion in mice ($Ire1\alpha^{Hepfe/-}$) resulted in altered hepatic lipid metabolism and ER stress in response to ER stress treatment with tunicamycin (TM), while no phenotypic differences were apparent under normal conditions relative to WT (K. Zhang et al., 2011). $Ire1\alpha^{Hepfe/-}$ mouse livers showed increased expression of lipogenic inducers such as PPARγ, C/EBPβ, DGAT2, and SCD1, and proapoptotic TFs ATF4 and CHOP, with slightly elevated hepatocyte apoptotic levels under TM induced ER stress (K. Zhang et al., 2011). Interestingly, conditional post-natal hepatic knockout of *Xbp1* (downstream of IRE-1) in mice led to a decrease in hepatic lipogenic genes such as *Scd1 and Dgat2* (A.-H. Lee et al., 2008). Indeed, XBP1s was confirmed by ChIP to bind to the promoters of these lipogenic genes under stress (A.-H. Lee et al., 2008). XBP1s

is not only important for proper lipogenic gene expression, but for hepatic lipoprotein secretion as well. XBP1s is needed for proper VLDL formation and secretion, which is used to transport fat and cholesterol from the liver throughout the body (A.-H. Lee et al., 2008; Zhu et al., 2018). XBP1s also serves as a connection between the UPR and the Kennedy pathway in order to regulate ER membrane biogenesis. It was shown that XBP1s stimulates the production of phosphatidylcholine and phosphatidylethanolamine, two major structural membrane lipids (Sriburi et al., 2007). Nutrient availability can be sensed by the IRE-1-XBP1 axis which induces COPII vesicle component expression and overall formation (L. Liu et al., 2019). XBP1s also plays a role in glucose metabolism by aiding in pancreatic alpha cell glucagon secretion and can stimulate adipocytes to increase glucose uptake as well (Akiyama et al., 2013). This adipocyte glucose uptake effect is likely linked to XBP1s' essential role in adipogenesis (Akiyama et al., 2013; Sha et al., 2009). *Xbp1* KO in MEF cells significantly reduced adipogenic potential by preventing proper adipogenic gene expression (Sha et al., 2009).

Adipogenesis requires a finely timed orchestration of a transcription factor expression pattern in which the UPR has been largely implicated in (L. Guo et al., 2015; Lowe et al., 2012; Sha et al., 2009; Zha & Zhou, 2012). During the early commitment phase of adipogenesis, C/EBPβ and C/EBPδ mRNA are upregulated which control the induction of the final adipogenic TFs PPARγ and then C/EBPα (L. Guo et al., 2015). This cascade promotes lipid droplet formation and mature adipocyte-specific gene expression. (L. Guo et al., 2015; Sha et al., 2009) In the early phase of adipogenesis, C/EBPβ directly stimulates transcription of the UPR gene, *Xbp1*. XBP1s TG then binds and upregulates *Cebpα* through its promoter during the late maturing phase of

adipogenesis (Sha et al., 2009). This XBP1s-dependent upregulation of C/EBPα was shown to be essential for adipogenesis in MEF or 3T3-L1 cells (Sha et al., 2009).

Like XBP1, ATF6α is also required for proper adipogenesis to occur (Lowe et al., 2012). Reduced mRNA expressions of key adipogenic factors C/EBPβ, PPARγ, SREBP1c, and GLUT4 were observed in ATF6α-deficient C3H10T1/2 cells differentiating into adipocytes over eight days (Lowe et al., 2012). Not surprisingly these ATF6α-dependent adipogenic gene inductions resulted in drastic inhibition of adipogenesis (Lowe et al., 2012). Also like XBP1, ATF6α can promote phospholipid synthesis and ER expansion through indirect induction of choline kinase isoforms *Chka* and *Chkb*, thus increasing phosphatidylcholine production (Bommiasamy et al., 2009). Similar to the *Ire1α*$^{Hepfe/-}$ mice, ATF6α-knockout mice do not exhibit any apparent phenotypes under normal physiological conditions (Chen et al., 2016; Yamamoto et al., 2010). When treated with ER stressor TM, ATF6α-knockout mice developed hepatic steatosis which was attributed to a reduction in FA oxidation and VLDL formation with simultaneous promotion of lipid drop formation with hepatocytes compared to WT (Chen et al., 2016; Yamamoto et al., 2010). Additionally, activated ATF6α can also interact with SREBP2 in the nucleus negatively coregulating its lipogenic activity. Other nuclear receptors that ATF6α can interact with PPARα and activate FA oxidation gene expression (*Cpt1*, *Cpt2*, *Acox1*, and *Pparα* itself) in mouse livers preventing hepatic steatosis (Chen et al., 2016). Additionally, PPARα and ATF6α expression in livers of mice during fasting state have a high correlation further strengthening their interplay and ATF6α's role in FA oxidation (Chen et al., 2016). Because of this, it is unsurprising that ATF6α is upregulated during glucose deprivation in HepG2 cells (Zeng et al., 2004).

During this low glucose-induced cellular stress ATF6α inhibits cholesterol synthesis through its SREBP2 coregulation (Zeng et al., 2004). Going along with ATF6α's role in glucose metabolism, *Atf6α*-knockout mice fed a HFD have reduced pancreatic beta cell insulin content and secretion and therefore were less tolerant to glucose, compared to WT (Usui et al., 2012). HFD fed *Atf6α*-knockout mice were reported to show higher levels of active *Xbp1s* mRNA compared to inactive *Xbp1*, indicating higher ER stress in their livers relative to WT (Usui et al., 2012).

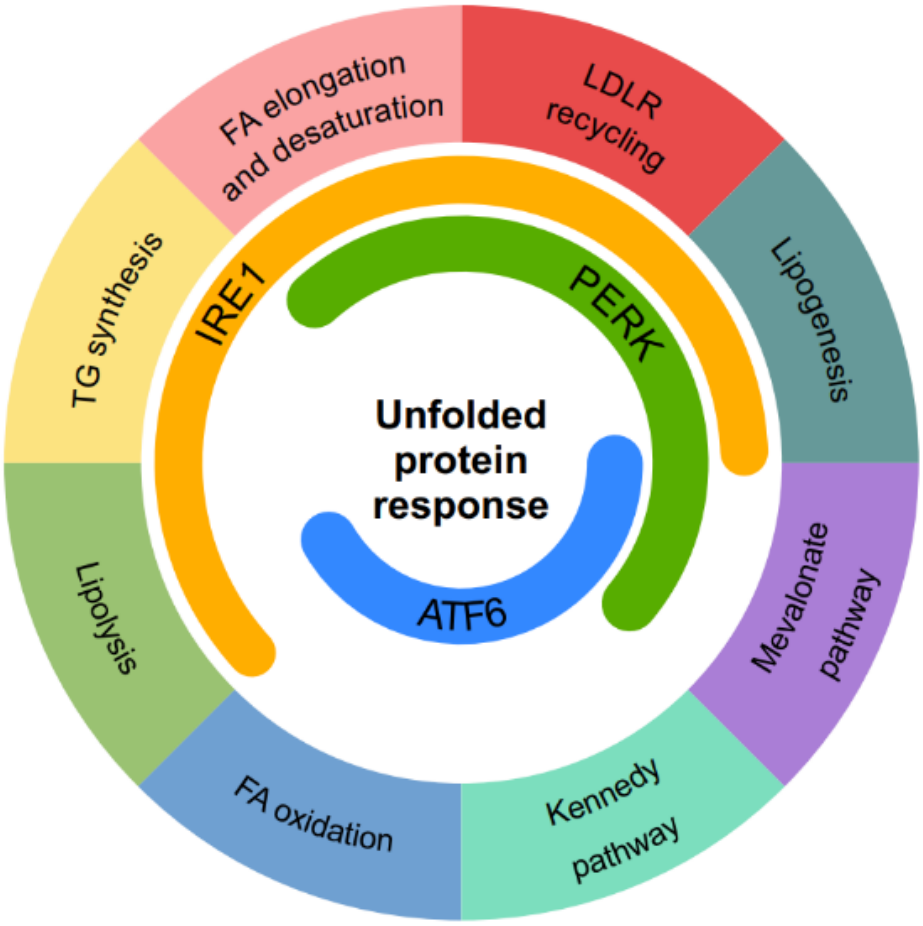

Figure 5: Unfolded Protein Response Regulation of Metabolic Processes. (Moncan et al., 2021)

1.5 Ca^{2+} Homeostasis and UPR

Ca^{2+} is an important second messenger in eukaryotic cells regulating many different physiological processes such as cell growth and death, differentiation, metabolism, secretion, muscle contraction, and neuronal action potentials (Davis et al., 2008; Forostyak et al., 2016; Lomax et al., 2002; Marcelo et al., 2016). Ca^{2+} also carries a positive charge of 2 which can also alter the polarization and electrochemical gradients of cellular organelles altering their function such as mitochondria (Boyman et al., 2020; Murphy & Steenbergen, 2021). Basal cytosolic Ca^{2+} concentration is typically kept at around 100nM with increases reaching up to 1-2uM (Davis et al., 2008; Lomax et al., 2002). Intracellular organelles, ER and Golgi apparatus, are significant cellular Ca^{2+} sinks and can hold 300uM up to 1000uM of Ca^{2+}(Davis et al., 2008; Lomax et al., 2002). Mitochondria maintain a similar [Ca^{2+}] to the cytosol at 100-200nM and is also capable of being elevated 10-fold (Boyman et al., 2020; Murphy & Steenbergen, 2021). Because of the integral importance of Ca^{2+} it is precisely regulated throughout the cell and its organelles. To accomplish this, cells possess a toolbox of Ca^{2+} sensors, pumps, and buffers. On the outer membrane of the cell is a Ca^{2+} channel that brings extracellular Ca^{2+} inside the cell called calcium release-activated calcium channel protein 1 (ORAI1) (Shen et al., 2021). ORAI1 channel permeability is regulated by ER-transmembrane protein stromal interaction molecule 1 (STIM1) (Shen et al., 2021). In the ER lumen, in the presence of high ER-Ca^{2+} stores STIM1 is bound and inhibited by Ca^{2+} ions (Shen et al., 2021). When ER-Ca^{2+} levels decrease and STIM1 is unbound, it dimerizes and binds to ORAI1 inducing a conformational change that opens the Ca^{2+} channel to increase cytosolic Ca^{2+} levels (Shen et al., 2021). The ER is the main Ca^{2+}

store in the cell as well as a sensor for too high or low Ca^{2+} levels (Davis et al., 2008; Lomax et al., 2002; Shen et al., 2021). To replenish ER-Ca^{2+} stores from cytosolic Ca^{2+}, a cytoplasm to ER Ca^{2+} pump powered by ATP called sarcoplasmic/endoplasmic reticulum Ca^{2+}-ATPase (SERCA) is constantly active, albeit at variable rates of ER-Ca^{2+} influx depending on factors such as ATP availability and ER-Ca^{2+} levels (de Marchi et al., 2011; S. Kang et al., 2016). Ca^{2+} is released from the ER mainly through two ER-membrane bound Ca^{2+} channels inositol 1,4,5-triphosphate receptor type 1 (IP3R) and ryanodine receptor (RyR) (Toprak et al., 2021; Xiao et al., 2018). ER-Ca^{2+} is released into the cytosol and regulates various Ca^{2+} dependent signaling ((Toprak et al., 2021; Xiao et al., 2018). Ca^{2+} release from the ER is also taken up by the mitochondria through mitochondria-associated ER membranes (MAMs) that physically connect it and the ER (Xiao et al., 2018). Mitochondrial Ca^{2+} influx can stimulate energy-producing reactions such as the TCA cycle and OXPHOS, increasing cellular respiration (de Marchi et al., 2014). However, overload of mitochondrial Ca^{2+} can cause mitochondrial dysfunction and induce apoptosis through depolarization of the mitochondrial membrane and subsequent release of apoptotic protein cytochrome c (Granatiero et al., 2019; Jambrina et al., 2003).

Ca^{2+} buffering proteins function to chelate and reduce free Ca^{2+} levels, particularly in the ER. Examples of Ca^{2+} buffering proteins include GRP78, calnexin, and calreticulin (CALR) can bind free ER-Ca^{2+} which reduces the basal ER-Ca^{2+} leakage (Burkewitz et al., 2020; Lin et al., 2021; Lomax et al., 2002; Marcelo et al., 2016). All three mentioned Ca^{2+} buffering proteins are known to be upregulated under ER stress through unfolded protein response element (UPRE) and/or ER stress

response elements (ERSEs) (Burkewitz et al., 2020; S. M. Park et al., 2021; Yamamoto1 et al., 2004; Yoshida et al., 1998). Intriguingly, the knockout of *Atf6α* in *Caenorhabditis elegans* led to the downregulation of CALR (Burkewitz et al., 2020). The reduction in CALR resulted in an increase in basal ER-Ca^{2+} leakage which stimulated mitochondrial activity (Burkewitz et al., 2020). This chronic increase in ER-Ca^{2+} leak and mitochondria activity provided *C. elegans* with a significantly extended lifespan (Burkewitz et al., 2020).

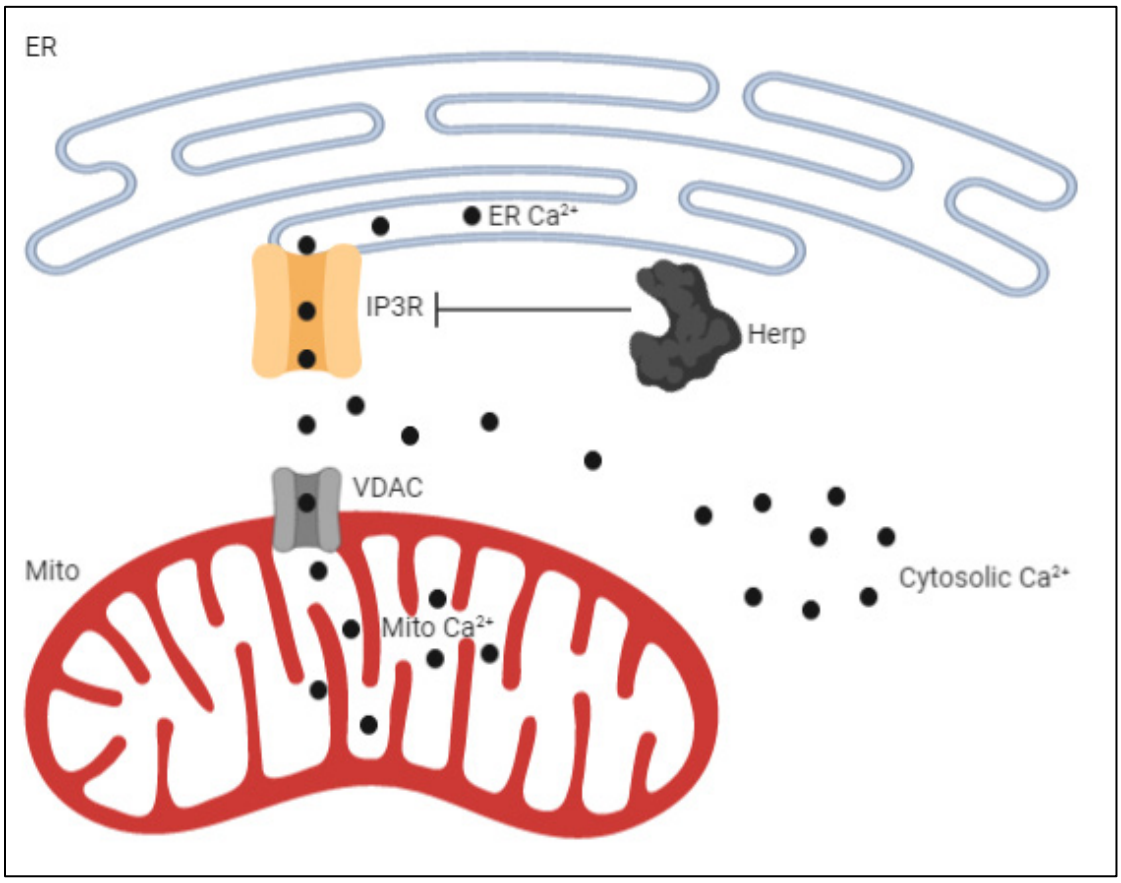

Figure 6: Ca^{2+} Homeostasis in Eukaryotic Cells. Intracellular Ca^{2+} levels are monitored in the ER lumen. Ca^{2+} is released from the ER through ER-Ca^{2+} efflux channels such as IP3R (InsP3R) into the cytosol or taken up by mitochondria in the cell.

Cytosolic Ca^{2+} is pumped back into the ER by SERCA. Herp protein can bind and degrade IP3R channels to prevent ER-Ca^{2+} release. (Created in BioRender)

1.6 Oxidative Stress and UPR

Oxidative stress occurs when there is an imbalance between oxidizing radicals, also known as reactive oxygen species (ROS) and the antioxidant elimination systems in cells/tissue. Elevated levels of ROS have been correlated to the pathogenesis of atherosclerosis, cancer, and neurodegenerative diseases (Bardaweel et al., 2018). The majority of ROS produced in mammalian cells arises as a metabolic byproduct from mitochondrial aerobic respiration through the ETC (Bardaweel et al., 2018). The electrons supercharging the mitochondrial membrane proton pump complexes exit by being transferred to a molecular oxygen molecule, O_2, producing a ROS called superoxide ($O_2^{\bullet -}$) (R. Guo et al., 2018; Scialò et al., 2016). Superoxide is then converted to another form of ROS, hydrogen peroxide (H_2O_2). This conversion can occur either spontaneously or through the action of Superoxide Dismutase 1 and 2 (SOD1 and 2) (Peoples et al., 2019). High levels of ROS can be detrimental to the cell and H_2O_2 can lead to even more deleterious oxidative species, therefore it is essential for cells to eliminate excess levels of H_2O_2 (Bardaweel et al., 2018; Peoples et al., 2019). Removal of H_2O_2 is accomplished in cells by the heme enzyme Catalase which breaks H_2O_2 down into water and oxygen alleviating the toxic levels of H_2O_2 (Jin et al., 2017; Y. Liu et al., 2009; Peoples et al., 2019). Under oxidative stress conditions, protein folding efficiency in the ER is typically reduced therefore subsequently causing

ER stress and activation of the UPR (Dandekar et al., 2015). Both XBP1 and ATF6α have been reported as links between ER and oxidative stress through their regulation of antioxidant genes (Jin et al., 2017; Y. Liu et al., 2009). XBP1-deficient MEF cells treated with H_2O_2 showed significant reductions in *catalase* and *Sod1* mRNA expressions which led to their susceptibility to the oxidative stress and higher levels of apoptosis compared to WT MEFs. (Y. Liu et al., 2009) The XBP1-dependent reductions in *catalase* and *Sod1* gene expression were attributed to an indirect effect, though still however confirming a role for XBP1 in preventing oxidative stress-induced apoptosis (Y. Liu et al., 2009). ATF6α was also shown to be essential for the protection from oxidative stress cell death in ischemia/reperfusion (oxygen deprivation which increases ROS) induced hearts of mice (Jin et al., 2017). The importance of ATF6α in oxidative stress was revealed by its binding to the ERSE-II promoter site of the *catalase* gene, activating its transcription and allowing Catalase to reduce H_2O_2 levels and for the cells to recover (Jin et al., 2017). At non-toxic levels, ROS is an important second messenger (Bardaweel et al., 2018). One example ROS acts as a second messenger is by the oxidation of amino acids residues of proteins such as cysteine residues, to promote disulfide bonding between protein dimers, thus affecting the activity of many enzymes and TFs (Sabaratnam et al., 2019; van der Reest et al., 2018). However, an overload of ROS has the ability to promote apoptosis in cells through stimulation of IP3R ER-Ca^{2+} release channel to activate Ca^{2+}-dependent mitochondrial programmed cell death (Farrukh et al., 2014; Jambrina et al., 2003; Peng & Jou, 2010; Rooney et al., 1991). Interestingly, slight increases in mitochondrial-derived ROS can actually stimulate anti-

aging processes to ultimately extend lifespan in yeast, *C. elegans*, and mice (Burkewitz et al., 2020; Scialò et al., 2016).

1.7 CREB3 Protein Family

There is another family of ER-membrane-bound TFs that function in a similar fashion to ATF6α and SREBP ER stress-associated proteins. These highly conserved proteins belong to the cyclic AMP response element-binding protein-3 (CREB3) basic-leucine zipper (bZIP) family of TFs. Indeed, CREB3 family proteins are also activated by ER stress, causing translocation to the Golgi and subsequent cleavage by S1P and S2P proteases to release the active TF N-terminus domain (C. P. Chan et al., 2011a; Sampieri et al., 2019). The N-terminus of CREB3 proteins then localizes to the nucleus and forms transcriptional complexes with various nuclear receptors and TFs. The mammalian CREB3 family consists of CREB3/LUMAN (known as LZIP in mice), CREB3L1/Oasis, CREB3L2/BBF2H7, CREB3L3/CREBH, and CREB3L4/AIbZIP (C. P. Chan et al., 2011a; Sampieri et al., 2019). These proteins contain a bZIP region which helps to anchor them in the ER membrane, with a DNA-binding domain permitting transcriptional regulation of genes (C. P. Chan et al., 2011a; Sampieri et al., 2019). All CREB3 family members have been reported to play a role in cellular secretion processes by stimulating gene transcription of COPII secretory vesicle formation components such as SEC23/24 or KDEL receptor (C. P. Chan et al., 2011a; Sampieri et al., 2019). Additional to secretory regulation, CREB3 family proteins have more

individualized functions that are still being uncovered (C. P. Chan et al., 2011a; Sampieri et al., 2019).

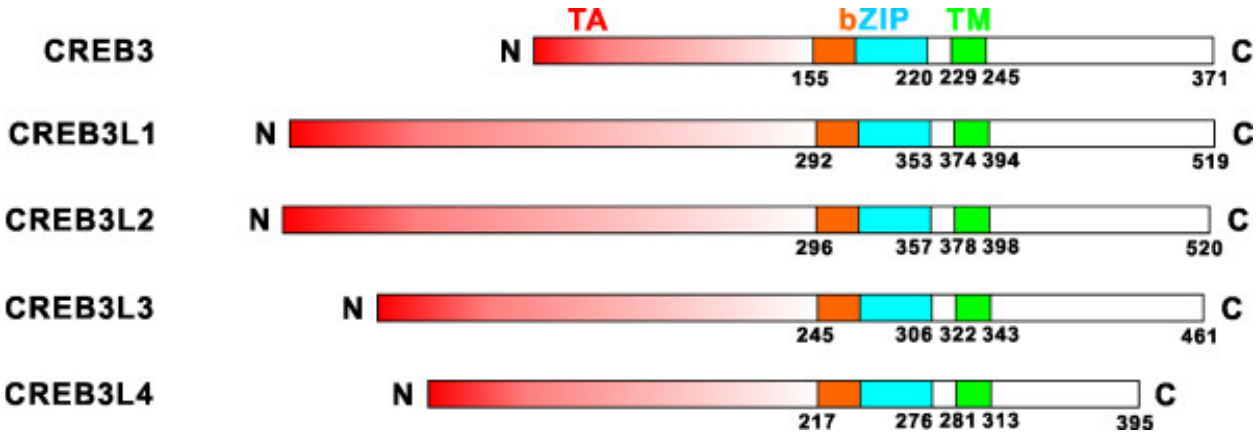

Figure 7: CREB3 Family Proteins. CREB3 family proteins are aligned by their bZIP and transmembrane (TM) regions. N-terminus side of bZIP contains the transactivation domain (TA). (Retrieved from: Chan et al., 2011)

1.7.1 CREB3L1 and CREB3L2

CREB3L1/OASIS was discovered in a screen for induced genes in aged astrocytes isolated from newborn mice (Honma et al., 1999). Under ER stress conditions CREB3L1's gene targets are *Grp78/BiP* and *Xbp1* (Murakami et al., 2009). In humans, CREB3L1 is most highly expressed in bone, heart, colon, pancreas, lung, placenta, and prostate tissue and found to be essential for bone formation, and important for astrocyte and goblet cell differentiation (M. Cui et al., 2015; Guillemyn et al., 2019; Honma et al., 1999; Murakami et al., 2009; Omori et al., 2002). CREB3L1 indeed regulates key osteogenesis genes type I collagen a1 and hypoxia-inducible

factor-1α (M. Cui et al., 2015; Murakami et al., 2009). In fact, humans with mutations in *Creb3l1* suffer from brittle bones due to dysfunctional osteogenesis (Guillemyn et al., 2019).

CREB3L2/BBF2H7 expression is highest in the heart, pancreas, placenta, ovaries, testis, and small intestine (Kondo et al., 2007; Panagopoulos et al., 2007). Other than the common induction of secretory genes of CREB3-Like proteins, CREB3L2 is reported to be a cartilage and bone differentiation factor similar to CREB3L1 (Hino et al., 2014; Saito et al., 2014). CREB3L2 regulates the Indian hedgehog (Ihh) signaling pathway involved in bone and cartilage development, as well as the cartilage matrix gene *Col2a1* (Hino et al., 2014; Saito et al., 2014). Additionally,CREB3L2 was found to be activated by SOX9 TF, a master regulator of chondrocyte/osteoblast differentiation (Hino et al., 2014; Saito et al., 2014).

1.7.2 CREB3L3

CREB3L3 is mainly expressed in the liver and intestines, but also occasionally found in muscle and both brown and white adipose tissue (Sa et al., 2014). CREB3L3 has a well-established role in the regulation of lipid and glucose metabolism and overall energy homeostasis (Nakagawa et al., 2016; Nakagawa & Shimano, 2018; Sa et al., 2014; Satoh et al., 2020; C. Zhang et al., 2012). CREB3L3 is a powerful co-activator of nuclear receptors involved in processes such as lipolysis, lipoprotein secretion, fatty acid oxidation, and gluconeogenesis (H. Kim et al., 2014; Nakagawa et al., 2016; Satoh et al., 2020). CREB3L3 is known to be induced and/or activated under fasting conditions by the PGC-1α/GR complex (H. Kim et al., 2014; M. W. Lee et al., 2010). CREB3L3

interacts with nuclear receptors through the trademark LxxLL nuclear receptor protein interaction domain (H. Kim et al., 2014; M. W. Lee et al., 2010). Proteins reported to interact through this domain with CREB3L3 include PGC-1α and PPARα (H. Kim et al., 2014; M. W. Lee et al., 2010; Nakagawa et al., 2016). Both CREB3L3 and PPARα are implicated together in the regulation of PGC-1α expression and activity through adjacent CRE-PPRE sites in the *Pgc1α* promoter . PGC-1α is a nuclear transcriptional co-activator with greatest expression in high oxidative capacity tissues such as liver, muscle, adipose, and heart tissue and commonly referred to as the master regulator of energy metabolism and mitochondrial biogenesis (Kressler et al., 2002; Puigserver et al., 1998; Rhee et al., 2003). It performs most of its protein-protein interactions through the LxxLL domain as well and its expression is induced under conditions like exercising, fasting, or cold-induced adaptive thermogenesis (Finck & Kelly, 2006; Kressler et al., 2002; Puigserver et al., 1998; Rhee et al., 2003). PGC-1α acts as a scaffold and promotes active complex formation between PGC-1α, and TFs such as CREB3L3 and PPARα (H. Kim et al., 2014; M. W. Lee et al., 2010; Nakagawa et al., 2016). These complexes have potent transcriptional activity targeting lipolysis, FA oxidation, gluconeogenic, and lipid transport gene programs (H. Kim et al., 2014; M. W. Lee et al., 2010; Nakagawa et al., 2016). Some other nuclear receptors PGC-1α co-regulates gene transcription with are PPARγ, GR, ER and ERRs, and thyroid hormone receptor (Knutti et al., 2000; Kressler et al., 2002; Puigserver et al., 1998). Overall, PGC-1α activity induces the overall breakdown of lipids for generating energy through β-oxidation and gluconeogenesis, thus increasing energy availability in times of need like fasting, exercise, or maintaining homeostatic body temperature. Interestingly, the PGC-1α-

CREB3L3-PPARα network are all known to transcriptionally induce each other in an apparent positive autoloop . PGC-1α contains both CRE and PPRE binding sites within its promoter, allowing CREB3L3 and PPARα as well as itself to upregulate its transcription while CREB3L3 and PPARα stimulate each other's gene expression through PPRE and CRE promoter binding sites, respectively (Finck & Kelly, 2006; Handschin & Spiegelman, 2006; M. W. Lee et al., 2010; Nakagawa et al., 2016; Puigserver et al., 1998; Sa et al., 2014; C. Zhang et al., 2012). Like PGC-1α, CREB3L3 is activated by fasting, however, it has also been reported to be activated by FAs (palmitate) and insulin (M. W. Lee et al., 2010; Nakagawa et al., 2016; Rhee et al., 2003; C. Zhang et al., 2012). *Creb3l3*-KO mice fed an atherogenic high-fat diet (AHF) showed significantly reduced weight gain, abdominal fat, with increased non-alcoholic steatohepatitis (NASH) and hypertriglyceridemia compared to WT (C. Zhang et al., 2012). Analysis of *Creb3l3*-KO mice livers revealed diminished hepatic mRNA expression of genes involved in lipogenic regulation, TG synthesis enzymes, lipolysis and lipid transport, FA elongation, FA oxidation, and cholesterol synthesis (C. Zhang et al., 2012). These reductions in hepatic lipid metabolism gene expression were also observed in livers of *Creb3l3*-KO mice on a normal diet, albeit to a lesser extent (C. Zhang et al., 2012). The sheer range of metabolic processes that appear to be regulated by CREB3L3 cement its importance in overall hepatic lipid metabolism. The apparent paradoxical control over opposing lipogenic and lipolysis genetic programs point to a potential co-regulation mechanism by interacting nuclear receptor proteins. These proteins may aid in controlling which metabolic gene promoter targets CREB3L3 binds to dependent on different metabolic conditions and/or cellular stresses.

1.7.3 CREB3L4

Like CREB3L3, CREB3L4 aids in lipid and glucose metabolism as evidenced by *Creb3l4*-knockout mice that were protected from HFD-induced weight gain (T.-H. Kim et al., 2014). This effect was not due to differences in food intake but instead hyperactive adipogenesis in which the authors identified CREB3L4 a novel negative regulator of (T.-H. Kim et al., 2014). The increase in adipogenesis led to an increase in smaller number adipocytes which aided in the protection from HFD-induced hyperglycemia and insulin resistance (T.-H. Kim et al., 2014). CREB3L4 is expressed in most tissues, but particularly high levels in male-specific tissue, such as the prostate gland. In fact, CREB3L4 has been strongly correlated with the proliferation of prostate cancer cells by co-activating AR gene targets in response to androgen hormone stimulation (T. H. Kim et al., 2017; Qi et al., 2002). Interestingly, like CREB3L3, CREB3L4 also performs a similar basal function while remaining tethered to the ER. In its full-length form, CREB3L4 binds and prevents translocation to the Golgi apparatus of fellow CREB3-Like protein, CREB3L1, and the subsequent cleavage and activation of CREB3L1 (X. Cui et al., 2016).

1.7.4 CREB3/LUMAN

CREB3 was discovered in 1997 by Lu *et al.* as a binding partner of cell cycle regulator Host Cell Factor 1 (HCF-1) and was involved in the dormancy of herpes simplex virus (R. Lu et al., 1997). Much of CREB3's physiological and cellular functions still remain unknown. CREB3 functions in a similar way to ATF6α or SREBP proteins once activated. Upon activation, CREB3 shuttles to the Golgi apparatus where it is

cleaved by S1P and S2P to release the N-terminus to the nucleus where it can interact with nuclear proteins and regulate gene transcription (Figure 8) (Raggo et al., 2002). It is thought that CREB3 provides crosstalk between ATF6α and XBP1 UPR proteins (Denboer et al., 2005; Liang et al., 2006; Yamamoto1 et al., 2004). CREB3 is known to bind to CRE, ERSE-II, and unfolded protein response elements (UPRE) (Denboer et al., 2005; Liang et al., 2006; R. Lu et al., 1997). It has previously been shown that CREB3's activated N-terminal can stimulate transcription of homocysteine-induced ER protein (*Herpud1*) gene by binding to the ERSE-II in the *Herpud1* promoter (Liang et al., 2006). HERP promotes the degradation of ER-Ca^{2+} channel IP3R, inhibiting ER-Ca^{2+} release linking CREB3 to Ca^{2+} homeostasis which has also been previously described in literature (S. L. Chan et al., 2004; Mirabelli et al., 2016; Torrealba et al., 2017). Recently, the chicken form of CREB3 structure was solved with X-ray crystallography and revealed a critical cysteine residue that moderated CREB3 dimerization capabilities depending on oxidation status (Sabaratnam et al., 2019). CREB3 also has an inhibiting counter-part protein, CREB3/Luman Recruitment Factor (CREBRF or LRF), that has been shown to bind the active N-terminus of CREB3 in the nucleus and promote its degradation (Audas et al., 2008). A genome-wide association study was conducted on a secluded population located on the Samoan Islands that had been reported to have the world's highest rate of obesity (Minster et al., 2016). Only one single nucleotide polymorphism (SNP) was found to be correlated with the obesity rates, and that SNP was in the *Crebrf* gene (Minster et al., 2016). This Arg457Gln missense SNP was significantly correlated to an average body mass index (BMI) increase of 1.4 kg/m2 per allele containing the SNP (Minster et al., 2016). Like CREBRF, CREB3 has also

recently been shown to interact with nuclear receptor GR (Martyn et al., 2012; Penney et al., 2018). Additionally, CREB3 deficiency in MEF cells resulted in significantly inhibited secretory capacity (Penney et al., 2018).

Full CREB3-knockout (*Creb3*$^{-/-}$) mice are incredibly rare compared to heterozygote (*Creb3*$^{+/-}$) mice, and when they do occur, it is a female suggesting a sex-specific role of CREB3 as well as being essential for developmental growth. Another observed phenotype of CREB3-deficient mice is the distinct lack of maternal care (Penney et al., 2017). Not surprisingly, due to this, pups reared by CREB3-deficient mothers have lower survival rates compared to pups born from a CREB3-deficient mother but cross-fostered and raised by a wild-type mouse mother (Penney et al., 2017). Additionally, CREB3-deficient mice were found to have a dysregulated Hypothalamus-Pituitary-Adrenal (HPA) axis and increased expression of Glucocorticoid Receptor (GR) with low levels of cortisol, the main stress response hormone in animals and plays vital roles in the HPA axis (Penney et al., 2017, 2018). The HPA axis controls the way mammals feel and experience behavioural stress. This HPA alteration of CREB3-deficient mice resulted in a blunted behavioural stress response (Penney et al., 2017). For example, when placed in a box that is half covered and dark while the other is open and exposed to light, WT mice hid in the dark portion of the box for longer periods of time in order to feel safe and protected (Penney et al., 2017). In contrast to this, CREB3-deficient mice were found to have no preference for either side of the box (Penney et al., 2017). Lastly, CREB3-deficient mice had stunted development growth with adults appearing to have a leaner body type, in particular, a distinct lack of abdominal adipose tissue compared to that of WT mice (Penney et al., 2017). Currently,

there is no published research directly implicating CREB3 in the regulation of energy metabolism.

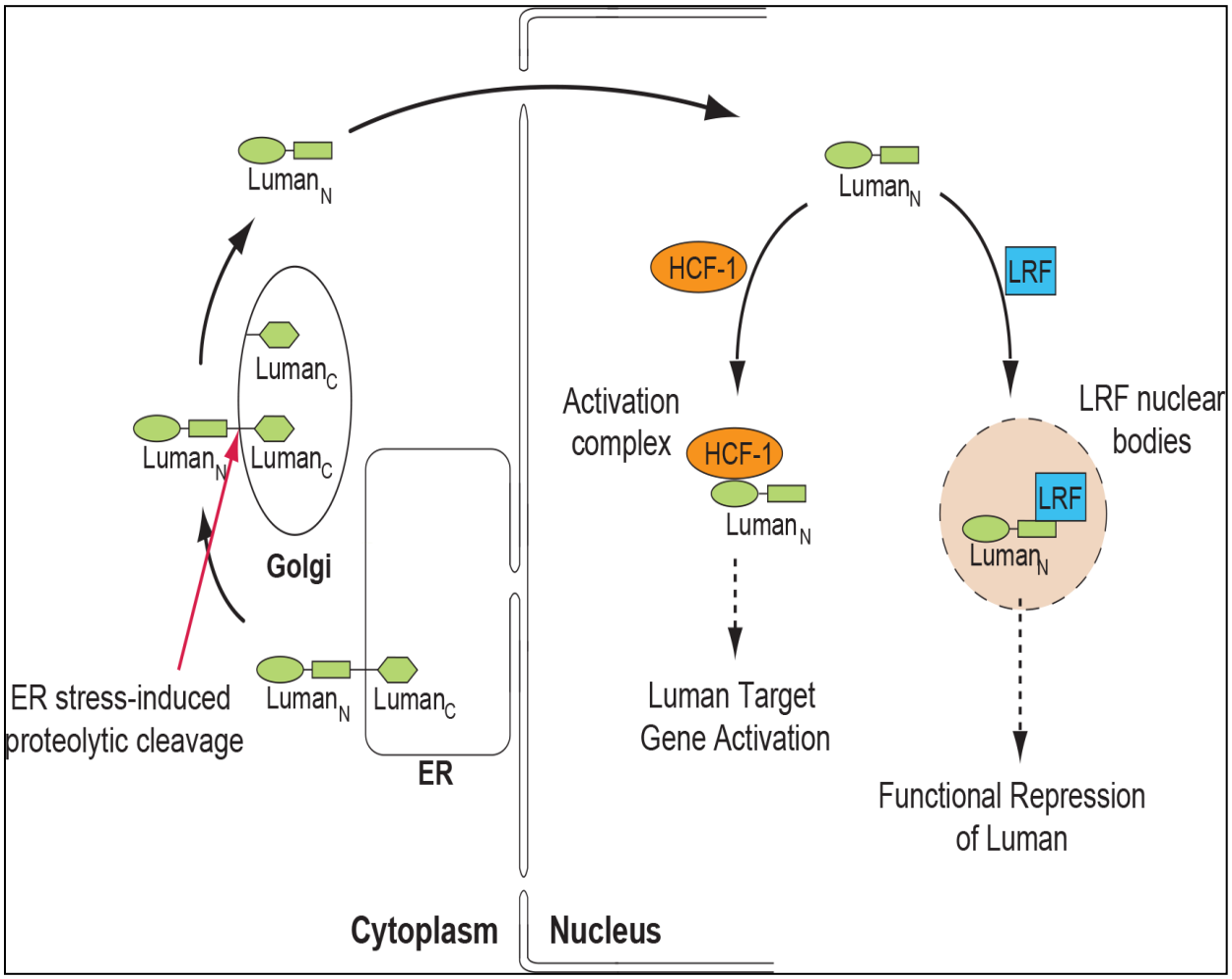

Figure 8: Activation mechanism of CREB3/LUMAN. Upon activation, full-length CREB3/Luman traffics to the Golgi apparatus where it is cleaved to release the N-terminus which then translocates to the nucleus to form transcription activation complexes with nuclear proteins such as HCF-1 or is repressed into nuclear bodies by CREBRF/LRF. (Audas et al., 2008)

1.8 Rationale and Objectives

Many of CREB3's physiological and cellular functions still remain unknown. It acts in a similar way to ATF6α and SREBPs of the UPR, while UPR proteins have been well connected to metabolic regulation in many previous studies. CREB3 can bind many of the promoter response elements that ATF6α can bind and has been thought to provide crosstalk between ATF6α and XBP1 of the UPR. CREB3's counterpart, CREBRF, has already been largely implicated in Samoans with obesity. CREB3-Like proteins CREB3L3 and CREB3L4 have very well described roles in energy metabolism which they perform through nuclear receptor protein interactions and promoter response element DNA binding capabilities. CREB3 contains these capabilities as well. Both CREB3L3- and CREB3L4-deficient mice are found to be lean, even when on a high-fat diet compared to WT. Taking all the previous pieces of information together it is hypothesized that CREB3 is a novel regulator of energy metabolism. To assess this hypothesis, WT and *Creb3*-deficient mice placed on control or high-fat diets were utilized to characterize metabolic phenotype differences with reductions in CREB3. Furthermore, the molecular mechanism of CREB3's potential role in energy metabolism will then be investigated using WT and *Creb3*-deficient mouse embryonic fibroblast (MEF) cells.

Chapter 2: Transcription factor CREB3 is a potent regulator of high-fat diet-induced obesity and energy metabolism.

Disclaimer:

High-fat Diet Measurement of Energy Expenditure by Indirect Calorimetry: Completed and analyzed by Dr. Robin E. Duncan, Kalsha Diaguarachchige De Silva, and Ashkan Hashemi at the University of Waterloo, Department of Kinesiology and Health Sciences.

Abstract

The endoplasmic reticulum senses alterations to cellular homeostasis that activates proteins involved in the Unfolded Protein Response (UPR). UPR proteins are known to aid in regulating glucose and lipid metabolism. Here we report that deficiency of a known UPR protein, Luman or CREB3, resulted in drastic metabolic changes in mice. Compared to wild-type (WT), *Creb3*-deficient mice had increased energy expenditure without any differences in high-fat diet (HFD) energy intake and an increased respiratory exchange ratio indicating a preference for carbohydrates as an energy substrate even on HFD. These metabolic changes resulted in *Creb3*-deficient mice possessing significant protection from HFD-induced weight gain, basal hyperglycemia, and sex-specific tissue lipid accumulation. Although both sexes of *Creb3*-deficient mice had significantly less fat and lean tissue on HFD, *Creb3*-deficient males, in particular, were protected from the accumulation of lipids in the liver and resisted HFD glucose intolerance compared to WT. On the other hand, only *Creb3*-deficient females were protected from lipid accumulation in skeletal muscle with dramatically reduced body fat percentage and plasma leptin levels relative to WT. Despite the drastic metabolic differences of *Creb3*-deficient mice on HFD, their lipid plasma levels did not differ from WT. Taken together, we postulate that CREB3 is a novel key regulator of diet-induced obesity and energy metabolism that warrants further investigation as a potential therapeutic target in metabolic disorders.

2.1 Introduction

Obesity is a modern worldwide pandemic with an estimated 42.4% of Americans with obesity according to the Centers for Disease Control and Prevention (CDC). The endoplasmic reticulum (ER) is a hub for sensing and alleviating alterations to nutrient homeostasis that causes stress to the cell (Basseri & Austin, 2012; Sampieri et al., 2019). The ER contains membrane-bound proteins that sense ER stress and activate unfolded protein response (UPR) to relieve cellular stress and restore homeostasis (Basseri & Austin, 2012; Piperi et al., 2016; Sampieri et al., 2019; Yoshida et al., 1998). ER stress-associated proteins are known to regulate glucose and lipid metabolism and therefore are connected to the pathogenesis of obesity (Basseri & Austin, 2012; Chen et al., 2016; Piperi et al., 2016; C. Zhang et al., 2012). Activating Transcription Factor 6 Alpha (ATF6α), for instance, a well-known UPR-associated protein which can induce hepatic fatty acid oxidation is critical for proper pancreatic β-cell insulin secretion and adipogenesis (Chen et al., 2016; Lowe et al., 2012; Usui et al., 2012; Yoshida et al., 1998).

Cyclic AMP response element-binding protein-3 (CREB3), also known as LUMAN in humans, or LZIP in mice, is an ER-membrane bound transcription factor (R. Lu et al., 1997). Like ATF6α, upon ER stress CREB3 is shuttled to the Golgi apparatus where it is cleaved to release the active N-terminus which translocate to the nucleus and acts as a transcription factor (Denboer et al., 2005; Liang et al., 2006; R. Lu et al., 1997; Raggo et al., 2002). The counterpart of CREB3, CREB3/LUMAN Recruitment Factor (CREBRF/LRF), when bound to CREB3, sequesters and targets it for degradation (Audas et al., 2008). A recent genome-wide association study was performed on a population of the Samoan Islands, which have one of the highest recorded rates of obesity in the world

(Minster et al., 2016). Interestingly, the study identified a particular single nucleotide polymorphism (SNP) in the CREBRF/LRF gene to be strongly associated with BMI with an effect size larger than any other known common obesity-risk variant in humans (Minster et al., 2016).

All CREB3 family proteins are bZIP transcription factors assumed to bind cyclic AMP response elements (CREs) in gene promoters, as well as contain at least one bona fide LxxLL nuclear receptor interaction domain allowing dimerization and co-regulation capabilities (C. P. Chan et al., 2011b; R. Lu et al., 1997; Sampieri et al., 2019; C. Zhang et al., 2012). A subfamily of CREB3-like (CREB3L) proteins consists of CREB3L1/Oasis, CREB3L2/BBF2H7, CREB3L3/CREB-H, and CREB3L4/AIbZIP (C. P. Chan et al., 2011b; T.-H. Kim et al., 2014; Sampieri et al., 2019; C. Zhang et al., 2012). While these CREB3-Like proteins are more tissue-specific, CREB3 expression is ubiquitous throughout all mouse tissues (T.-H. Kim et al., 2014; Ying et al., 2015; C. Zhang et al., 2012). All CREB3-family members have been reported to stimulate secretory vesicle forming genes such as *Sec23/24* or *KDEL* receptor, but also have functions related to metabolism (C. P. Chan et al., 2011b; Penney et al., 2018; Sa et al., 2014; Sampieri et al., 2019). CREB3L3 is mainly expressed in the liver and can regulate lipid and glucose homeostasis (Nakagawa et al., 2016; Sa et al., 2014; Satoh et al., 2020; C. Zhang et al., 2012) while CREB3L4 negatively regulates adipogenesis (T.-H. Kim et al., 2014).

Creb3-deficient mice have previously been shown to have a blunted behavioral stress response phenotype (Penney et al., 2017). They depict less anxious and more “daredevil-like” behavior when compared to wild-type mice under stressful conditions (Penney et al., 2017). Currently, no metabolic phenotypes of *Creb3*-deficient models have

been reported. Therefore, examining the cellular functions of CREB3 may aid in understanding how metabolism is regulated under dietary stress and the pathogenesis of obesity and obesity-related diseases. Here, we hypothesize that CREB3 acts as a novel regulator of energy metabolism. To test this hypothesis, we assessed energy and metabolic homeostasis in wild-type (WT) and *Creb3*-deficient mice fed control (CD) and high-fat diets (HFD).

2.2 Methods

Animals

The *Creb3* gene knockout mouse line was generated in collaboration with the International Gene Trap Consortium. Chimeric mice were backcrossed to C57BL/6NTac mice to produce a 99.9% congenic mouse strain. Mouse ear notches were collected at 21 days old, and DNA extracted using 75uL alkaline lysis solution (25mM NaOH and 0.2mM Na_2EDTA in ddH_2O) heated at 95^oC for 30 minutes. The lysis reaction was neutralized with an equal volume of 40mM Tris-HCl. Genotyping was accomplished by PCR amplification of the WT *Creb3* gene and *lacZ* selection cassette using specific primers (Sup Table 1). Mice were group-housed with same-sex siblings maintained on a 12-h light/dark cycle (10:00–22:00). Temperature was maintained at 21–24°C. Mice were provided tap water, and a control diet (Teklad Global 14% protein rodent maintenance diet: calories from 20% protein, 13% fat, and 67% carbohydrates) ad libitum. Due to low *Creb3* homozygous knockout survival, *Creb3*$^{+/-}$ mice were used in all experiments. 8-week-old WT or *Creb3*$^{+/-}$ mice either remained on CD or were placed on a HFD (Research

Diets Inc., NJ, USA; calories from 20% protein, 45% fat, and 35% carbohydrates) for 8 weeks. Weights were monitored weekly. HFD intestinal fat absorption was monitored by collection of feces from single-housed WT (n=5) and *Creb3*$^{+/-}$ mice (n=4) over 1 week. Feces were mixed with saline, and the lipid phase was isolated and extracted using chloroform: methanol phase separation. Lipid liquid phases were transferred to pre-weighed glass tubes and left to evaporate for 3 days then weighed again to determine the mass of total fecal lipids (bile, cholesterol, fatty acids) per g of feces. The University of Guelph approved all conducted procedures.

Analysis of Body Composition and Fat Distribution

16-week-old WT (males n=6; females n=7) and *Creb3*$^{+/-}$ mice (males n=9; females n=8) on HFD for 8 weeks were euthanized by cervical dislocation and scanned by dual x-ray absorptiometry (DXA) at Ontario Veterinary Clinic Animal Hospital, University of Guelph. Two scans per mouse were obtained, and the average body composition results were used for analysis. Scans were performed and analyzed on GE Healthcare Lunar Prodigy DXA system.

Measurement of Energy Expenditure by Indirect Calorimetry

WT (CD: males/females n=4; HFD: males n=10, females n=5) and *Creb3*$^{+/-}$ mice (CD males/females n=4; HFD males/females n=8) were monitored with an open circuit indirect calorimeter for animal research (Oxymax/CLAMS, University of Waterloo). CLAMS software integrates the data for food and water intake, O2 intake (VO2 in ml/kg/hour), and CO2 exhalation (V CO2 in ml/kg/hour) allowing the calculation of the respiratory exchange

ratio VCO2/VO2 (RER) and the heat production (kcal/hour) over 48 hours. The data collected during the last 24 hours were used for further analysis.

Intraperitoneal Glucose Tolerance Test (IGTT)

WT and *Creb3*$^{+/-}$ mice on either CD (n=5) or HFD (n=5) for 8 weeks fasted overnight, and intraperitoneally injected with 20% sterile filtered glucose in dH2O solution. The amount (in µL) of glucose solution injected was determined by mouse weight (g) X 10 = µL injected. Tips of mouse tails were scored to access and measure blood glucose levels at 0, 15, 30, 60, and 120 minutes. The integrated glucose clearance, the area under the IGTT curve (AUC), was used for comparison between WT and *Creb3*$^{+/-}$ mice.

Plasma Measurements

At the end of the treatment, blood was collected from overnight fasted WT (CD males n=11; HFD males n=4; CD females n=13; HFD females n=4) and *Creb3*$^{+/-}$ (CD males n=7; HFD males n=4; CD females n=5; HFD females n=6) mice by terminal cardiac puncture. Plasma was separated and stored at -80°C. Plasma insulin was determined using Ultra-Sensitive Mouse Insulin ELISA Kit (Crystal Chem# 90080) and leptin using Mouse ELISA Kit (Enzo Life Sciences# ADI-900-019A) and both were detected using Multiskan GO (Thermo-Fisher). The remaining plasma was analyzed for total and HDL cholesterol, non-esterified fatty acids (NEFA), and triglycerides (TG) at the Animal Health Lab facility, University of Guelph.

Gene Expression Analysis

RNA was extracted from mouse liver using Omega E.Z.N.A. Total RNA Kit II. The samples were DNase treated (Thermo-Fisher #EN0525) then reverse transcribed to cDNA (qScript

#G490) and transcript levels measured by qRT-PCR using PerfeCTa SYBR green on a StepOnePlus Real-Time PCR System (Applied Biosystems, Carlsbad, CA, United States). Genes tested include the genes for lipid transport: apolipoprotein A-IV [*ApoA4*] and microsomal triglyceride transfer protein [*Mtp*]; fatty acid synthesis: stearoyl-CoA desaturase [*Scd1*] and fatty acid synthase [*Fasn*]; fatty acid oxidation: Pparγ-coactivator 1a [*Pgc-1α*], peroxisome proliferator-activated receptor-alpha [*Pparα*] and acyl-CoA oxidase 1 [*Acox1*]. Additional genes include the cholesterol synthesis gene squalene epoxidase (*Sqle*), the gluconeogenic gene phosphoenolpyruvate carboxykinase (*Pepck*) and glucocorticoid receptor (*GR*). The list of primers used is in the supplementary Table 1S.

Western Blotting

Frozen epididymal or gonadal white adipose tissue was homogenized with a glass dounce in RIPA buffer (150mM NaCl, 50mM Tris, 1% (v/v) triton x-100, 0.5% (v/v) sodium deoxycholate, 0.1% (v/v) SDS), and run through a QIAshredder (Qiagen #79656) as per manufacturers instructions. Protein lysates were normalized to 1µg/µL using the Bradford Protein Assay (Bio-Rad # 5000002). Protein samples were prepared with 2x Laemmli Sample Buffer (20% glycerol, 0.125M Tris, 4% SDS, 10% 2-mercaptoethanol, and 0.004% bromphenol blue) in a 1:1 ratio (0.5µg/µL) and boiled at 95°C for 10 minutes. 15µg of protein was loaded into each well in a 10% SDS-Page. Gels were run at 150V for 1.5 hours, then wet transferred to PVDF membrane at 50V for 2 hours. Blots were blocked in 5% (m/v) skim milk in PBS-0.1% Tween (PBS-T) for 1 hour at room temperature. Then probed with anti-UCP1 (1:600 in 5% skim milk, ProteinTech #23673-1-AP), and anti-Actin (1:1000 in 5% skim milk, GenScript #A00730) overnight at 4°C. The following day, blots

were washed with PBS-T and probed with secondary horseradish peroxidase (HRP)-conjugated antibodies used at (1:7500 in 5% skim milk, Promega) for 2 hours at room temperature then washed again with PBS-T prior to imaging on a ChemiDoc XRS+ System (Bio-Rad) using ECL imaging substrate (GE Healthcare, Piscataway, NJ).

Tissue Histology and Triglyceride Assays

Mouse tissue sectioning and staining were performed at the University of Guelph Animal Health Laboratory facility. Representative H&E micrographs were examined for the liver and adipocyte lipid droplets and the size of adipocytes determined with ImageJ.

For TG analysis, the liver and quadricep muscle tissues from WT and *Creb3*$^{+/-}$ (n=5 each) mice were homogenized in NP40 lysis buffer provided by Triglyceride Colorimetric Assay Kit (Cayman Chemicals, No. 10010303) and protocol followed as per manufacturer's instructions.

TOF-MS Lipid Analysis

After an 8-week HFD, male WT and *Creb3*$^{+/-}$ livers (n=3 each) were analyzed at the University of Toronto lipidomic facility. Liver samples were spiked with known amount of internal standard mix. After extraction, an aliquot of lipid extract was infused by electrospray ionization in positive and negative modes on a SCIEX 6600 TripleTOF mass spectrometer. Data acquisition was performed using an MS/MSAll method. Data analysis was carried out using Lipid View SoftwareTM (SCIEX). Peak intensities represent the relative abundance of each class and species. Glycerolipid, glycerophospholipid, and sphingolipid classes and their subspecies were analyzed. Fatty acid species profiles were measured for glycerolipids and glycerophospholipids.

Statistical Analysis

Statistical analyses were performed using either a two-way ANOVA followed by Tukey post hoc multiple comparisons or a Student's *t*-test. Results were considered significant when $p < 0.05$. Heatmaps were generated using Heatmapper with Pearson Distance Measurement Method and Single Linkage clustering (Babicki et al., 2016).

2.3 Results

2.3.1 Creb3-deficient mice are resistant to high-fat diet-induced obesity.

To determine the effect of HFD on body weight, 2-month-old WT and *Creb3*$^{+/-}$ male and female mice were placed on HFD for 8 weeks. As shown in Fig. 9A, *Creb3*$^{+/-}$ mice had significantly reduced weight gain compared to WT at various time points and for the entire treatment period (AUCs). This was further corroborated with DXA post-HFD measurements and attributed to a reduced body fat in both *Creb3*$^{+/-}$ male and female mice (Figure 9B, C). HFD weight in *Creb3*$^{+/-}$ males was reduced by 34% and females by 39.5% from WT males and females respectively (Figure 9A, AUC). No statistically significant difference in body fat percentage was found between WT (44.3% ± 0.69) and *Creb3*$^{+/-}$ males (40.4% ± 0.86) when placed on HFD. On the other hand, WT females had 41.17% ± 1.731 fat while *Creb3*$^{+/-}$ females had significantly less at 26.07% ± 2.502 (Figure 9B). *Creb3*$^{+/-}$ males had a 4.3% and females a significant 15.5% increase in lean muscle percentage relative to WT (Figure 9B). Both male and female *Creb3*$^{+/-}$ mice had drastic absolute body fat mass reductions (WT males: 16.5g ± 0.37; *Creb3*$^{+/-}$ males: 12.17g ± 0.71; WT females: 12.64g ± 0.99; *Creb3*$^{+/-}$ females: 5.13 ± 0.8) (Figure 9C). Despite the

increase in lean mass percent (Figure 9B), *Creb3*$^{+/-}$ mice had significant reductions in absolute lean mass (WT males: 20.75g ± 0.77; *Creb3*$^{+/-}$ males: 17.78g ± 0.6; WT females: 17.71g ± 0.58; *Creb3*$^{+/-}$ females: 13.63 ± 0.35) (Figure 9C). *Creb3*$^{+/-}$ mice body weight reductions were not attributed to altered food intake or total feces lipid levels (Figure 9D).

The liver images show that only HFD treated WT mice developed hepatic steatosis as indicated by a pale liver colour (Figure 9E) and accumulation of lipid (TG) droplets (Figure 9F). When quantified for total TG content (Figure 9G), *Creb3*$^{+/-}$ male livers had 1.7-fold lower TG (37.20 mg/dl ± 5.193) compared to WT males (62.30 mg/dl ± 4.586). Differences in total liver TG were however not significant between female groups (Figure 9G). On CD, no hepatic TG accumulation was observed in any of the groups showing that liver lipid accumulation was diet and sex specific.

Examination of quadricep muscle TG levels showed that WT females accumulated more TG in the muscle than WT males fed HFD. *Creb3*$^{+/-}$ females however resisted HFD induced increases in muscle TG, with a reduction relative to WT females of 3.6-fold (Figure 9H). Differences in muscle TG levels were not significant between male groups and diets (Figure 9H). Gonadal/epididymal adipose tissue was used to determine the average adipocyte size and number. On both CD and HFD (Figure 9I), compared to WT, both *Creb3*$^{+/-}$ male and female mice contained a significantly greater number of smaller adipocytes.

Blood biochemistry was analyzed to compare plasma lipid levels between WT and *Creb3*$^{+/-}$ mice on CD and HFD. Paradoxically there were no differences in lipid levels despite the dramatic phenotype of *Creb3*$^{+/-}$ mice on HFD (Figure 10). Taken together, the data shows that when placed on HFD both male and female *Creb3*$^{+/-}$ mice resisted the

weight gain while consuming similar amounts of HFD food, but in a tissue-specific manner, with bigger protective effects from HFD on male liver and female muscle, while having no effect on plasma lipid levels.

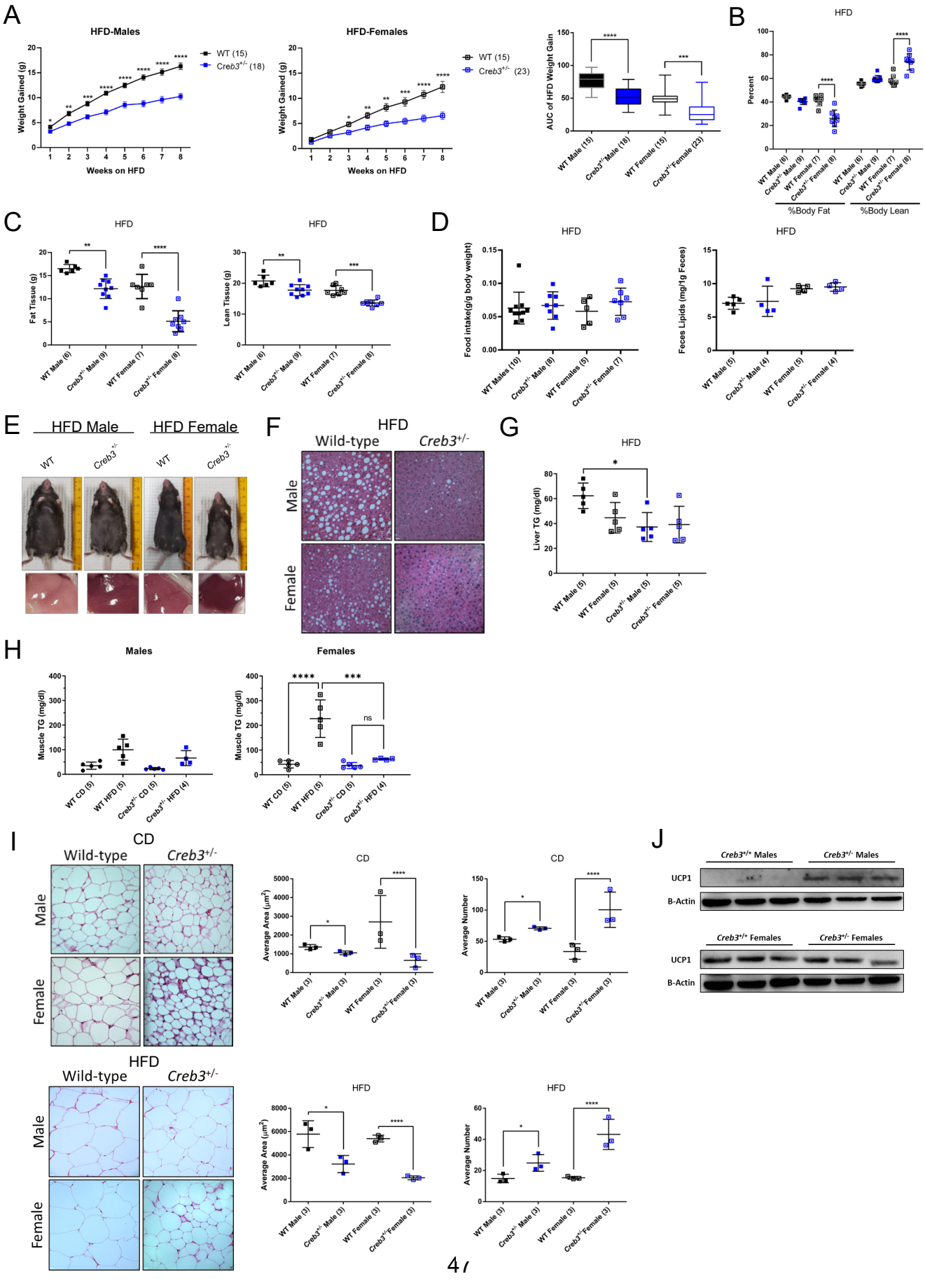
A
HFD-Males
Weight Gained (g)
Weeks on HFD
WT (15)
Creb3+/- (18)
HFD-Females
WT (15)
Creb3+/- (23)
AUC of HFD Weight Gain
WT Male (15)
Creb3+/- Male (18)
WT Female (15)
Creb3+/- Female (23)
B
HFD
Percent
WT Male (6)
Creb3+/- Male (9)
WT Female (7)
Creb3+/- Female (8)
%Body Fat
%Body Lean
C
HFD
Fat Tissue (g)
Lean Tissue (g)
D
HFD
Food intake(g/g body weight)
WT Males (10)
Creb3+/- Male (8)
WT Females (5)
Creb3+/- Female (7)
Feces Lipids (mg/1g Feces)
WT Male (5)
Creb3+/- Male (4)
WT Female (5)
Creb3+/- Female (4)
E
HFD Male
HFD Female
WT
Creb3+/-
F
HFD
Wild-type
Creb3+/-
Male
Female
G
HFD
Liver TG (mg/dl)
WT Male (5)
WT Female (5)
Creb3+/- Male (5)
Creb3+/- Female (5)
H
Males
Females
Muscle TG (mg/dl)
WT CD (5)
WT HFD (5)
Creb3+/- CD (5)
Creb3+/- HFD (4)
ns
I
CD
Wild-type
Creb3+/-
Male
Female
Average Area (μm2)
Average Number
WT Male (3)
Creb3+/- Male (3)
WT Female (3)
Creb3+/- Female (3)
HFD
J
Creb3+/+ Males
Creb3+/- Males
UCP1
B-Actin
Creb3+/+ Females
Creb3+/- Females

Figure 9: *Creb3*-deficient mice are resistant to high-fat diet-induced obesity and hepatic steatosis. 16-week-old male and female WT, and *Creb3*$^{+/-}$ C57BL/6NTac mice fed a CD or HFD for 8- weeks. **(A)** HFD body weight (g) gained since the start of an 8-week diet. n=15 WT males (solid black squares), n=18 *Creb3*$^{+/-}$ males (solid blue squares), n=15 WT females (open black squares), n=23 *Creb3*$^{+/-}$ females (open blue squares). **(B-C)** HFD body percent and absolute fat and lean masses determined by dual-energy x-ray absorptiometry (DXA). n=6 WT males, n=9 *Creb3*$^{+/-}$ males, n=7 WT females, n=8 *Creb3*$^{+/-}$ females. **(D)** HFD food consumption (n=10 WT males, n=8 *Creb3*$^{+/-}$ males, n=5 WT females, n=8 *Creb3*$^{+/-}$ females) over 24h and feces lipid excretion (n=4-5 per group) **(E)** Male and female WT and *Creb3*$^{+/-}$ whole body and liver tissue images. **(F)** H&E-stained liver sections at 40x magnification. **(G)** Male and female WT and *Creb3*$^{+/-}$ on HFD total triglyceride content of liver tissue, n=5 per group. **(H)** Male and female WT and *Creb3*$^{+/-}$ on HFD total triglyceride content of muscle tissue, n=5 per group **(I)** Control diet male and female WT and *Creb3*$^{+/-}$ H&E-stained abdominal adipose sections at 40x magnification and quantified average size and number of adipocytes, n=3 per group. **(J)** Western blots of WT and *Creb3*$^{+/-}$ eWAT (males) and gWAT (females) protein lysate after HFD, n=3 per group. Graphs depict mean ± SD. Two-way ANOVA with Tukey post hoc, *P < 0.05, **P< 0.01, ***P< 0.001, ****P< 0.0001.

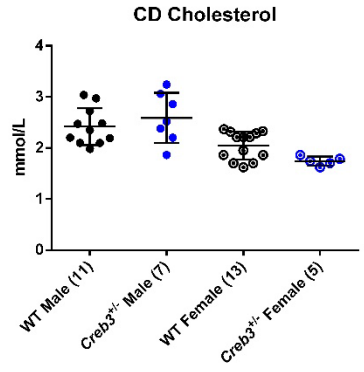
CD Cholesterol
mmol/L
0
1
2
3
4
WT Male (11)
Creb3+/- Male (7)
WT Female (13)
Creb3+/- Female (5)

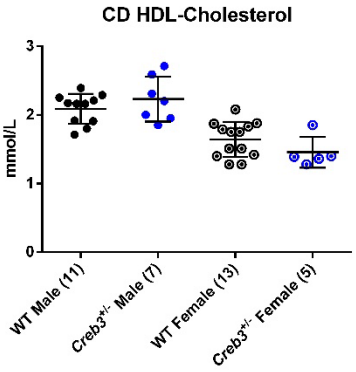
CD HDL-Cholesterol
mmol/L
0
1
2
3
WT Male (11)
Creb3+/- Male (7)
WT Female (13)
Creb3+/- Female (5)

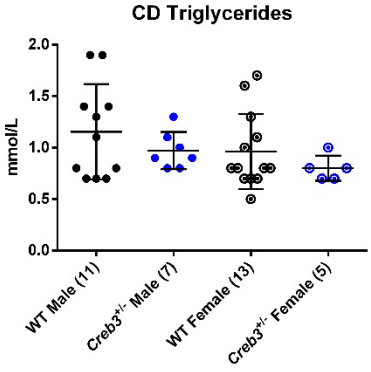
CD Triglycerides
mmol/L
0.0
0.5
1.0
1.5
2.0
WT Male (11)
Creb3+/- Male (7)
WT Female (13)
Creb3+/- Female (5)

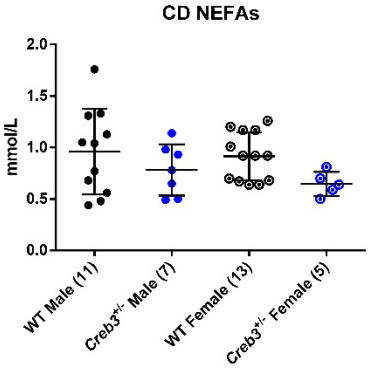
CD NEFAs
mmol/L
0.0
0.5
1.0
1.5
2.0
WT Male (11)
Creb3+/- Male (7)
WT Female (13)
Creb3+/- Female (5)

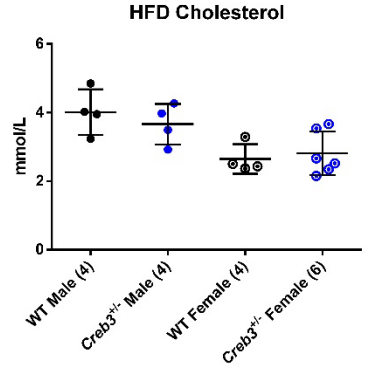
HFD Cholesterol
mmol/L
0
2
4
6
WT Male (4)
Creb3+/- Male (4)
WT Female (4)
Creb3+/- Female (6)

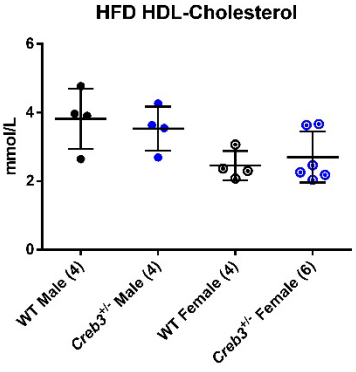
HFD HDL-Cholesterol
mmol/L
0
2
4
6
WT Male (4)
Creb3+/- Male (4)
WT Female (4)
Creb3+/- Female (6)

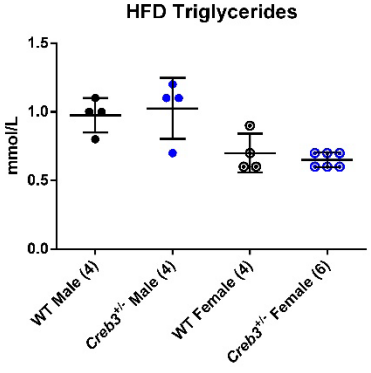
HFD Triglycerides
mmol/L
0.0
0.5
1.0
1.5
WT Male (4)
Creb3+/- Male (4)
WT Female (4)
Creb3+/- Female (6)

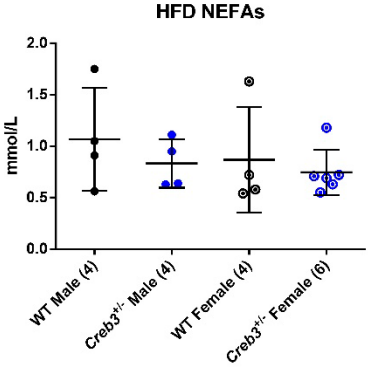
HFD NEFAs
mmol/L
0.0
0.5
1.0
1.5
2.0
WT Male (4)
Creb3+/- Male (4)
WT Female (4)
Creb3+/- Female (6)

Figure 10: WT and *Creb3*$^{+/-}$ fasted plasma lipid analysis on CD or HFD. 16-week-old WT and *Creb3*$^{+/-}$ male and female mice fed CD or HFD for 8 weeks. Males: n=11 CD WT, n=4 HFD WT, n=7 CD *Creb3*$^{+/-}$, n=4 HFD *Creb3*$^{+/-}$. Females: n=13 CD WT, n=4 HFD WT, n=5 CD *Creb3*$^{+/-}$, n=6 HFD *Creb3*$^{+/-}$. Data is represented as the mean ± SD. Two-way ANOVA with Tukey post hoc, *P< 0.05.

2.3.2 Creb3-deficient mice have increased energy expenditure without differences in energy intake.

To assess differences in energy expenditure and energy substrate utilization as a potential reason for the *Creb3*$^{+/-}$ mice resistance to HFD induced obesity we measured VO2 consumption, VCO2 exhalation, and calculated body heat production and RER (Figure 11). On CD no significant differences in heat production or RER were observed between *Creb3*$^{+/-}$ and WT mice (Figure 11A, B). When placed on HFD, both *Creb3*$^{+/-}$ sexes had higher RER and increased heat production relative to WT (Figure 11C, D). T-test analysis also revealed significant heat increases in *Creb3*$^{+/-}$ versus WT mice ($p = 0.0142$). *Creb3*$^{+/-}$ males and females had 46% and 40% respective increases in body heat relative to WT mice on HFD (Figure 11C). Agreeing with this in *Creb3*$^{+/-}$ male mice heat production, *Creb3*$^{+/-}$ males also showed significant induction of thermogenic protein UCP1 in epididymal white adipose (eWAT) tissue (Figure 9J). However, no differences were detected in gonadal white adipose tissue (gWAT) between female genotypes (Figure 9J). HFD RERs increased 17.5% and 25% in *Creb3*$^{+/-}$ males and females, respectively, from WT, indicating a greater preference towards carbohydrate utilization for energy (Figure 11D). Despite the increases in energy expenditure of *Creb3*$^{+/-}$ mice fed a HFD there were no differences in HFD energy intake compared to WT (Figure 9D),

suggesting that changes in energy expenditure are contributing to the decrease in body weight and fat mass of *Creb3*$^{+/-}$ mice. Male *Creb3*$^{+/-}$ mice appeared to expend this energy through UCP1 dependent mitochondrial uncoupling in eWAT, while *Creb3*$^{+/-}$ females showed no difference from WT, suggesting they expend energy/heat from another metabolic tissue such as muscle.

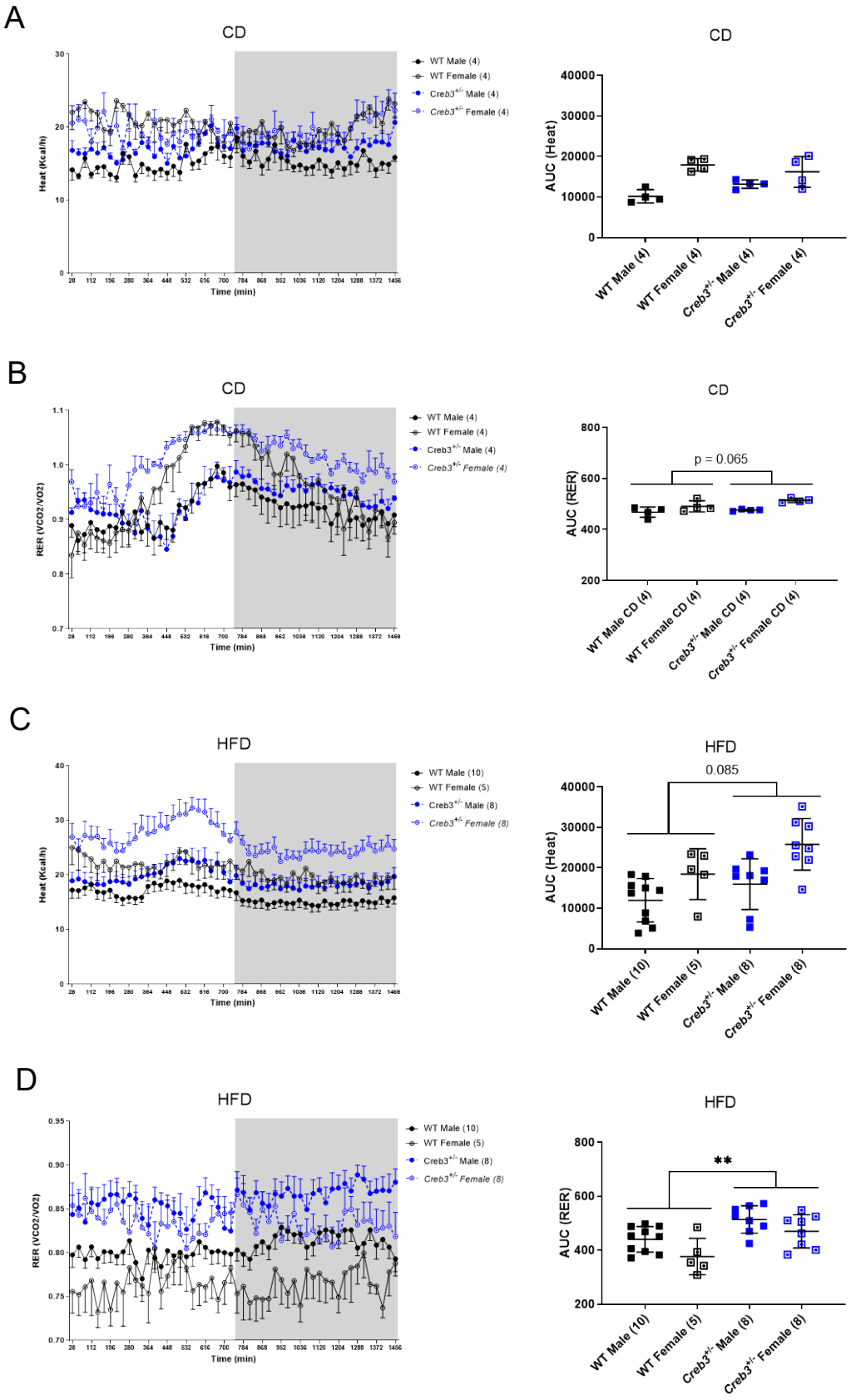
A
CD
Heat (Kcal/h)
Time (min)
WT Male (4)
WT Female (4)
Creb3+/- Male (4)
Creb3+/- Female (4)
CD
AUC (Heat)
WT Male (4)
WT Female (4)
Creb3+/- Male (4)
Creb3+/- Female (4)
B
CD
RER (VCO2/VO2)
Time (min)
WT Male (4)
WT Female (4)
Creb3+/- Male (4)
Creb3+/- Female (4)
CD
AUC (RER)
p = 0.065
WT Male CD (4)
WT Female CD (4)
Creb3+/- Male CD (4)
Creb3+/- Female CD (4)
C
HFD
Heat (Kcal/h)
Time (min)
WT Male (10)
WT Female (5)
Creb3+/- Male (8)
Creb3+/- Female (8)
HFD
0.085
AUC (Heat)
WT Male (10)
WT Female (5)
Creb3+/- Male (8)
Creb3+/- Female (8)
D
HFD
RER (VCO2/VO2)
Time (min)
WT Male (10)
WT Female (5)
Creb3+/- Male (8)
Creb3+/- Female (8)
HFD
**
AUC (RER)
WT Male (10)
WT Female (5)
Creb3+/- Male (8)
Creb3+/- Female (8)

Figure 11: *Creb3*-deficient mice have increased energy expenditure and respiratory exchange ratio on HFD. 16-week-old male and female WT, and *Creb3*$^{+/-}$ mice fed a CD or HFD for 8 weeks. **(A)** CD body heat production over 24 hours and AUC, n=4 per group (CD WT males: solid black circles, *Creb3*$^{+/-}$ males: solid blue circles, WT females: open black circles, *Creb3*$^{+/-}$ females: open blue circles) **(B)** CD respiratory exchange ratio over 24 hours and AUC, n=4 per group. **(C)** HFD body heat production over 24 hours and AUC, n=10 WT males, n=8 *Creb3*$^{+/-}$ males, n=5 WT females, n=8 *Creb3*$^{+/-}$ females **(D)** HFD respiratory exchange ratio over 24 hours and AUC, n=10 WT males, n=8 *Creb3*$^{+/-}$ males, n=5 WT females, n=8 *Creb3*$^{+/-}$ females. Data is represented as the mean ± SEM (line graphs) and the mean ± SD (AUC). Two-way ANOVA with Tukey post hoc, *P < 0.05, **P < 0.01.

2.3.3 Creb3-deficient mice maintain normal glucose levels on high-fat diet.

As expected, WT mice had significantly elevated blood glucose on HFD compared to CD, i.e., WT males showed 2.17-fold increase (328.7 ± 31.54 mg/dl on HFD and 151.6 ± 7.34 mg/dl) and WT females showed 1.33-fold increase (172.8 ± 9.609 mg/dl on HFD and 129.6 ± 13.77 mg/dl) on CD (Figure 12A, B). *Creb3*$^{+/-}$ mice however maintained blood glucose on CD and HFD, i.e., *Creb3*$^{+/-}$ males had 167.5 mg/dl ± 7.393 on CD and 162.0 mg/dl ± 8.62 on HFD and *Creb3*$^{+/-}$ females had 119.7 mg/dl ± 8.67 on CD and 121.3 mg/dl ± 10.42 glucose on HFD (Figure 12A, B).

The IGTT test further showed that WT mice developed glucose intolerance on HFD (Figure 12C-F). On the other hand, *Creb3*$^{+/-}$ males had preserved glucose tolerance on HFD (Figure 12C, E) while female *Creb3*$^{+/-}$ showed little to no reduction compared to WT females (Figure 12D, F). Insulin and leptin measurements (Figure 12G, H) showed that

Creb3$^{+/-}$ male mice displayed a mild basal reduction in blood insulin (*Creb3*$^{+/-}$ male: 0.7776 ng/mL ± 0.1292) compared to WT males (1.167 ng/mL ± 0.1701) while female insulin did not differ (Figure 12G). However, female *Creb3*$^{+/-}$ mice had 3.26-fold reduction (246.0 pg/mL ± 13.47) in basal leptin levels compared to WT female (802.8 pg/mL ± 209.4) (Figure 12H). Taken together, WT males are more sensitive to HFD increased fasted glucose levels than WT females, that was reflected in larger reductions in *Creb3*$^{+/-}$ glucose and insulin in males than females. Additionally, the preference for carbohydrates as an energy substrate due to increased RER of *Creb3*$^{+/-}$ mice on HFD (Figure 11D) is likely contributing to their improved fasted blood glucose and glucose intolerance in *Creb3*$^{+/-}$ males. However female *Creb3*$^{+/-}$ had dramatically reduced basal (CD) leptin levels possibly because of reductions in adipose tissue, that was apparently protective.

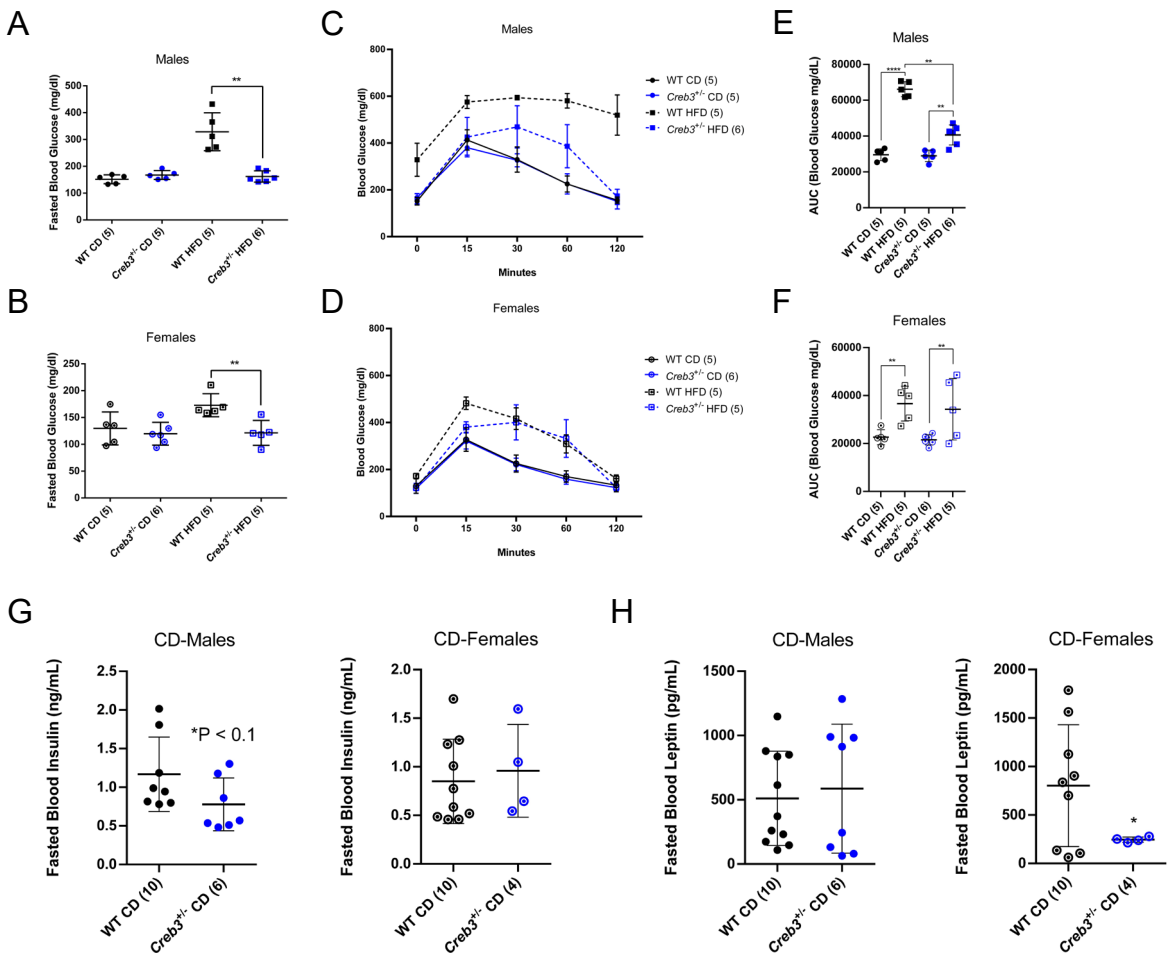

Figure 12: *Creb3*-deficient mice preserve glucose tolerance on HFD. 16-week-old WT and *Creb3*$^{+/-}$ male and female mice fed either a CD or HFD for 8 weeks. **(A-B)** Fasted blood glucose levels, n=5-6 per group. **(C-D)** Intraperitoneal glucose tolerance tests on CD or HFD, fasted overnight, n=5-6 per group. **(E-F)** Area under curve analyses of intraperitoneal glucose tolerance tests. **(G-H)** Fasted blood insulin and leptin levels on CD, n=10 WT males, n=6 *Creb3*$^{+/-}$ males, n=10 WT females, n=4 *Creb3*$^{+/-}$ females. Data is represented as the mean ± SD. Two-way ANOVA with Tukey post hoc, *P< 0.05, **P< 0.01, ***P< 0.001, ****P< 0.0001.

2.3.4 Creb3-deficient mice have differential expression of liver lipid and UPR genes.

To understand the differences in the liver and plasma lipid phenotype observed on HFD, WT and *Creb3*$^{+/-}$ mice were analyzed for the expression of key metabolic genes known to be directly or indirectly affected by hepatic CREB3 subfamily member, CREB3L3 (Figure 13A). Both *Creb3*$^{+/-}$ sexes showed a 3-fold increase in the expression of mitochondrial biogenesis regulator *Pgc-1α*, and the key enzyme for oleic acid synthesis *Scd1*. The fatty acid oxidation enzyme *Acox1* and *GR* were also upregulated greater than 1.5-fold in both *Creb3*$^{+/-}$ livers. *Creb3*$^{+/-}$ males specifically showed ~2-fold increase in the gluconeogenic enzyme *Pepck* and the fatty acid oxidation regulator *Pparα*, while the lipoprotein gene *ApoA4* was significantly reduced. Female *Creb3*$^{+/-}$ had increased expression of the lipoprotein assembly gene *Mtp* and the fatty acid synthesis gene *Fasn*, with a significant reduction in the sterol biosynthesis gene *Sqle*.

To assess ER stress levels in the livers of HFD fed WT and CREB3-deficient mice, hepatic mRNA of key UPR activity indicator genes were measured (Figure 13B). *Creb3*$^{+/-}$ mice had a 2.5-fold induction of inactive *Xbp1* mRNA while no differences were found in active *Xbp1-s* mRNA levels compared to WT mice of both sexes. Additionally, *Creb3*$^{+/-}$ mouse livers showed reductions in mRNA of UPR indicators *Grp78* and *Chop* by 68% and 74% relative to WT, respectively. In terms of oxidative stress, only *Creb3*$^{+/-}$ female livers revealed large reductions in antioxidant genes *Catalase* and *Sod1* by 82% and 89% compared to WT females.

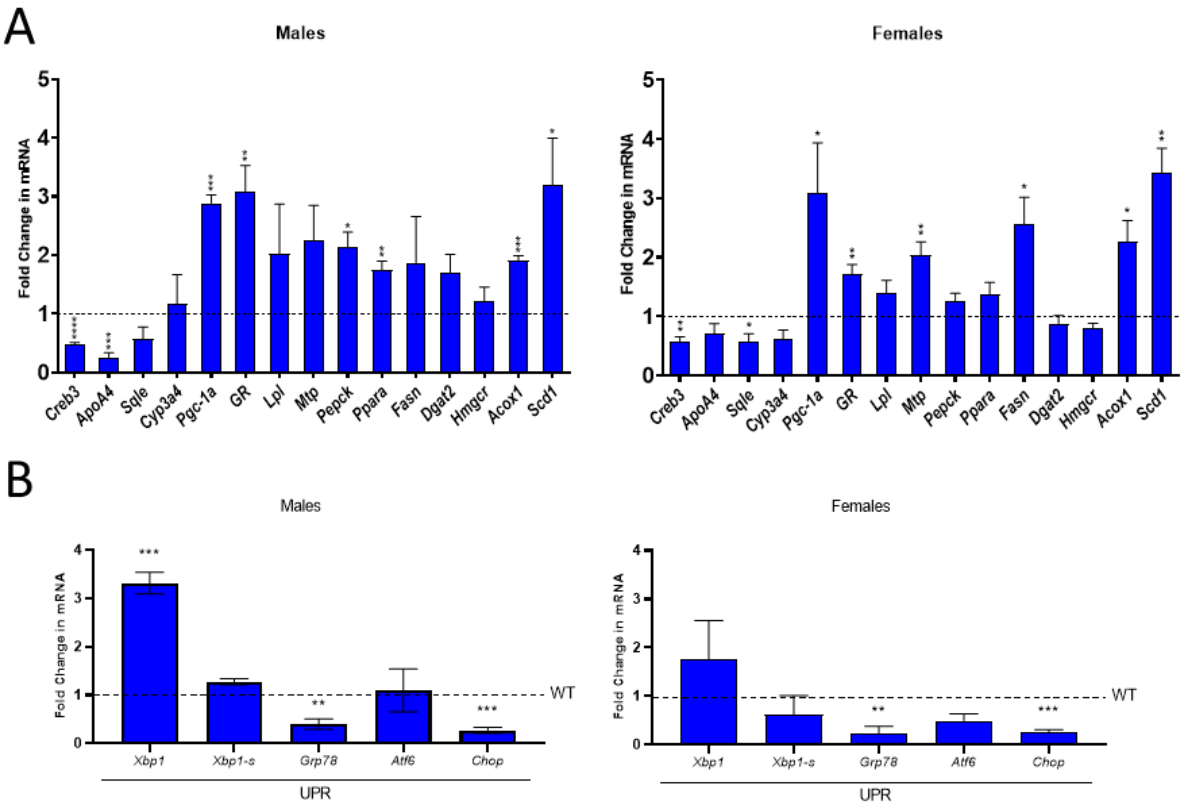

Figure 13: *Creb3*-deficient mice have altered hepatic lipid and UPR gene expression. 16-week-old male and female WT and *Creb3*$^{+/-}$ mice fed HFD for 8 weeks. Relative changes in *Creb3*$^{+/-}$ gene expression data from reverse-transcribed mRNA isolated from mouse livers (WT=1, dash line). n=3 WT males, n=3 *Creb3*$^{+/-}$ males, n=4 WT females, n=6 *Creb3*$^{+/-}$ females. **(A)** Metabolic gene expression panel **(B)** UPR and oxidative stress response gene expression panel (WT=1, dash line). n=3. Data is represented as the mean ± SD. Student's *t* test, *P< 0.05, **P< 0.01, ***P< 0.001, ****P< 0.0001.

2.3.5 Creb3-deficient mice have decreased hepatic glycerolipids and increased glycerophospholipids on HFD.

Since WT male mice developed fatty liver on HFD (Figure 9E-G), hepatic lipid profiles of *Creb3*$^{+/-}$ males were investigated by Maldi-TOF-MS. Specific glycerolipids, phospholipids, and sphingolipids and their fatty acid compositions were analyzed to assess potential dysfunction of lipid synthesis/metabolism. Surprisingly, *Creb3*$^{+/-}$ and WT males did not differ in most lipid species and fatty acid compositions. However, there was a drastic reduction in *Creb3*$^{+/-}$ total TG and an increase in individual phospholipids. Compared to WT, there was a 71% reduction in hepatic TG in *Creb3*$^{+/-}$ mice (Figure 14A). Similarly, a 55% reduction in monoacylglycerol (MAG), and a 68% reduction in diacylglycerol (DAG) from WT livers were observed in *Creb3*$^{+/-}$ livers (Figure 14A). Inversely, *Creb3*$^{+/-}$ hepatic phosphatidylcholine (PC), phosphatidylethanolamine (PE), and phosphatidylserine (PS) were increased by 60%, 78%, and 52%, respectively (Figure 14B).

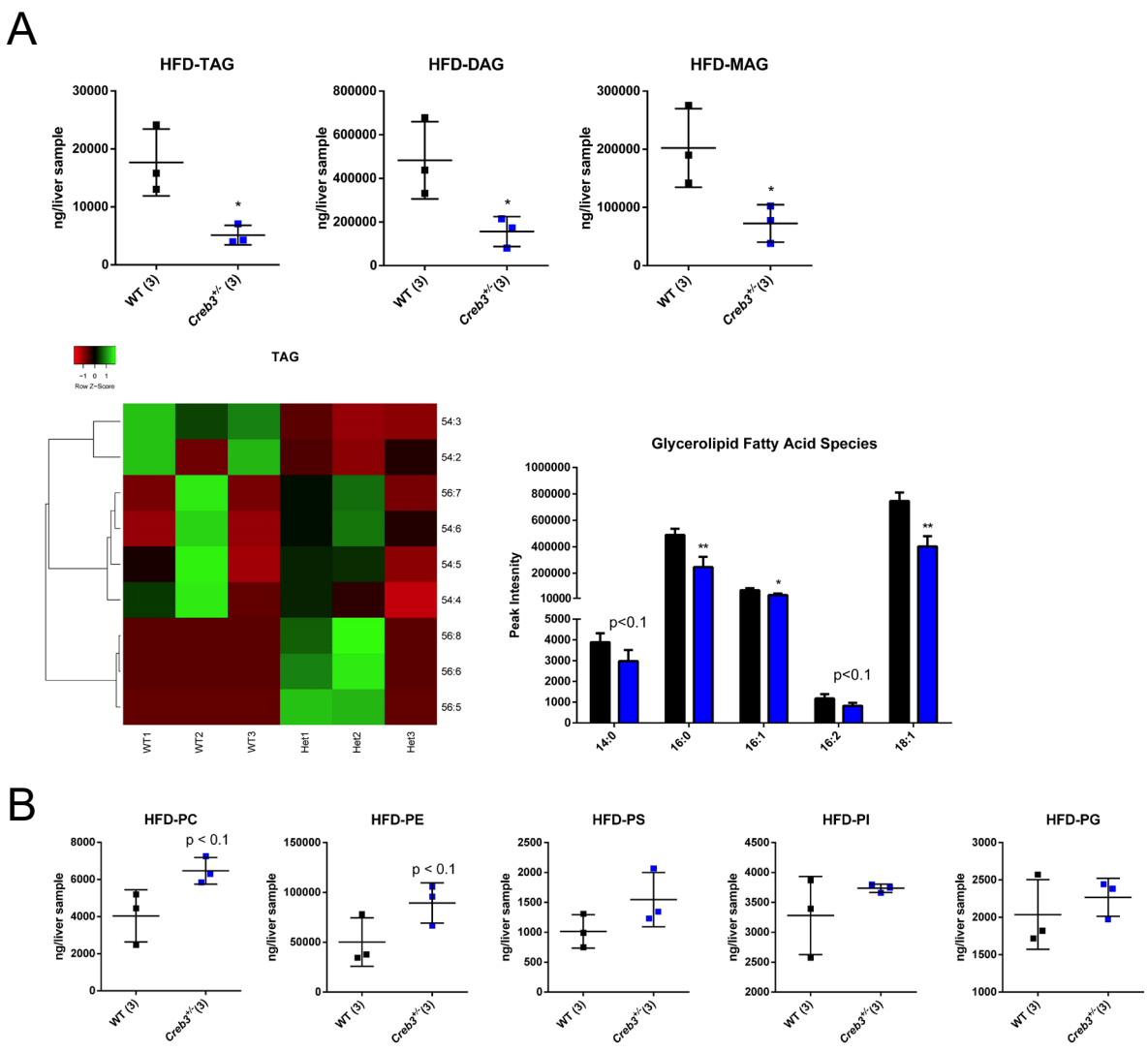

Figure 14: *Creb3*-deficient mice have altered hepatic lipid profiles on HFD. (A) HFD male WT and *Creb3*$^{+/-}$ hepatic glycerolipids class (TAG, DAG, MAG), TAG species, and fatty acid species MS/MS semi-quantification **(B)** HFD male WT and *Creb3*$^{+/-}$ hepatic glycerophospholipids MS/MS semi-quantification profile (n=3 WT males, n=3 *Creb3*$^{+/-}$ males on HFD). Data is represented as the mean ± SD. Student's *t* test, *P < 0.05.

2.4 Discussion

In this first metabolic study of *Creb3*-deficient mice, we report that *Creb3*$^{+/-}$ mice develop a desirable metabolic phenotype that offers protection from HFD induced obesity, basal hyperglycemia, glucose intolerance, and sex-specific tissue lipid accumulation. This phenotype was attributed to a distinct of increased energy expenditure of *Creb3*$^{+/-}$ mice with no differences in energy intake compared to WT. Notably, despite these drastic observations *Creb3*$^{+/-}$ mice had no difference in plasma lipids relative to WT. The high resistance of *Creb3*$^{+/-}$ mice to HFD-induced obesity was evidenced by a significant reduction in body fat mass in both males and females (Figure 9A, B, C). In agreement with the observed lean phenotype, we found that both male and female *Creb3*$^{+/-}$ mice possess an increased number of smaller adipocytes on both CD and HFD. Indicating a sex-specific effect of CREB3, *Creb3*$^{+/-}$ mice resisted the HFD weight gain in a tissue-specific manner, with *Creb3*$^{+/-}$ males being protected from TG accumulation in the liver and *Creb3*$^{+/-}$ females from TG accumulation in the skeletal muscle. In accordance with the observed reduction in hepatic steatosis, HFD *Creb3*$^{+/-}$ males accumulated reduced amounts of glycerolipids (TG, DAG, and MAG) and had increased levels of membrane phospholipids (PC, PE, and PS) relative to WT male liver. Since increased hepatic glycerolipids and decreased phospholipids are seen in obese mice, *Creb3*$^{+/-}$ livers that display the opposite of this trend agrees with the fatty liver resistant phenotype (Sanyal & Pacana, 2015).

Despite the HFD challenge, both *Creb3*$^{+/-}$ sexes had normal blood glucose and possessed significantly higher RER than WT, indicating a preference for carbohydrate utilization as an energy substrate. *Creb3*$^{+/-}$ males resisted HFD induced glucose

intolerance and *Creb3*$^{+/-}$ females on the other hand overcame glucose increases possibly due to a significant reduction in extramyocellular lipids compared to WT females, accompanied with dramatically reduced levels of leptin. Human leptin levels are in a direct relationship with body weight and body fat, and low leptin levels indicate chronic starvation (K. K. Miller et al., 1998). Muscle TG metabolism is typically stimulated by leptin indicating that the *Creb3*$^{+/-}$ females regulation of muscle TG metabolism is unrelated to leptin (Baldwin et al., 2011). *Creb3*$^{+/-}$ males showed increased expression of thermogenic protein, UCP1, in eWAT which corrolates well to the increased heat production of *Creb3*$^{+/-}$ mice. Female *Creb3*$^{+/-}$ mice on the other hand did not show an upregulation of gWAT UCP1 expression suggesting *Creb3*$^{+/-}$ females generate their increased energy expenditure through another tissue, such as muscle, and should be further investigated.

The UPR has been implicated in various metabolic processes such as lipid and glucose metabolism in the liver, as well as adipocyte differentiation. *Creb3*$^{+/-}$ mice showed reductions in hepatic UPR mRNA such as *Grp78* and *Chop* signifying less diet-induced hepatic steatosis associated ER stress and apoptosis when compared to WT. UPR protein ATF6α is critical for proper induction of adipogenic gene expression, with ATF6α knockdown in mouse embryonic fibroblast (MEF) cells resulting in significantly inhibited adipogenesis compared to WT (Lowe et al., 2012). Another UPR protein, XBP1, is also required for upregulation of mid-late adipogenesis genes (Sha et al., 2009; Yoshida et al., 2001). Indeed, *Xbp1*$^{-/-}$ MEFs also have significantly diminished adipogenic potential compared to WT (Sha et al., 2009). Interestingly, CREB3 is not only structurally like ATF6α and the lipogenic transcription factor SREBP-1c (Brown & Goldstein, 1997; Raggo et al., 2002; Yoshida et al., 2000), it is also believed to provide

crosstalk between ATF6α and XBP1 UPR pathways (Denboer et al., 2005; Liang et al., 2006; Yamamoto1 et al., 2004). CREB3 family of proteins are all involved in the UPR, some of which are involved in metabolic regulation (T.-H. Kim et al., 2014; Sa et al., 2014; C. Zhang et al., 2012). Recently, it has been discovered that CREB3L4 is a negative regulator of adipogenesis (T.-H. Kim et al., 2014). *Creb3l4*-knockout mice had increased adipogenesis that led to smaller and increased number of adipocytes (T.-H. Kim et al., 2014). This increase in number of adipocytes led to improved basal glucose levels, glucose tolerance, and protection from insulin resistance (T.-H. Kim et al., 2014). Here, we found that *Creb3*$^{+/-}$ mice possess a similar phenotype of an increased number of smaller adipocytes, and improved glucose tolerance and plasma levels on HFD compared to WT. Further investigation is needed to elucidate the role of CREB3, and the interplay between UPR and CREB3 family proteins in regulating adipogenic capabilities and gene expression.

CREB3L3/CREBH, which is the most similar protein to CREB3, has been shown to regulate metabolic processes in the liver such as fatty acid oxidation, lipolysis, lipogenesis, and lipid transport during cellular stress (Nakagawa et al., 2016; Sa et al., 2014; Satoh et al., 2020; C. Zhang et al., 2012). *Creb3l3* transgenic (*Creb3l3*-Tg) and *Creb3*$^{+/-}$ mice fed a HFD had strikingly similar phenotypes (Satoh et al., 2020). Both had reduced weight gain and body fat, with no difference in food intake compared to WT mice fed HFD (Satoh et al., 2020). Additionally, *Creb3*$^{+/-}$ mice had reduced hepatic lipid accumulation which was also observed in *Creb3l3-Tg* mice (Nakagawa et al., 2016). *Creb3*$^{+/-}$ mice showed an inverse hepatic gene expression profile to *Creb3l3*-KO with significant upregulation of key metabolic regulator *Pgc-1a*, TG synthesis enzymes *Fasn*

and *Scd1*, and fatty acid oxidation inducers *Pparα* and *Acox1* (Satoh et al., 2020). CREB3 and CREB3L3 proteins have been shown to interact with and co-regulate nuclear proteins (H. Kim et al., 2014; R. Lu et al., 1997; Nakagawa et al., 2016; Penney et al., 2018). It may be conceivable that CREB3 interacts with CREB3L3 and modulates its activity on various gene targets. Here we show that CREB3 indirectly influenced *Pgc-1a* hepatic gene expression. Previously, PGC-1a was reported to interact with and co-regulated by cell cycle protein Host Cell Factor 1 (Ruan et al., 2012). CREB3 was initially discovered through its interaction with Host Cell Factor 1 (HCF-1) (R. Lu et al., 1997). Therefore, it may be plausible that CREB3 indirectly affects *Pgc-1a* expression through HCF-1, or even directly regulate PGC-1a via a co-regulation interaction through nuclear receptor binding sites as CREB3 was found to do with GR (Penney et al., 2017), another known binding partner of PGC-1a, which notably also interacts with CREB3L3 (Nakagawa & Shimano, 2018). CREB3L3 also forms a transcriptional activation complex with another PGC-1a co-regulator, PPARα, to stimulate energy expenditure genes through CRE-PPAR-response element-binding motifs such as *Pgc1a* (H. Kim et al., 2014; Sa et al., 2014). Taken together, there is a complex network of protein interactions between PGC-1a, HCF-1, CREB3L3, PPARα, and GR that influence energy homeostasis in which CREB3 is likely also involved and warrants further investigation.

Creb3$^{-/-}$ mice were sub-viable; only one female null mouse survived which showed exaggerated phenotype as *Creb3*$^{+/-}$ females, and thus, this study focused on *Creb3*$^{+/-}$ mice. Therefore, various tissue-specific conditional knockout models would be a valuable tool in further delineating the precise role of CREB3 in regulating whole-body energy

metabolism. Additionally, since our data revealed a preference for carbohydrates as an energy substrate and an improvement in glucose homeostasis of *Creb3*$^{+/-}$ mice, studying *Creb3*$^{+/-}$ mice fed a high-carbohydrate diet instead of HFD may further elucidate CREB3's role in glucose metabolism.

In conclusion, it was found that *Creb3*-deficiency in mice led to a in increased energy expenditure without any differences in HFD energy intake which resulted in significant protection from HFD induced weight gain with sex-specific tissue lipid accumulation, and basal hyperglycemia. Despite these drastic metabolic differences, *Creb3*$^{+/-}$ mice possessed unchanged plasma lipid concentrations from WT mice on HFD. From this study, we show that CREB3 is a novel regulator of diet-induced obesity and energy homeostasis in a sex-specific manner warranting further investigation as a potential therapeutic target in obesity-related disorders.

Chapter 3: CREB3-deficiency in MEF cells leads to increased respiration and ROS production and altered Ca^{2+} homeostasis

Disclaimer:

Live ER-Ca^{2+} Imaging: Experiment and data analysis conducted by Tristen Hewitt of the Lalonde Lab at the University of Guelph.

Abstract

In mammalian cells, mitochondrial respiration produces reactive oxygen species (ROS) such as superoxide (O^{-}_{2}). Superoxide is then converted by the SOD1 enzyme into hydrogen peroxide (H_2O_2), the predominant form of cytosolic ROS. ROS at high levels can be toxic, but below this threshold are important for physiological processes acting as a second messenger similar to Ca^{2+}. Mitochondrial Ca^{2+} influx from the ER is known to increase ROS and ATP production, while ROS and ATP are capable of regulating Ca^{2+} homeostasis, alluding to an intricate mutual interplay between Ca^{2+}, ROS, and ATP synthesis. To protect cells from toxic levels of ROS, oxidative stress response enzymes such as SOD1 and Catalase systematically break down ROS into non-toxic H_2O and O_2. The Unfolded Protein Response (UPR) proteins ATF6 and XBP1 which typically activate in response to endoplasmic reticulum stress also contribute to protection from oxidative stress through upregulation of *Sod1* and *Catalase* genes. Here, UPR-associated protein CREB3 is shown to play a role in balancing Ca^{2+}, ROS, and ATP homeostasis. *Creb3*-deficient mouse embryonic fibroblast cells ($MEF^{-/-}$) had elevated basal cytosolic ROS and were more susceptible to oxidative stress-induced cell death compared to WT MEFs ($MEF^{+/+}$). $MEF^{-/-}$ cells also depicted an increased ER-Ca^{2+} release and subsequent elevated basal mitochondrial Ca^{2+} levels compared to WT. $MEF^{-/-}$ cells consumed significantly more oxygen and produced higher amounts of ATP relative to $MEF^{+/+}$. Gene expression analysis revealed drastic downregulation of *Catalase* and *Sod1* expression despite the high levels of basal ROS in *Creb3*-deficient MEF cells compared to WT. These results suggest CREB3 is essential for maintaining proper Ca^{2+}, ROS, and ATP balance

likely through preventing elevated ROS levels by induction of *Catalase* and *Sod1* antioxidant genes.

3.1 Introduction

Cellular stress occurs when there is a deviation from homeostasis within eukaryotic cells. This can be caused by changes in temperature, nutrient levels, ion concentrations, elevated reactive oxygen species (ROS), and most notably the accumulation of unfolded proteins in the endoplasmic reticulum (ER). The ER is a central hub for sensing homeostatic changes in the cell and a major intracellular Ca^{2+} store (Landolfi et al., 1998). ER-Ca^{2+} is released through receptors into the cytosol to act as an important second messenger that regulates cellular functions such as cell survival/death, neuronal action potentials, secretion, gene expression, and metabolism (Bartok et al., 2019; de Marchi et al., 2014; Landolfi et al., 1998; Lomax et al., 2002). Ca^{2+} released from the ER also enters the mitochondria and increases ATP production via oxidative phosphorylation stimulation, although too much will induce cytochrome C release and apoptosis (de Marchi et al., 2014; Granatiero et al., 2019; Indiveri et al., 2020; Jambrina et al., 2003; Peng & Jou, 2010). A byproduct of oxidative phosphorylation is ROS which at non-toxic levels has also been identified as a critical second messenger. ROS has been reported to stimulate ER-Ca^{2+} efflux (Bánsághi et al., 2014; Cooper et al., 2013; Lin et al., 2021), while ATP can activate SERCA and consequentially increase ER-Ca^{2+} influx (Brookes et al., 2004; Hofer et al., 1996). Taken together, there is a complex finely tuned mutual interplay between organelle Ca^{2+} levels, ROS, and ATP production, and often when one becomes dysregulated, the other two are affected as well.

The ER contains transmembrane proteins that in response to various stresses stimulate downstream pathways and gene transcription to alleviate the specific type of stress present. These ER stress-related proteins make up the Unfolded Protein Response (UPR). Activating Transcription Factor 6 alpha (ATF6α) is a UPR protein that has been implicated in regulating a variety of cellular processes like ER protein folding/degradation, cell survival, apoptosis, glucose and lipid metabolism, secretion, ROS protection, and Ca^{2+} homeostasis (Burkewitz et al., 2020; Chen et al., 2016; Jin et al., 2017; Usui et al., 2012; Yoshida et al., 1998, 2000). In *C. elegans*, activated ATF6α alters ER-Ca^{2+} stores through transcriptional activation of ER-Ca^{2+} chelator calreticulin, and thus reduces ER-Ca^{2+} release (Burkewitz et al., 2020). Knockout of ATF6α in *C. elegans* extends lifespan by promoting ER-Ca^{2+} release and stimulating basal mitochondrial function which is known to decline throughout the aging process (Burkewitz et al., 2020).

ATF6α as well as another UPR protein XBP1 have been reported to link ER stress with oxidative stress by providing protection from ROS (H_2O_2) (Jin et al., 2017; Y. Liu et al., 2009). Overexpression of native ATF6α offered rat cardiac myocytes significantly increased protection from H_2O_2-induced cell death (Jin et al., 2017). This protective quality was attributed to direct regulation of key H_2O_2 clearance gene, *Catalase* through the ER stress response element (ERSE) (Jin et al., 2017; Yoshida et al., 1998, 2000). XBP1 however was described to indirectly upregulate antioxidant genes *catalase*, *Sod1*, and *Trx1*, and results in an increased susceptibility to H_2O_2-induced oxidative stress when knocked out in mouse embryonic fibroblast (MEF) cells (Y. Liu et al., 2009).

Originally discovered through its interaction with Host Cell Factor 1 (HCF-1), Cyclic AMP Response Element Binding Protein-3 (CREB3), also known as LUMAN in humans,

or LZIP in mice, is another UPR associated ER-membrane bound transcription factor (Denboer et al., 2005; R. Lu et al., 1997; Raggo et al., 2002). Detailed molecular and physiological functions of CREB3 remain to be defined. Recently we have found that CREB3-deficient mice increased energy expenditure/heat production without any difference in energy intake and had a preference for carbohydrates as an energy substrate while fed a high-fat diet compared to WT mice (Chapter 2). These metabolic changes provided CREB3-deficient mice significant protection from HFD induced weight gain, basal hyperglycemia, and sex-specific tissue lipid accumulation. Here I aim to probe the molecular mechanism that is potentially involved in Ca^{2+} and ROS homeostasis and consequent metabolic changes in MEF cells.

CREB3 is thought to provide crosstalk between ATF6α and XBP1 (Denboer et al., 2005; Liang et al., 2006; Yamamoto1 et al., 2004). Like ATF6α, upon ER stress CREB3 is shuttled to the Golgi apparatus where it is cleaved to release the active N-terminus which translocates to the nucleus and regulates the transcription of target genes (Raggo et al., 2002; Yoshida et al., 2000). CREB3 has also been implicated in the regulation of Ca^{2+} homeostasis in neurons through its transcriptional regulation of Homocysteine Inducible ER Protein with Ubiquitin Like Domain 1 (*Herpud1*) gene (Liang et al., 2006; Mirabelli et al., 2016). The protein, HERP, inhibits ER-Ca^{2+} release by binding and promoting the degradation of ER-Ca^{2+} release channel Inositol Trisphosphate Receptor (IP3R) (Mirabelli et al., 2016; Torrealba et al., 2017). Recently, the X-ray structure of chicken CREB3 was established and revealed a redox-dependent cysteine residue that appeared to promote dimerization with CREB3 and other CREB3-family members under oxidizing conditions (Sabaratnam et al., 2019). Therefore, in this study, we sought to

elucidate CREB3's impact on ATP production through Ca^{2+} and ROS homeostatic regulation in MEF cells.

3.2 Methods

Cell Culture

All CREB3 $MEF^{+/+}$, $MEF^{+/-}$, and $MEF^{-/-}$ cells were previously collected in the lab from embryos of each genotype. Cells were grown in Dulbecco's Modified Eagle's Medium high glucose media (Wisent #319-005-CL) supplemented with 10% fetal bovine serum (Wisent #098-150) and 1% penicillin/streptomycin antibiotics (Thermo Fisher Scientific #15140122). Cells were maintained at 37°C and 5% CO_2 humidified atmosphere and passaged every 2-3 days.

Calcium Imaging

$MEF^{+/+}$ and $MEF^{-/-}$ cells (n=300, 3 separate experiments with 100 individual cells measured each time) were seeded onto 35mm glass-bottom dishes (MatTek, Ashland, MA, United States) 24h prior to imaging. Cells were loaded with 2μM of a Ca^{2+} sensitive cytosolic probe (Fluo-4; Thermo Fisher Scientific #F14201) diluted in a HEPES imaging solution containing Ca^{2+} (10mM HEPES pH 7.3, 140mM NaCl, 5mM KCl, 2mM CaCl2, 1mM MgCl2, and 10mM glucose) for 45 minutes. Cells were then washed and incubated in Ca^{2+}-containing HEPES imaging solution for 20 minutes at 37°C for de-esterification. Cells were then washed in Ca^{2+} free HEPES imaging solution (10mM HEPES pH7.3, 140mM NaCl, 5mM KCl, 3mM MgCl2, and 10mM glucose) and incubated for 10 minutes. Images were collected on a Nikon Eclipse Ti2 with ex/em 494/506 nm. Baseline fluorescence measurements were taken at 1 frame/5 second for 3 minutes. Next, thapsigargin was added directly to the media at a final concentration of 2μM. 10 minutes later, Ca^{2+} free HEPES imaging solution was replaced with Ca^{2+} containing HEPES

imaging solution. Image processing and analysis were done using NIS Elements (Nikon, Minato City, TYO) and Microsoft Excel.

Mitochondrial Function Analysis

A Seahorse XFe24 Analyzer was used to measure cellular oxygen consumption rate (OCR) to calculate basal respiration, ATP-linked respiration, H^+ (proton) leak, maximal respiration, spare respiratory capacity, and non-mitochondrial respiration while using the Agilent Mito Stress Test Kit. 35,000 $MEF^{+/+}$ (n=15) or $MEF^{-/-}$ (n=14) cells per well were seeded onto a Seahorse 24-well plate the day prior to the experiment. During the experiment, OCR was measured while cellular respiration modulators at final concentrations of 1.5μM oligomycin, 2μM FCCP, and 0.5μM rotenone/antimycin A were added at timed intervals. Upon completion, OCR readings were made relative to cell density by crystal violet staining.

Intracellular ROS Measurements

$MEF^{+/+}$ and $MEF^{-/-}$ cells (n=3) were seeded onto 6-well plates with coverslips for fluorescent microscopy, or a black-walled clear bottom 96-well plate for microplate assay the day before the experiment. Cells were loaded with 2μM Hoescht 33342 (Abcam #ab228551), and 20μM 2',7' –dichlorofluorescein diacetate (DCFDA) (Abcam #ab113851) at 37°C for 45 minutes. After, cells were washed and then fluorescence measured by MultiSkan GO (Thermo Fisher Scientific, Waltham, MA, United States) microplate reader or imaged by fluorescence spectroscopy on a Leica DMRA2 microscope with a Hamamatsu ORCA-ER digital camera and Openlab imaging software (PerkinElmer) with ex/em at 485nm/535 nm.

Cytotoxicity Assay

$MEF^{+/+}$ and $MEF^{-/-}$ cells (n=3) were seeded onto 12-well plates and treated the next day with 0μM, 500μM, 750μM, 1000μM, or 2000μM H_2O_2 for 24 hours. After treatment, media supernatants containing dead or detached cells were collected and combined with the adhered cells collected using trypsin. Cells were spun at 4000 rpm to pellet and resuspended in growth media. A 10μL representative sample was combined with 10μL of 0.04% Trypan Blue (Bio-Rad #1450003) and cell viability measured with a TC20 Automated Cell Counter (Bio-Rad, Hercules, CA, United States).

Western Blotting

Cells were washed in three times in PBS and collected in RIPA buffer (150mM NaCl, 50mM Tris, 1% (v/v) triton x-100, 0.5% (v/v) sodium deoxycholate, 0.1% (v/v) SDS) and homogenized with QIAshredders (Qiagen #79656) as per manufacturers instructions. Protein lysates were normalized to 1μg/μL using the Bradford Protein Assay (Bio-Rad # 5000002). Protein samples were prepared with 2x Laemmli Sample Buffer (20% glycerol, 0.125M Tris, 4% SDS, 10% 2-mercaptoethanol, and 0.004% bromphenol blue) in a 1:1 ratio (0.5μg/μL) and boiled at 95°C for 10 minutes. 15-20μg of protein was loaded into each well of a 10-well 10% SDS-Page, while 5-10μg was loaded in 15-well 10% SDS-Page. Gels were run at 150V for 1.5 hours, then wet transferred to PVDF membrane at 50V for 2 hours. Blots were blocked in 5% (m/v) skim milk in PBS-0.1% Tween (PBS-T) for 1 hour at room temperature. Then probed with anti-HERPUD1 (1:500 in 5% skim milk, OriGene #TA507019), anti-CREB3 (1:1000 in 5% skim milk, ProteinTech #11275-1-AP), anti-IPT3R (1:400 in 5% skim milk, ProteinTech #19962-1-AP), or anti-Actin (1:1000 in 5% skim milk, GenScript #A00730) overnight at 4°C. The following day, blots were

washed with PBS-T and probed with secondary horseradish peroxidase (HRP)-conjugated antibodies used at (1:7500 in 5% skim milk, Promega) for 2 hours at room temperature then washed again with PBS-T prior to imaging on a ChemiDoc XRS+ System (Bio-Rad) using ECL imaging substrate (GE Healthcare, Piscataway, NJ).

Quantitative Reverse Transcription Polymerase Chain Reaction

RNA was extracted from $MEF^{+/+}$, $MEF^{+/-}$, and $MEF^{-/-}$ cells (n=3) using Omega E.Z.N.A. Total RNA Kit II. The samples were DNase treated (Thermo-Fisher #EN0525) then reverse transcribed to cDNA (qScript #G490) and transcript levels measured by qRT-PCR using PerfeCTa SYBR green Supermix with 6-carboxy-X-rhodamine (ROX) (Quanta Biosciences, Inc., Gaithersburg, MD, United States) on a QuantStudio 3 Real-Time PCR System (Applied Biosystems, Carlsbad, CA, United States). Genes tested include the genes for oxidative stress: catalase [*Cat*], superoxide dismutase 1 [*Sod1*], and superoxide dismutase 2 [*Sod2*]; and UPR/ER stress: CCAAT-enhancer-binding protein homologous protein [*Chop*], activated X-Box binding protein 1 [*Xbp1-s*] as well as the inactive form [*Xbp1*], and glucose regulatory protein 78 [*Grp78*]. Both glyceraldehyde-3-phosphate dehydrogenase [*Gapdh*] and beta-actin [*Actin*] were used as endogenous reference genes and CT values averaged for each sample's final reference gene CT and used to determine ΔCT. The list of primers used can be found in Supplementary Figure 1S.

Statistical Analysis

Statistical analyses were performed using a one-way ANOVA followed by multiple comparisons, or a two-tailed student *t*-test (GraphPad Prism 9). Results were deemed significant when $p < 0.05$.

3.3 Results

3.3.1 Creb3-knockout in MEF cells results in increased susceptibility to H_2O_2 and higher basal ROS levels.

To first investigate the potential role of CREB3 in the protection of cells from oxidative stress, we investigated the ROS cytotoxicity in MEF cells with different *Creb3*-genotypes. MEF cells were treated with 0μM, 500μM, 750μM, 1000μM, or 2000μM H_2O_2 for 24 hours then cell viability was measured to evaluate oxidative stress susceptibility differences between *Creb3*-genotypes. We found that, in the absence of CREB3, there was a ~25% drop of survivability at 750μM and 1mM H_2O_2 compared to WT MEF cells (Figure 15A). Next, to assess basal antioxidant homeostasis between *Creb3*-genotypes, basal ROS (H_2O_2) levels were measured. Cells were loaded with a fluorescent cytosolic ROS probe (DCFDA) and nuclear probe (Hoescht 33342) then imaged on a fluorescent microscope (Figure 15B) or quantitatively measured by a microplate reader (Figure 15C). We found that $MEF^{-/-}$ cells contained ~6.5-fold higher basal intracellular ROS fluorescence relative to $MEF^{+/+}$ (Figure 15B, C) suggesting CREB3 plays a significant role in maintaining basal oxidative homeostasis.

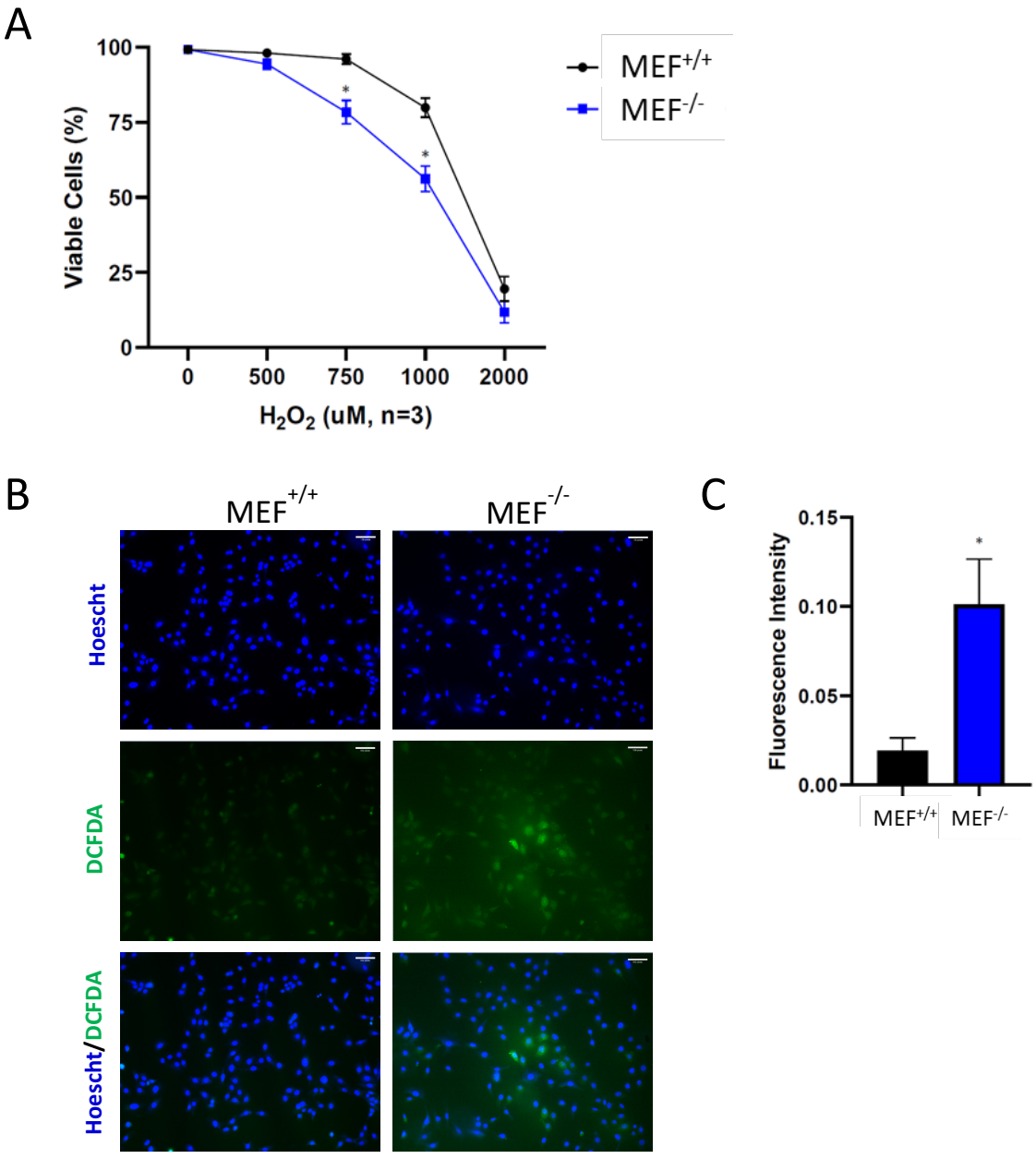

Figure 15: MEF$^{-/-}$ cells are susceptible to H_2O_2 and have elevated ROS levels. MEF$^{+/+}$ and MEF$^{-/-}$ cells **(A)** H_2O_2 cytotoxicity curve. n=3. **(B)** Fluorescent images of cytosolic ROS staining with DCFDA (green) and Hoescht 33342 (blue). n=3. **(C)** Microplate cytosolic ROS DCFDA assay. n=3. Data is represented as the mean ± SD. Student's t-test, *P< 0.05.

3.3.2 Creb3-knockout MEFs have increased cellular respiration and mitochondrial ATP production.

To assess the potential role of CREB3 in affecting mitochondrial function as a potential cause of increased ROS levels, we measured the oxygen consumption rate of $MEF^{+/+}$ and $MEF^{-/-}$ cells by a Seahorse mitochondrial stress test assay. It was found that $MEF^{-/-}$ cells had 161% and 165% higher basal and maximal respiration (measured after addition of FCCP) respectively, relative to $MEF^{+/+}$ (Figure 16A, B). The percent increase from basal to maximal respiration indicates spare respiratory capacity percentage which was significantly higher in $MEF^{-/-}$ (273% ± 11.4%) than $MEF^{+/+}$ (239% ± 5.2%). The coupling efficiency (percentage of basal respiration being used for ATP production determined after oligomycin addition) was 7.62% ± 3.46% higher in $MEF^{-/-}$ (90.29% ± 3.53%) compared to $MEF^{+/+}$ cells (82.67% ± 0.59%). The remaining mitochondrial basal respiration is due to proton leak which $MEF^{-/-}$ cells had 170% more (53.94 ± 1.84 pmol/min) than $MEF^{+/+}$ (31.80 ± 2.49 pmol/min). After rotenone/antimycin A is added to inhibit all mitochondrial respiration, the non-mitochondrial respiration by enzymes can then be determined. Although not statistically significant ($p=0.059$), $MEF^{-/-}$ cells (32.87 ± 4.94 pmol/min) had slightly higher non-mitochondrial respiration than $MEF^{+/+}$ (21.83 ± 2.83 pmol/min).

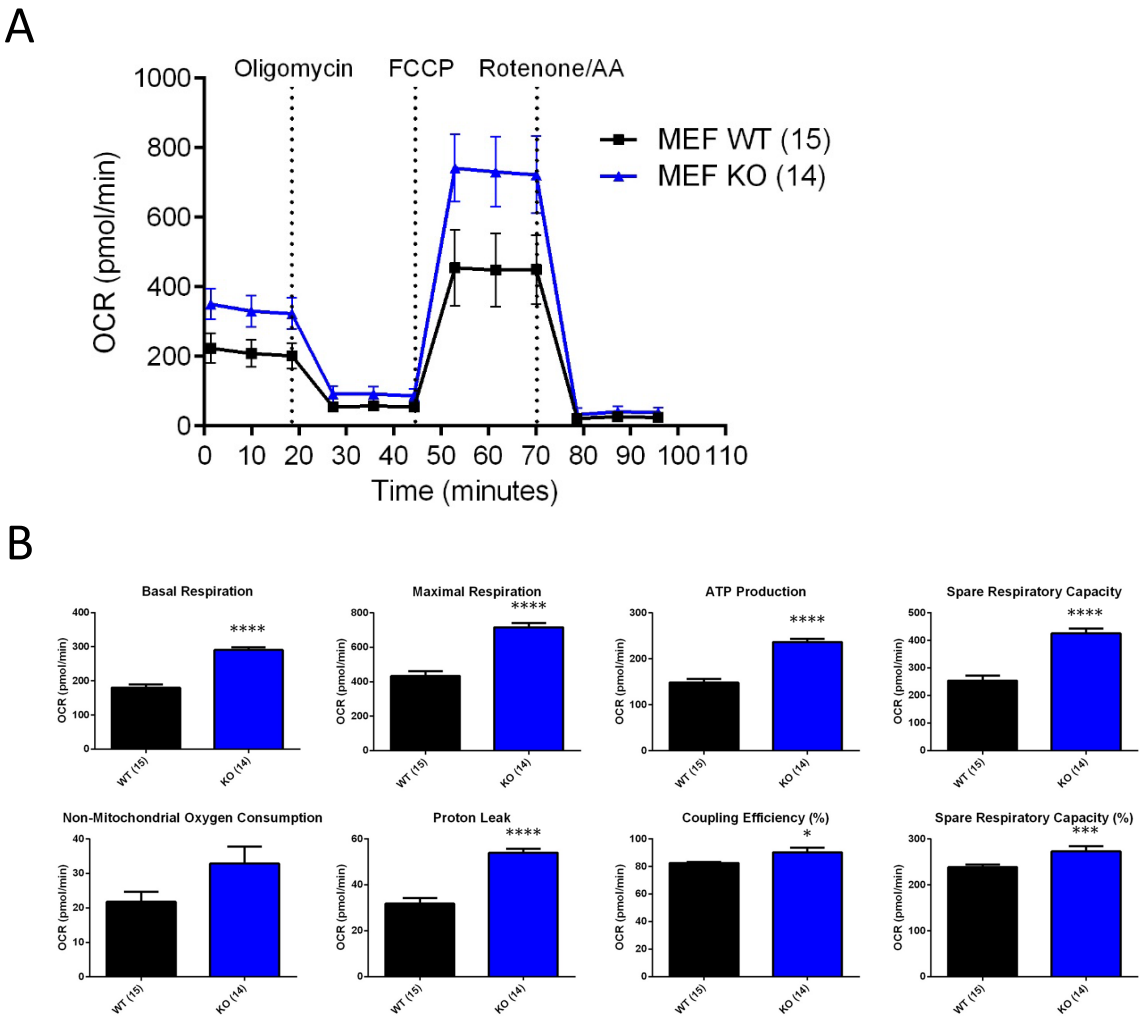

Figure 16: MEF$^{-/-}$ cells have increased cellular respiration and ATP production. MEF$^{+/+}$ and MEF$^{-/-}$ cells **(A)** Total oxygen consumption rate (OCR) over 95 minutes under basal, oligomycin, FCCP, or Rotenone/AA treatments. n=14-15. **(B)** Mitochondrial parameters calculated from total OCR graph. n=14-15. Data is represented as the mean ± SD. Student's *t* test, *P< 0.05, **P< 0.01, ***P< 0.001, ****P< 0.0001.

3.3.3 Creb3-knockout MEFs have increased ER Ca^{2+} efflux and mitochondrial $[Ca^{2+}]$.

To determine if CREB3 is required for proper ER and mitochondria Ca^{2+} homeostasis, we first measured Ca^{2+} efflux from the ER by live-cell thapsigargin induced ER-Ca^{2+} release imaging assay. Following 2μM thapsigargin treatment in $MEF^{+/+}$ cells, cytosolic Ca^{2+} levels increased 2.89-fold from basal fluorescence and obtained an area under the curve (AUC) of 171.4 ± 6.65, reflecting basal ER-Ca^{2} stores and release rates (Figure 17A). On the other hand, $MEF^{-/-}$ cells treated with 2μM thapsigargin increased 3.67-fold from basal and had an AUC of 203.5 ± 9.55. This was a 127% and 119% higher peak fold increase and AUC, respectively, in $MEF^{-/-}$ compared to $MEF^{+/+}$ cells (Figure 17A). It is known that Ca^{2+} released from the ER can enter the mitochondria, therefore basal $[Ca^{2+}]_m$ was assessed using mitochondria specific Ca^{2+} fluorescent probe Rhod-2 relative to total mitochondria probe MitoTracker. It was seen that $MEF^{+/+}$ cells had 0.75-fold ± 0.12 and $MEF^{-/-}$ cells 1.63-fold ± 0.028 $[Ca^{2+}]_m$ fluorescence relative to total mitochondria fluorescence (Figure 17B). These results suggest that CREB3 promotes ER-Ca^{2+} retention, therefore, reducing basal ER to mitochondrial Ca^{2+} influx and subsequently $[Ca^{2+}]_m$.

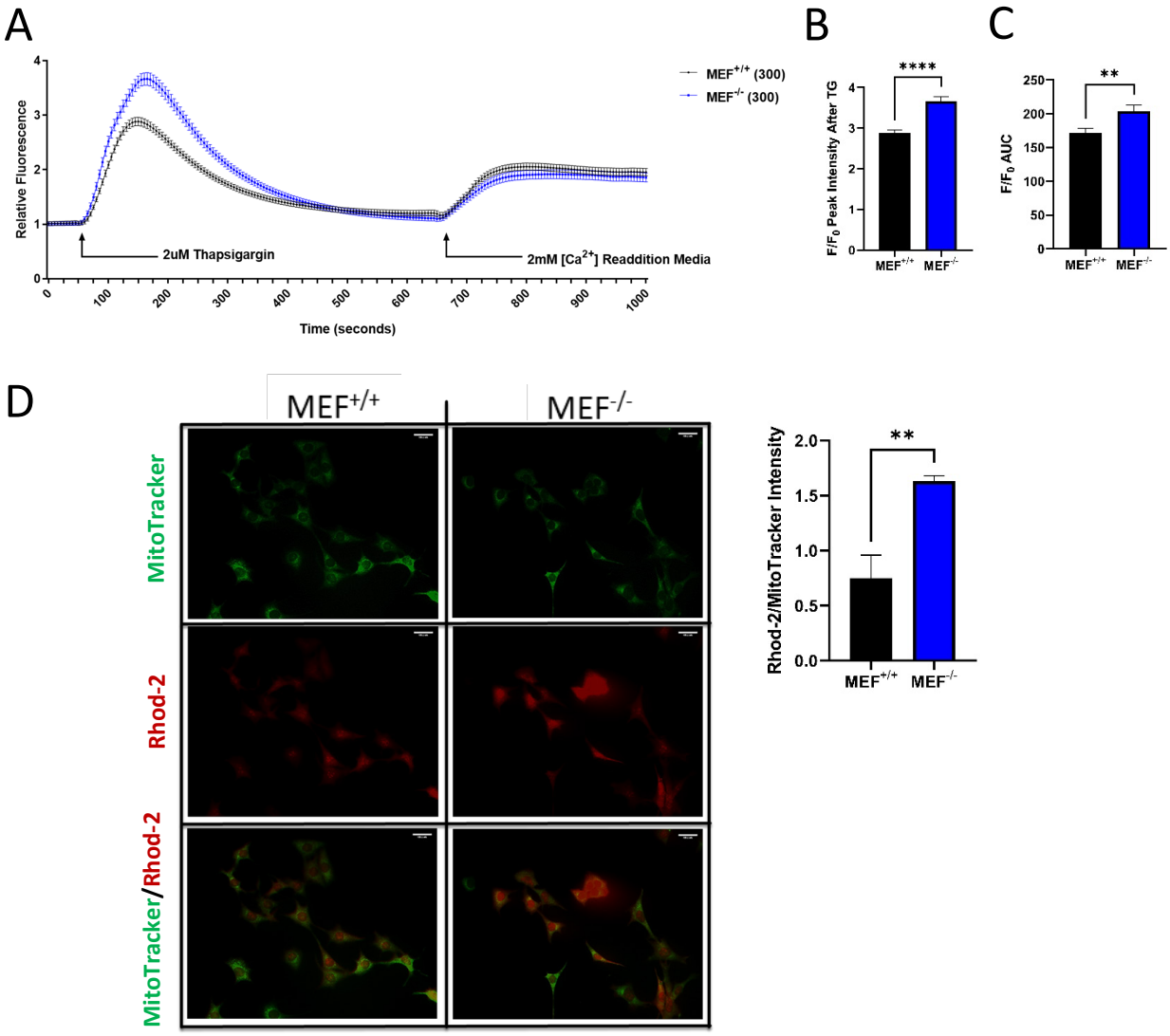

Figure 17: MEF$^{-/-}$ cells have increased ER-Ca^{2+} efflux and mitochondrial [Ca^{2+}]. MEF$^{+/+}$ and MEF$^{-/-}$ cells **(A)** Live ER-Ca^{2+} release imaging in response to thapsigargin treatment over 1000s. n=300. **(B-C)** F/F_0 peak intensity and AUC analysis post-thapsigargin treatment. n=300. **(D)** Fluorescent microscopy imaging of mitochondrial Ca^{2+} fluorescence (Rhod-2 in red) relative to total mitochondria (MitoTracker in green) and quantified Rhod-2/MitoTracker intensity ratios. n=3. Data is represented as the mean ± SD. Student's *t* test, *P< 0.05, **P< 0.01, ***P< 0.001, ****P< 0.0001.

3.3.4 CREB3 is not cleaved in response to H_2O_2, palmitate, or homocysteine.

CREB3 undergoes proteolytic cleavage during the UPR, we wanted to investigate if CREB3 is also triggered to be cleaved/activated by elevated ROS (H_2O_2), palmitate, homocysteine, or glucose. $MEF^{+/+}$ cells were treated with each compound and the lysate was probed for CREB3 via western blotting. 400nM Brefeldin A treatment for 6 hours was used as a positive control for activated CREB3 cleavage with the activated CREB3 band appearing at 40-45 kDa (Figure 18A). No CREB3 activation was detected in response to 6-, 12-, or 24-hour 500μM H_2O_2 (concentration that showed significant CREB3-dependant H_2O_2 cytotoxic susceptibility) treatments (Figure 18B). Additionally, the fatty acid ER stressor palmitate between concentrations 100μM and 400μM for 6- or 12-hours also did not produce activated CREB3 (Figure 18). Lastly, CREB3 was also not activated by homocysteine at 100μM for 12 hours or 30mM glucose for 6-12 hours (Figures 18B, C). These results suggest the activation of CREB3 may be more complex than singular ER stress treatments, and additional factors may be required for stimulating the cleavage of CREB3 under metabolic-related conditions.

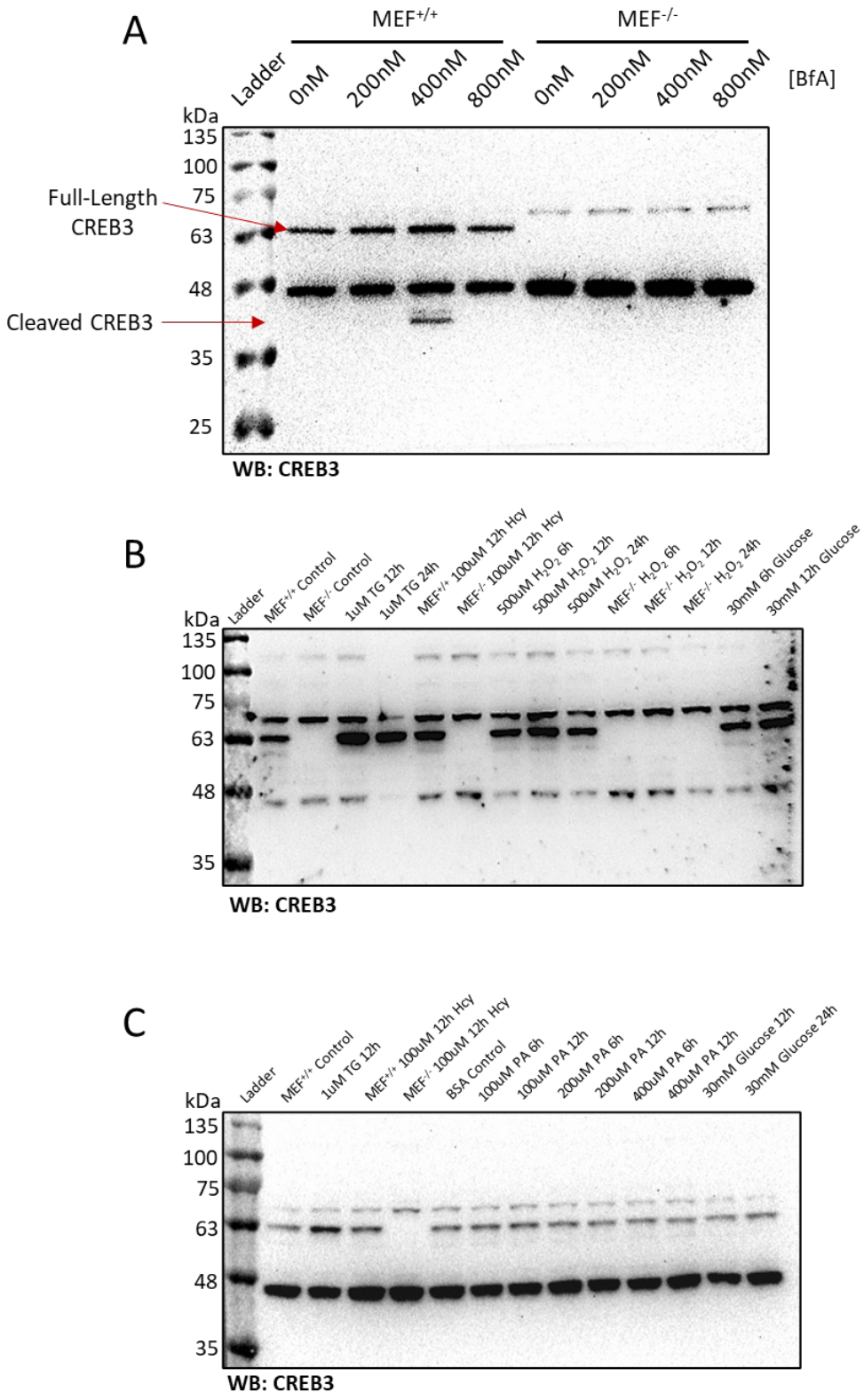

Figure 18: CREB3 activation blots in MEF cells under BfA, homocysteine (Hcy), palmitate (PA), H_2O_2, and glucose treatments.

3.3.5 No significant differences in HERP or IP3R expression levels in Creb3-KO MEFs under basal or stress-induced conditions.

We were interested to investigate if the ER-Ca^{2+} differences observed in CREB3 null MEFs can be attributed to CREB3 regulation of HERP and thus its degradation of IP3R ER-Ca^{2+} efflux channel. Protein levels of HERP and IP3R were compared in $MEF^{+/+}$, $MEF^{+/-}$, and $MEF^{-/-}$ cells under basal and stressed conditions. First, a traditional ER stressor known to stimulate HERP expression, thapsigargin (TG), was used. Concentrations of TG between 0.5μM and 2μM were successful at inducing HERP expression, although no consistent differences were observed between MEF *Creb3* genotypes (Figure 19). In fact, there was quite a drastic variability of HERP expression between experiments of the same untreated/treated samples. Next, another known ER stress inducer of HERP expression typically accumulated through diet and alters redox status of cells, homocysteine, was tested. Surprisingly homocysteine at varying concentrations was unable to increase HERP protein levels in WT or CREB3-deficient MEF cells (Figures 20A, B, C). H_2O_2 at 500μM for 6-, 12-, and 24-hours was also unsuccessful to increase HERP protein expression (Figure 20D). Lastly, BfA at the previously determined treatment concentration (400nM) that activated CREB3 cleavage was used to assess potential HERP expression differences under BfA induced cellular stress. Again, HERP levels varied between experiments within the same sample groups indicating more factors may be involved in the regulation of HERP (Figure 21).

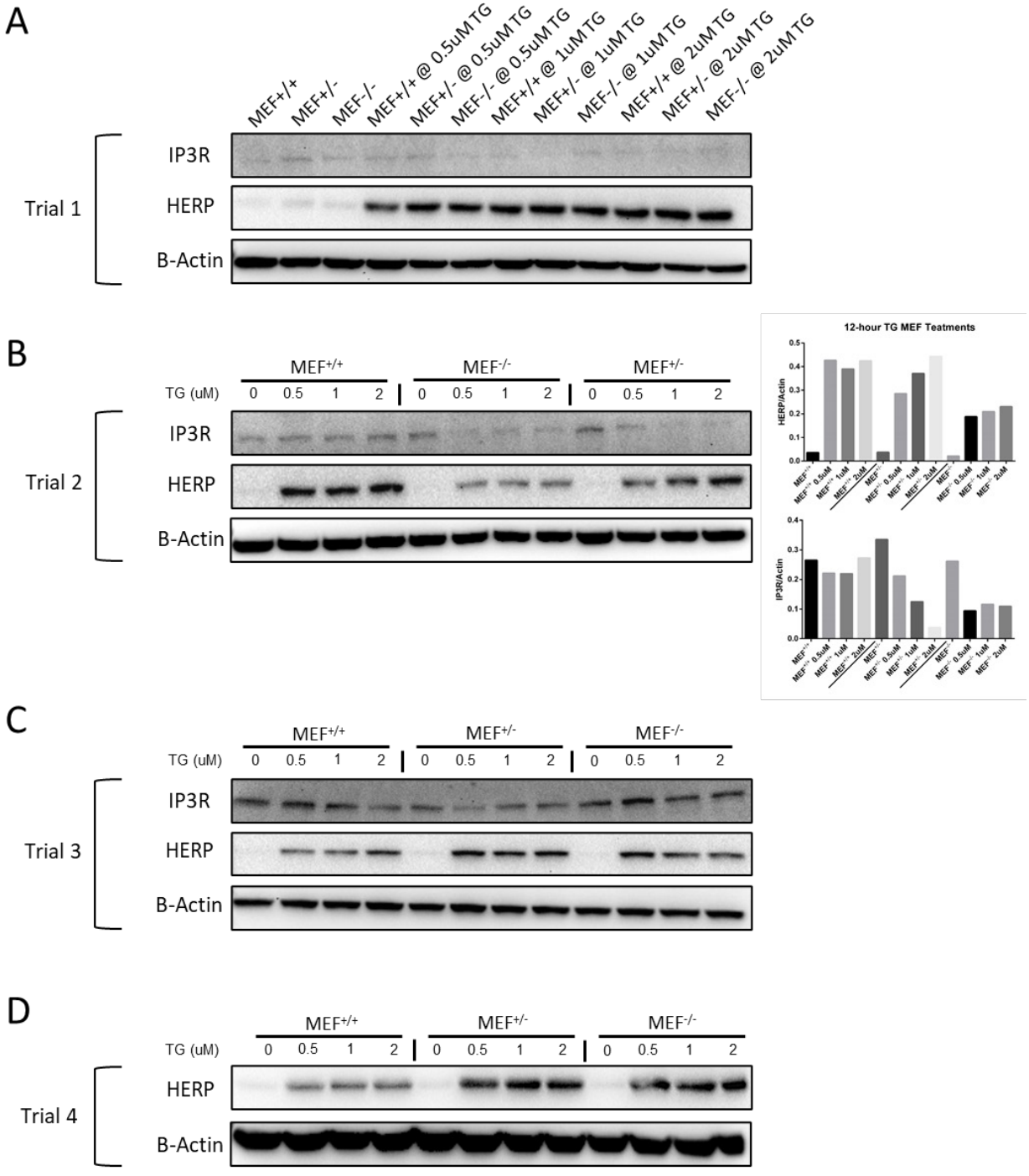

Figure 19: HERP and IP3R expression in basal and thapsigargin (TG) treated $MEF^{+/+}$, $MEF^{+/-}$, and $MEF^{-/-}$ cells.

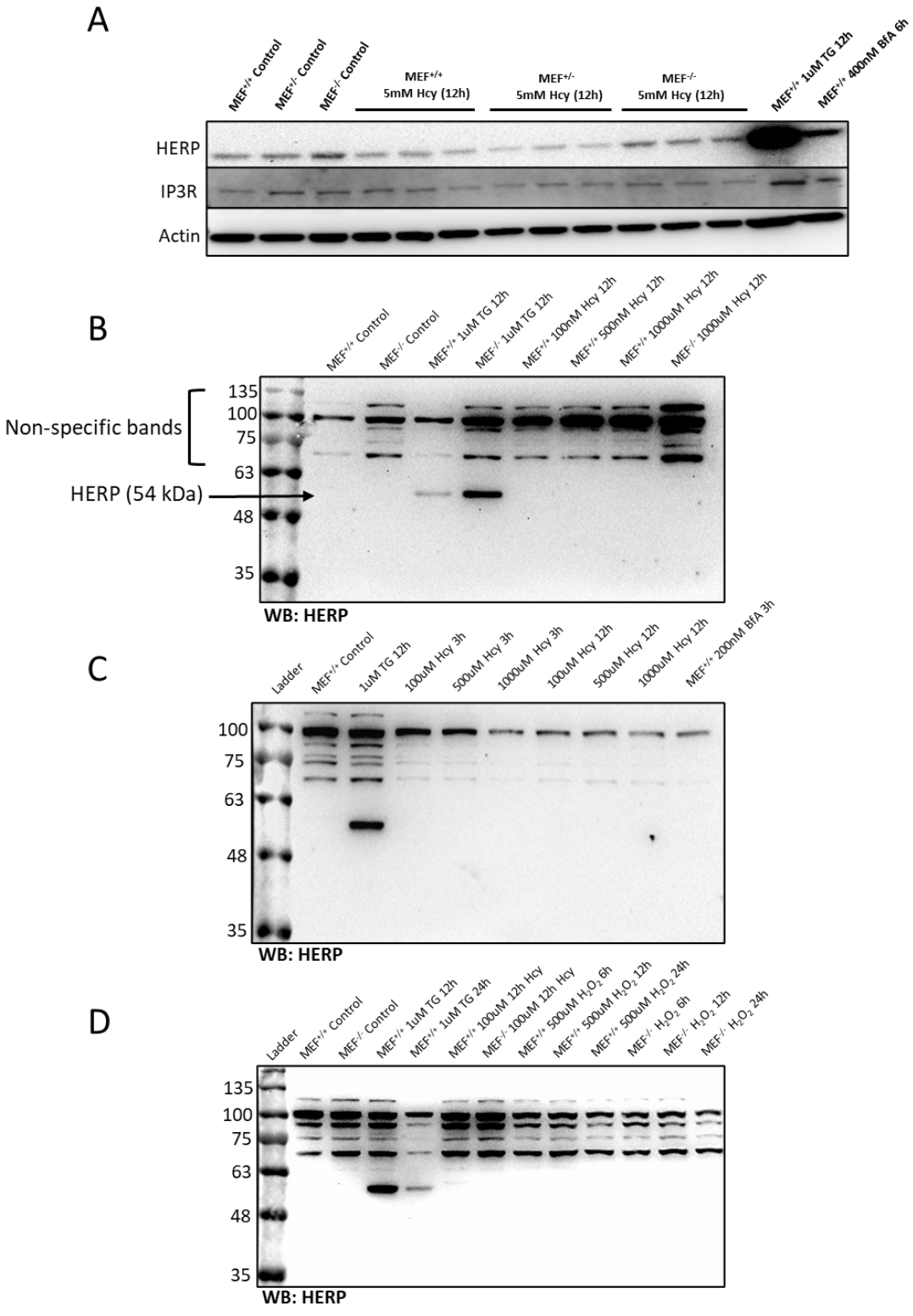

Figure 20: HERP and IP3R expression in basal, homocysteine (Hcy), and H_2O_2 treated MEF$^{+/+}$, MEF$^{+/-}$, and MEF$^{-/-}$ cells.

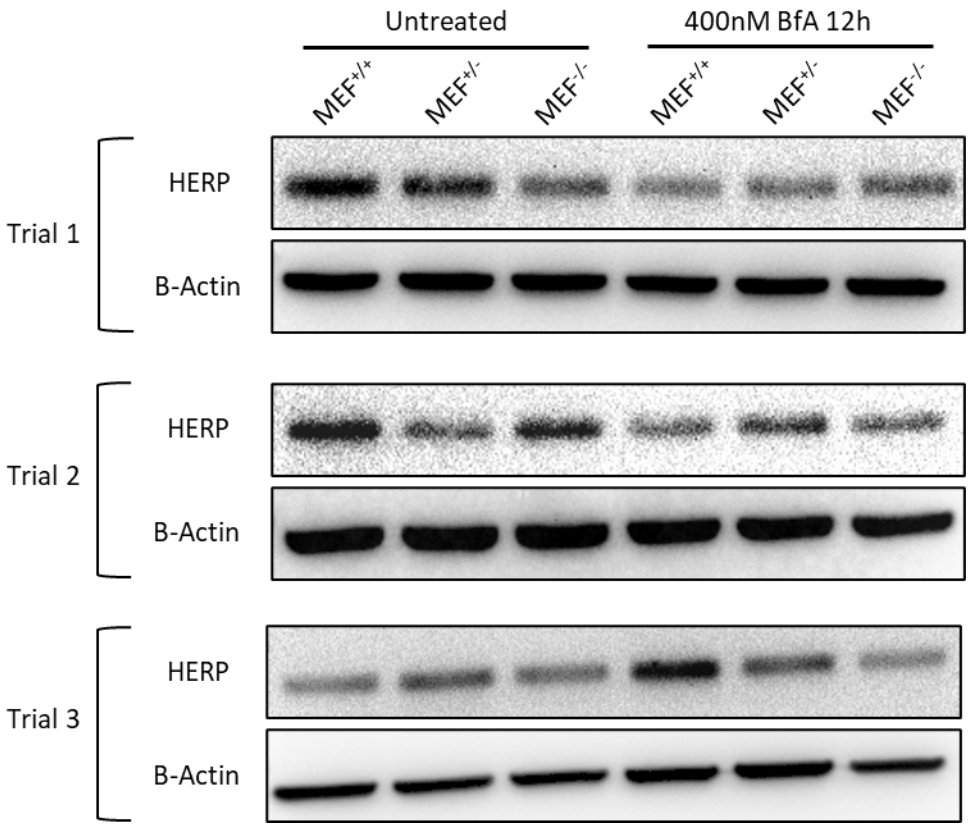

Figure 21: Variable basal and BfA treated MEF HERP protein expression.

3.4 Discussion

In this study, the cellular impact of CREB3-deficiency potentially affecting the finely tuned interplay between ROS protection, Ca^{2+} homeostasis, and ATP production was investigated. *Creb3* knockout in MEF cells led to drastic homeostatic alterations to all three mentioned compared to WT. CREB3-deficiency in MEF cells led to increased susceptibility to ROS (H_2O_2), as well as elevated basal ROS levels potentially suggesting elevated mitochondrial activity and/or defective antioxidant capabilities. A Seahorse assay confirmed that $MEF^{-/-}$ cells indeed had significantly increased basal mitochondrial respiration and ATP production compared to $MEF^{+/+}$, likely contributing to elevated ROS in $MEF^{-/-}$ cells. Additionally, relative to $MEF^{+/+}$, mitochondria of $MEF^{-/-}$ cells had greater spare respiratory capacity, or metabolic flexibility when energy is in high demand. Although $MEF^{-/-}$ cells had a higher coupling efficiency of basal respiration to ATP production, they also had increased basal proton leak compared to $MEF^{+/+}$. Basal proton leak contributes to the remaining basal respiration that is not coupled to ATP production as it produces heat instead of ATP as a product and is reflective of the metabolic rate of the cells (Amo et al., 2008; Lomax et al., 2002). Due to this, increases in both coupling efficiency and basal proton leak compared to $MEF^{+/+}$ was likely due to the significant increase in overall respiration and metabolic rate of $MEF^{-/-}$ cells.

When looking into the potential cause for the increased metabolic rate of $MEF^{-/-}$ cells, ER-Ca^{2+} efflux rates which correlate with basal ER-Ca^{2+} leak (Lomax et al., 2002), were found to be significantly increased in $MEF^{-/-}$ cells compared to $MEF^{+/+}$, which also led to increased $[Ca^{2+}]_m$. While an overload of $[Ca^{2+}]_m$ is known as an initiating signal for apoptosis, mild $[Ca^{2+}]_m$ increases can stimulate ATP production via oxidative

phosphorylation, and thus ROS levels as well (de Marchi et al., 2014; Jambrina et al., 2003; Peng & Jou, 2010). An increase in intracellular [ATP] stimulates the ATPase, SERCA, which pumps cytosolic Ca^{2+} into the ER increasing ER-Ca^{2+} stores and leakage, entering the mitochondria and beginning the cycle over again. What remained to be elucidated was where the obvious break in the tightly regulated Ca^{2+}-ATP-ROS cycle was in $MEF^{-/-}$ cells.

Previously, CREB3 has been reported to induce transcription of the *Herpud1*gene through an ERSE-II promoter recognition site (Liang et al., 2006). The protein of this gene, HERP, binds and promotes the degradation of the IP3R ER-Ca^{2+} channel and thus reduces ER-Ca^{2+} efflux (Mirabelli et al., 2016; Torrealba et al., 2017). From this, one might infer that CREB3 may then prevent ER-Ca^{2+} efflux through the HERP-IP3R pathway, indirectly regulating $[Ca^{2+}]_m$ and mitochondrial activity. Indeed, the knockout of CREB3 in MEF cells resulted in greatly increased ER-Ca^{2+} efflux, $[Ca^{2+}]_m$, and mitochondria activity, however, surprisingly no consistent differences were observed in basal HERP or IP3R compared to WT. Intriguingly, with all conditions kept the same, HERP expression varied between each western blot within the same sample groups in both $MEF^{+/+}$ and $MEF^{-/-}$ cells. It has been shown that MEF cells experience a circadian rhythm-dependent gene expression (B. H. Miller et al., 2007; Wible et al., 2018). Both HERP and CREB3's counterpart, CREB3 Recruitment Factor (CREBRF) which inhibits CREB3's activity, are expressed in a circadian dependent manner (Li et al., 2016; B. H. Miller et al., 2007; Tamaru et al., 2013). It may then be possible that the potential CREBRF-CREB3-HERP pathway is indeed also dependent on circadian rhythm and future investigation may require a cell cycle synchronization step prior to experiments. Adjusting for different cell

cycle population ratios within and between tissue culture dishes/cell lines will aid in accounting for alterations in cell cycle-dependent protein expression or activity variability between experiment repeats, creating more reliable and robust results. Synchronization can be accomplished through irreversible cell cycle arresting in a specific phase before experiments. Alternatively, reversible cell cycle arrest followed by the simultaneous release of this inhibition between cell lines thus synchronizing their progressing cell cycles before experimenting is another viable option if not interested in gathering data during a certain cell cycle phase.

UPR proteins ATF6α and XBP1s contribute to protection from oxidative stress through direct and indirect *catalase* transcriptional activation respectively (Jin et al., 2017; Y. Liu et al., 2009; Yoshida et al., 1998). ATF6α induces *catalase* through the ERSE-II promoter site in which CREB3 is also known to bind (Jin et al., 2017; Liang et al., 2006; Raggo et al., 2002). XBP1 also indirectly induces the antioxidant gene *Sod1* (Y. Liu et al., 2009). Here, despite the significant increase in basal ROS observed in $MEF^{-/-}$ cells, CREB3-deficient MEFs were found to have significantly decreased basal *catalase* and *Sod1* expression compared to WT. Therefore, it may be plausible that CREB3 directly regulates *catalase* and *Sod1* gene expression, or indirectly co-regulates their expression through crosstalk between ATF6α and XBP1s (Denboer et al., 2005; Liang et al., 2006; Yamamoto1 et al., 2004). Follow-up experiments should be aimed at comparing antioxidant gene expression differences between WT and CREB3-deficient MEF cells under oxidative stress conditions relative to basal, as well as assessing CREB3's regulatory impact on the *catalase* gene promoter, beginning with the ERSE-II site.

Although not statistically significant, there appeared to be an inverse correlation between *Creb3* genotype and *Chop* expression. MEF$^{-/-}$ cells showed the highest average *Chop* expression followed by MEF$^{+/-}$ and then MEF$^{+/+}$. These elevated *Chop* mRNA levels in MEF$^{-/-}$ cells are not all that surprising due to the increase in ROS with simultaneous reductions in *catalase* and *Sod1* gene expression compared to WT causing oxidative stress, which can then lead to ER stress and thus UPR activation (Huang et al., 2015; Lin et al., 2021; Y. Liu et al., 2009). Interestingly, in contrast to the slightly increased *Chop* levels, CREB3-deficient MEFs had significantly reduced *Grp78* expression relative to WT suggesting CREB3 may be involved in the upregulation of *Grp78*.

Interestingly, the cellular respiration phenotype reported here of CREB3-deficient MEF cells correlates well with the previously described metabolic phenotype of CREB3-deficient mice. Both had increased oxygen consumption rates with CREB3-deficient mice possessing increased metabolic rates and heat generation while CREB3-deficient MEF cells showed increased mitochondrial activity as well as proton leak which produces heat as a by-product. It may be worth noting that higher ER-Ca^{2+} efflux due to ATF6α knockout increases metabolism and lifespan in *C. elegans* while overactivation of SERCA and thus ER-Ca^{2+} stores in leptin mice can reverse various obesity-related pathologies (Burkewitz et al., 2020; S. W. Park et al., 2010). Although full *Creb3* knockout in mice is sub-viable and MEF$^{-/-}$ cells have elevated ROS and *Chop* levels, *Creb3*$^{+/-}$ mice are viable with highly desirable metabolic changes and resistance to high-fat diet-induced obesity. Therefore, only partial, and not full knockdown of CREB3 may offer an overall metabolic advantage without being damaging to the organism.

Taken together, this study shows that CREB3 is essential for maintaining proper cellular homeostasis. CREB3 may serve as a link between oxidative and ER stress and be essential for proper antioxidant homeostasis and gene expression leading to elevated basal ROS and susceptibility to exogenous ROS (H_2O_2) of $MEF^{-/-}$ cells. ROS is known to stimulate ER-Ca^{2+} release by opening the IP3R ER-Ca^{2+} channel, while ATP can activate SERCA-dependent ER-Ca^{2+} influx. Consistent with this, we found that CREB3-deficiency in MEFs resulted in an increased ER-Ca^{2+} efflux leading to elevated $[Ca^{2+}]_m$. Mitochondrial Ca^{2+} influx may stimulate the electron transport chain activity producing greater amounts of ATP and ROS in $MEF^{-/-}$ cells. These results warrant further investigation in the elucidation of specific role(s) of CREB3 in maintaining energy and oxidative homeostasis as a novel therapeutic target for various metabolic disorders.

Chapter 4: Discussion and Future Directions

Obesity and obesity-related disorders are a modern global pandemic with UPR proteins known to play a role in their pathogenesis. CREB3/LUMAN is a UPR associated ER-membrane bound transcription factor with nuclear receptor co-regulation abilities. However, much of CREB3's physiological and cellular functions remain unclear. In this thesis, it was hypothesized that CREB3 controls energy metabolism through the regulation of Ca^{2+} homeostasis and oxidative stress. To test this, the first objective was to metabolically characterize WT and CREB3-deficient mice on CD or HFDs. It was found that CREB3 deficiency in mice led to a in increased energy expenditure with no significant differences in energy intake compared to WT. This effect offered CREB3-deficient mice a significant resistance to diet-induced weight gain, hyperglycemia, and sex-specific tissue lipid accumulation. The second objective was to elucidate CREB3's molecular mechanism by investigating WT and CREB3-deficient MEF cells. It was seen that CREB3-deficient MEF cells also have an increased metabolic rate, which may be due to increased ER-Ca^{2+} efflux leading to mitochondrial Ca^{2+} influx and thus stimulating the production of ATP and ROS.

4.1 CREB3's Role in Energy Homeostasis

From the data presented in this thesis, it is evident that CREB3 plays an integral role in the regulation of energy homeostasis in both mice and MEF cell cultures. Both

CREB3-deficient mice on HFD and MEF cells exhibited significantly increased metabolic rate/respiration with CREB3-deficient mice having an increased heat production and $MEF^{-/-}$ cells increased ATP production when compared to WT. This suggests that CREB3 functions as a metabolic brake. Since CREB3 is known to activate under specific ER stress treatments, CREB3 then may respond in times of metabolic stress in which mitochondrial activity is causing stress on the cell potentially through elevated ROS. Although metabolic/dietary treatments to MEF cells such as homocysteine, H_2O_2, or palmitate did not activate CREB3 cleavage alone, perhaps a certain combination of conditions is required. Another possibility is the resistance of MEF cells to metabolic treatments which therefore a more metabolically relevant cell line such as hepatocytes, adipocytes, or pancreatic beta cells may be necessary for *in vitro* CREB3 activation by metabolic treatments. Additionally, other CREB3-related proteins such as CREBRF and CREB3L3 as well as CREB3 gene target *Herpud1* are regulated by circadian rhythm, therefore it may be possible CREB3 activation could also be cell cycle-dependent.

4.2 CREB3 and Adipogenesis

In this thesis, it was observed that *Creb3*$^{+/-}$ mice possess a significant reduction in fat mass on HFD, with an increased number of smaller-sized white adipocytes on both CD and HFD compared to WT (Figure 9I). CREB3-Like protein, CREB3L4, was previously described as a negative regulator of adipogenesis (T.-H. Kim et al., 2014). Similar to *Creb3*$^{+/-}$ mice*, Creb3l4*-KO in mice also resulted in an increased number of

smaller-sized adipocytes (hyperplasia) present in their white adipose tissue compared to WT (T.-H. Kim et al., 2014). The increased number of smaller adipocytes was determined to be a result of increased adipogenesis with the relief from CREB3L4 inhibition of key adipogenic genes *Cebpα* and *Pparg2* (T.-H. Kim et al., 2014). The increased number of smaller adipocytes in *Creb3l4*-KO mice was the determining factor behind the improved glucose tolerance and fasted blood glucose levels observed compared to WT on HFD. In direct correlation with this, *Creb3*$^{+/-}$ mice also retained normal fasted blood glucose levels with *Creb3*$^{+/-}$ males having improved glucose tolerance compared to WT on HFD (Figures 12A-F).

UPR proteins ATF6α and XBP1 have also been described as essential for proper adipogenic gene expression (Lowe et al., 2012; Sha et al., 2009). Deficiency of either ATF6α or XBP1 resulted in significantly reduced adipogenic potential in MEF cells (Lowe et al., 2012; Sha et al., 2009). Despite these promising connections between the UPR protein CREB3 and adipogenic potential, it is impossible to rule out the resulting smaller adipocytes being due to the overall leanness of *Creb3*$^{+/-}$ mice. Further functional studies will be required to decipher whether or not CREB3 truly does play an integral role in the adipogenesis process.

4.3 CREB3, CREB3L3, and PGC-1α

It is hard to ignore the connections between CREB3 and CREB3L3 other than their sequence similarities. *Creb3l3*-Tg mice overexpressing CREB3L3 had a surprisingly similar metabolic phenotype to that of CREB3-deficient mice (Sa et al.,

2014; Satoh et al., 2020; C. Zhang et al., 2012). As previously discussed, both had reduced weight gain, body fat, and hepatic lipid accumulation with no differences in food intake on HFD compared to WT mice. Additionally, *Creb3l3*-KO mice show an inverse hepatic gene expression profile to CREB3-deficient mice (Sa et al., 2014; Satoh et al., 2020; C. Zhang et al., 2012). Since CREB3 and CREB3L3 are known to interact with nuclear receptors, and CREB3 family proteins can dimerize through LxxLL sites, it may be plausible that CREB3 negatively co-regulates CREB3L3 similarly to CREBRF inhibition on CREB3 (Audas et al., 2008). CREB3L3 also plays a basal role in lipid metabolism. In its inactive form, it binds to and promotes the formation and anchoring of the INSIG-SCAP-SREPB complex within the ER membrane, preventing SCAP-SREBP translocation to the Golgi (Nakagawa et al., 2021). Indeed, deficiency of CREB3L3 led to an increase in nuclear SREBPs and an increase in TG synthesis (Nakagawa et al., 2021). This was attributed to both the direct inhibition of CREB3L3 on SREBP trafficking and also through CREB3L3 physically competing with SREBPs for S1P and S2P cleavage in the Golgi (Nakagawa et al., 2021). In contrast, overexpression of inactive CREB3L3 prevented SREBP cleavage and nuclear accumulation and thus TG synthesis while overexpression of active CREB3L3 showed no effect on SREBP function or activity (Nakagawa et al., 2021). Like CREB3L3's basal role of tethering the lipogenic SCAP-SREBP1 complex in the ER, CREB3L4 also performs a similar role. It has been found that CREB3L4 binds and retains CREB3L1 within the ER-membrane, inhibiting CREB3L1 activation (X. Cui et al., 2016). CREB3's potential co-regulating abilities of nuclear receptors similar to CREB3L3 and CREB3L4, its ER-membrane localization, and apparent effect on metabolism under basal conditions shown in

Chapters 2 and 3 of this thesis suggest it too could be regulating basal lipid metabolism from the ER-membrane. Since CREB3L3 has a complex role in lipid metabolism in that it can induce both lipogenesis and lipolysis and FA oxidation, another possibility is that CREB3 may form a transcriptional complex with CREB3L3 that alters its transcriptional gene targets to more lipogenic and lipid transport genes. Here it is shown that hepatic *Pgc-1α* was indirectly or directly induced with a reduction in *Creb3* expression (Figure 13A). CREB3L3 is known to form a complex with both PPARα and PGC-1α to induce energy expenditure, lipolysis, and FA oxidation genes, including *Pgc-1α* itself (H. Kim et al., 2014; M. W. Lee et al., 2010; Nakagawa et al., 2016). Since known CREB3 binding partner HCF-1 also interacts and co-regulates PGC-1α function, CREB3 could indirectly be influencing PGC-1α through HCF-1, or even directly through the LxxLL nuclear receptor binding site (Ruan et al., 2012). These not so coincidental correlations warrant further investigation into the complex interactions between CREB3, CREB3L3, PGC-1α, PPARα, and HCF-1.

4.4 CREB3 and Ca^{2+} Homeostasis

CREB3 has previously been linked to the regulation of Ca^{2+} flow in neurons through the regulation of the IP3R ER-Ca^{2+} channel inhibitor protein, HERP (S. L. Chan et al., 2004; Mirabelli et al., 2016). It has been shown the overexpression of HERP reduced ER-Ca^{2+} release through its degradation of IP3R (Torrealba et al., 2017). Agreeing with this research, it was found in this thesis that CREB3-deficient MEFs indeed had increased ER-Ca^{2+} release leading to increased mitochondrial Ca^{2+} uptake

and subsequent ATP and ROS production. Although surprisingly HERP was variably expressed in MEFs independent of *Creb3* genotype and known HERP inducers, homocysteine, thapsigargin, and H_2O_2. This still however could be a possible mechanism behind CREB3's regulation of mitochondrial function since the cell cycle was not controlled for in the experiments performed in this thesis. As stated previously HERP, as well as CREB3 inhibitor, CREBRF, are both regulated by cell cycle which may account for the inconsistencies of HERP expression found here in $MEF^{+/+}$, $MEF^{+/-}$, and $MEF^{-/-}$ cells (Li et al., 2016; B. H. Miller et al., 2007; Tamaru et al., 2013). HERP may not be the only CREB3 target involved in Ca^{2+} homeostasis either. As previously shown, UPR protein ATF6α is responsible for the induction of ER-Ca^{2+} chelator, calreticulin, therefore it may be worthwhile to investigate other integral Ca^{2+} homeostasis genes upregulated by ER stress and UPR activation (Burkewitz et al., 2020).

4.5 CREB3 and Oxidative Stress

UPR proteins ATF6α and XBP1 already have previously reported functions in the protection from oxidative stress through direct or indirect regulation of antioxidant genes (Jin et al., 2017; Y. Liu et al., 2009). ATF6α in particular binds to the ERSE-II present in the promoter of *Catalase* to induce its transcription and reduce oxidative stress (Jin et al., 2017). CREB3 is also known to induce transcription through ERSE-II and it is shown in this thesis that $MEF^{-/-}$ cells containing significantly higher basal ROS levels are also susceptible to 24-hour H_2O_2-induced oxidative stress treatments (Liang et al., 2006).

Due to this, CREB3's potential regulation of antioxidant gene expression warrants further investigation.

4.6 Sex-specific Role of CREB3

The data presented in this thesis reveal a sex-specific function of CREB3. The first indication of this effect is that even though *Creb3*$^{-/-}$ mice are sub-viable, about 1 *Creb3*$^{-/-}$ mouse is birthed per year when mating *Creb3*$^{+/-}$ mice together and has always been born a female. While both *Creb3*$^{+/-}$ sexes depicted resistance to HFD-induced weight gain, female *Creb3*$^{+/-}$ showed much more drastic reductions in body fat and adipocyte sizes than *Creb3*$^{+/-}$ males compared to WT. *Creb3*$^{+/-}$ males showed more protection from hepatic lipid accumulation while *Creb3*$^{+/-}$ females were more protected from intramuscular fat accumulation. Additionally, while *Creb3*$^{+/-}$ males maintained somewhat normal glucose tolerance post-HFD compared to WT, *Creb3*$^{+/-}$ females did not. The estrogen receptor (ERα) is structurally and functionally similar to GR and do indeed interact with and co-regulate one another (Kumar et al., 2011; Uht et al., 1997). GR is one of CREB3's known nuclear receptor binding partners and co-regulates promoter binding of at glucocorticoid response elements (GREs) of genes and is upregulated in the absence of CREB3 in mice and MEF cells (Penney et al., 2018). ERα has been found to bind the promoters and induce hepatic gluconeogenic genes *Pck-1*, *G6Pase* and lipogenic genes *Fasn* and *Acc1* (Qiu et al., 2017). CREB3 may therefore contribute to regulating ERα activity indirectly through GR or perhaps directly through co-regulation interactions. *Creb3*$^{+/-}$ males also showed significant induction of UCP1

thermogenic protein expression in WAT compared to WT, while *Creb3*$^{+/-}$ and WT females had equivalent UCP1 expression to each other. Indeed, UCP1 is known to have sex-specific expression differences (Moschinger et al., 2019; Rodríguez et al., 2002; Zhenqi et al., 2020). Females are more prone to higher levels of brown and white adipose tissue UCP1 expression than males, largely as a result of transcriptional induction of *Ucp1* by estradiol/estrogen activation of ERα (Moschinger et al., 2019; Zhenqi et al., 2020). Additionally, testosterone acts oppositely as to estrogen as it inhibits *Ucp1* transcription (Moschinger et al., 2019; Rodríguez et al., 2002). Previously reported drastic reductions in testosterone levels of *Creb3*$^{+/-}$ male mice compared to WT could explain the significant increase of UCP1 in their eWAT (Penney, 2017).

4.7 General Future Directions

This thesis will serve as a basis for many follow-up experiments. Of course, there is much more to be elucidated about CREB3's specific role in metabolic regulation. Firstly, mice used in experiments in this thesis were fasted prior to euthanization and/or examinations. Since high nutrient influx from feeding can cause cellular/ER stress, it may be of interest to study CREB3 under non-fasted conditions such as a fast then refeed scenario both in mice and cell culture. Additionally, since mouse studies here compared CD to HFD while CREB3-deficient mice show an increased preference for glucose as an energy substrate, a high-carbohydrate diet may help further elucidate CREB3's metabolic effects, particularly in glucose metabolism.

Although not discussed in depth in this thesis, CREB3 is known to contribute to secretory vesicle formation through transcriptional upregulation of key COPII structural genes (Penney et al., 2018). Secretion of key metabolic hormones such as insulin/glucagon, or growth hormones may be of significance to study in CREB3-deficient models.

4.8 Limitations

Since *Creb3*$^{-/-}$ mice are non-viable, it may be of value to perform studies on conditional *Creb3* knockout mice to bypass the developmental mortality phenotype of *Creb3*$^{-/-}$ mice. On top of this, since whole-body *Creb3*$^{+/-}$ mice were used in this study tissue-specific conditional knockouts would be even more advantageous in determining in which tissue(s) CREB3 predominantly affects metabolism. In particular, liver, adipose, muscle, pancreas, and brain knockouts would be of the most interest due to their metabolic nature and/or CREB3 expression levels, or previous data on CREB3.

Unfortunately, due to COVID-19 lockdown, 2 CD cohorts (~25 mice) were lost that were to be used to help generate a control diet weight curve, more plasma lipids, and insulin/leptin measurements, as well as muscle, pancreas, liver, and adipose dissections and tissue analysis. Additionally, 2 other HFD cohorts (~25 mice) worth of data was also lost during the lockdown in which were to be used for more metabolic cage measurements, plasma lipids and insulin/leptin measurements, muscle, pancreas, liver, adipose tissue dissections and analysis. This resulted in reduced sample size numbers, and a lack of HFD plasma insulin and leptin data.

4.9 Significance of Research and Conclusion

This first of its kind research on CREB3's role in metabolism serves multiple significant purposes. This novel study directly implicates CREB3 in the regulation of overall organismal and cellular metabolism. Due to this, data produced in this thesis will provide a basis for all future CREB3 research in the field of metabolism and provide insight into other processes CREB3 may be involved in such as oxidative stress response and protection. Secondly, and not surprisingly, energy metabolism, as well as oxidative stress, are vastly implicated in obesity and many other metabolic disorders. Therefore, CREB3 may then provide an exciting new potential therapeutic target warranting further investigation in this context. Not only do energy metabolism and oxidative stress correlate to many metabolic diseases but are also very much involved in neurodegenerative disorders. Coincidentally, CREB3-deficient mice were previously reported to have a neurological phenotype described as a blunted "behavioural stress response" further reinforcing the possible neurological applications of CREB3 as well.

References

Adeva-Andany, M. M., Carneiro-Freire, N., Seco-Filgueira, M., Fernández-Fernández, C., & Mouriño-Bayolo, D. (2019). Mitochondrial β-oxidation of saturated fatty acids in humans. In *Mitochondrion* (Vol. 46, pp. 73–90). Elsevier B.V. https://doi.org/10.1016/j.mito.2018.02.009

Akiyama, M., Liew, C. W., Lu, S., Hu, J., Martinez, R., Hambro, B., Kennedy, R. T., & Kulkarni, R. N. (2013). X-Box binding protein 1 is essential for insulin regulation of pancreatic α-cell function. *Diabetes*, *62*(7), 2439–2449. https://doi.org/10.2337/db12-1747

Amo, T., Yadava, N., Oh, R., Nicholls, D. G., & Brand, M. D. (2008). Experimental assessment of bioenergetic differences caused by the common European mitochondrial DNA haplogroups H and T. *Gene*, *411*(1–2), 69–76. https://doi.org/10.1016/j.gene.2008.01.007

Audas, T. E., Li, Y., Liang, G., & Lu, R. (2008). A Novel Protein, Luman/CREB3 Recruitment Factor, Inhibits Luman Activation of the Unfolded Protein Response. *Molecular and Cellular Biology*, *28*(12), 3952–3966. https://doi.org/10.1128/mcb.01439-07

Averous, J., Bruhat, A., Jousse, C., Carraro, V., Thiel, G., & Fafournoux, P. (2004). Induction of CHOP Expression by Amino Acid Limitation Requires Both ATF4 Expression and ATF2 Phosphorylation. *Journal of Biological Chemistry*, *279*(7), 5288–5297. https://doi.org/10.1074/jbc.M311862200

Babicki, S., Arndt, D., Marcu, A., Liang, Y., Grant, J. R., Maciejewski, A., & Wishart, D. S. (2016). Heatmapper: web-enabled heat mapping for all. *Nucleic Acids Research*, *44*, 147–153. https://doi.org/10.1093/nar/gkw419

Back, S. H., Schröder, M., Lee, K., Zhang, K., & Kaufman, R. J. (2005). ER stress signaling by regulated splicing: IRE1/HAC1/XBP1. *Methods*, *35*(4), 395–416. https://doi.org/10.1016/J.YMETH.2005.03.001

Badiola, N., Penas, C., Miñano-Molina, A., Barneda-Zahonero, B., Fadó, R., Sánchez-Opazo, G., Comella, J. X., Sabriá, J., Zhu, C., Blomgren, K., Casas, C., & Rodríguez-Alvarez, J. (2011). Induction of ER stress in response to oxygen-glucose deprivation of cortical cultures involves the activation of the PERK and IRE-1 pathways and of caspase-12. *Cell Death and Disease*, *2*(4). https://doi.org/10.1038/cddis.2011.31

Baldwin, K. M., Joanisse, D. R., Haddad, F., Goldsmith, R. L., Gallagher, D., Pavlovich, K. H., Shamoon, E. L., Leibel, R. L., Rosenbaum, M., Baldwin, K. M., & Joanisse, D. R. (2011). CALL FOR PAPERS Integrative and Translational Physiology: Integrative Aspects of Energy Homeostasis and

Metabolic Diseases Effects of weight loss and leptin on skeletal muscle in human subjects. *Am J Physiol Regul Integr Comp Physiol*, *301*, 1259–1266. https://doi.org/10.1152/ajpregu.00397.2011.-Maintenance

Bánsághi, S., Golenár, T., Madesh, M., Csordás, G., RamachandraRao, S., Sharma, K., Yule, D. I., Joseph, S. K., & Hajnóczky, G. (2014). Isoform- and species-specific control of inositol 1,4,5-trisphosphate (IP3) receptors by reactive oxygen species. *Journal of Biological Chemistry*, *289*(12), 8170–8181. https://doi.org/10.1074/jbc.M113.504159

Barberá, M. J., Schlüter, A., Pedraza, N., Iglesias, R., Villarroya, F., & Giralt, M. (2001). Peroxisome proliferator-activated receptor α activates transcription of the brown fat uncoupling protein-1 gene. A link between regulation of the thermogenic and lipid oxidation pathways in the brown fat cell. *Journal of Biological Chemistry*, *276*(2), 1486–1493. https://doi.org/10.1074/jbc.M006246200

Bardaweel, S. K., Gul, M., Alzweiri, M., Ishaqat, A., Alsalamat, H. A., & Bashatwah, R. M. (2018). Reactive oxygen species: The dual role in physiological and pathological conditions of the human body. In *Eurasian Journal of Medicine* (Vol. 50, Issue 3, pp. 193–201). AVES İbrahim KARA. https://doi.org/10.5152/eurasianjmed.2018.17397

Barrera, M. J., Aguilera, S., Castro, I., Cortés, J., Bahamondes, V., Quest, A. F. G., Molina, C., González, S., Hermoso, M., Urzúa, U., Leyton, C., & González, M. J. (2016). Pro-inflammatory cytokines enhance ERAD and ATF6α pathway activity in salivary glands of Sjögren's syndrome patients. *Journal of Autoimmunity*, *75*, 68–81. https://doi.org/10.1016/J.JAUT.2016.07.006

Bartok, A., Weaver, D., Golenár, T., Nichtova, Z., Katona, M., Bánsághi, S., Alzayady, K. J., Thomas, V. K., Ando, H., Mikoshiba, K., Joseph, S. K., Yule, D. I., Csordás, G., & Hajnóczky, G. (2019). IP3 receptor isoforms differently regulate ER-mitochondrial contacts and local calcium transfer. *Nature Communications*, *10*(1). https://doi.org/10.1038/s41467-019-11646-3

Basseri, S., & Austin, R. C. (2012). Endoplasmic reticulum stress and lipid metabolism: Mechanisms and therapeutic potential. In *Biochemistry Research International*. https://doi.org/10.1155/2012/841362

Berger, J. P. (2005). Role of PPARγ, transcriptional cofactors, and adiponectin in the regulation of nutrient metabolism, adipogenesis and insulin action: View from the chair. *International Journal of Obesity*, *29*(SUPPL. 1). https://doi.org/10.1038/sj.ijo.0802904

Bobrovnikova-Marjon, E., Hatzivassiliou, G., Grigoriadou, C., Romero, M., Cavener, D. R., Thompson, C. B., & Alan Diehl, J. (2008). *PERK-dependent regulation*

of lipogenesis during mouse mammary gland development and adipocyte differentiation. www.pnas.org/cgi/content/full/

Bommiasamy, H., Back, S. H., Fagone, P., Lee, K., Meshinchi, S., Vink, E., Sriburi, R., Frank, M., Jackowski, S., Kaufman, R. J., & Brewer, J. W. (2009). ATF6α induces XBP1-independent expansion of the endoplasmic reticulum. *Journal of Cell Science*, *122*(10), 1626–1636. https://doi.org/10.1242/jcs.045625

Boyman, L., Karbowski, M., & Lederer, W. J. (2020). Regulation of Mitochondrial ATP Production: Ca2+ Signaling and Quality Control. *Trends in Molecular Medicine*, *26*(1), 21–39. https://doi.org/10.1016/J.MOLMED.2019.10.007

Brookes, P. S., Yoon, Y., Robotham, J. L., Anders, M. W., & Sheu, S. S. (2004). Calcium, ATP, and ROS: A mitochondrial love-hate triangle. In *American Journal of Physiology - Cell Physiology* (Vol. 287, Issues 4 56-4). https://doi.org/10.1152/ajpcell.00139.2004

Brown, M. S., & Goldstein, J. L. (1997). The SREBP Pathway: Regulation Review of Cholesterol Metabolism by Proteolysis of a Membrane-Bound Transcription Factor. In *Cell* (Vol. 89).

Burkewitz, K., Feng, G., Dutta, S., Kelley, C. A., Steinbaugh, M., Cram, E. J., & Mair, W. B. (2020). Atf-6 Regulates Lifespan through ER-Mitochondrial Calcium Homeostasis. *Cell Reports*, *32*(10). https://doi.org/10.1016/j.celrep.2020.108125

Chan, C. P., Kok, K. H., & Jin, D. Y. (2011a). CREB3 subfamily transcription factors are not created equal: Recent insights from global analyses and animal models. In *Cell and Bioscience* (Vol. 1, Issue 1). https://doi.org/10.1186/2045-3701-1-6

Chan, C. P., Kok, K. H., & Jin, D. Y. (2011b). CREB3 subfamily transcription factors are not created equal: Recent insights from global analyses and animal models. In *Cell and Bioscience* (Vol. 1, Issue 1). https://doi.org/10.1186/2045-3701-1-6

Chan, S. L., Fu, W., Zhang, P., Cheng, A., Lee, J., Kokame, K., & Mattson, M. P. (2004). Herp stabilizes neuronal Ca2+ homeostasis and mitochondrial function during endoplasmic reticulum stress. *Journal of Biological Chemistry*, *279*(27), 28733–28743. https://doi.org/10.1074/jbc.M404272200

Chaudhry, R., & Varacallo, M. (2021). *Biochemistry, Glycolysis*. StatPearls Publishing, Treasure Island (FL). http://europepmc.org/books/NBK482303

Chen, X., Zhang, F., Gong, Q., Cui, A., Zhuo, S., Hu, Z., Han, Y., Gao, J., Sun, Y., Liu, Z., Yang, Z., Le, Y., Gao, X., Dong, L. Q., Gao, X., & Li, Y. (2016). Hepatic ATF6 increases fatty acid oxidation to attenuate hepatic steatosis in mice

through peroxisome proliferator-activated receptor α. *Diabetes*, *65*(7), 1904–1915. https://doi.org/10.2337/db15-1637

Cheng, C.-F., Ku, H.-C., & Lin, H. (2018). *Molecular Sciences PGC-1α as a Pivotal Factor in Lipid and Metabolic Regulation*. https://doi.org/10.3390/ijms19113447

Cooper, L. L., Li, W., Lu, Y., Centracchio, J., Terentyeva, R., Koren, G., & Terentyev, D. (2013). Redox modification of ryanodine receptors by mitochondria-derived reactive oxygen species contributes to aberrant Ca 2+ handling in ageing rabbit hearts. *The Authors. The Journal of Physiology C*, *591*, 5895–5911. https://doi.org/10.1113/jphysiol.2013.260521

Cui, M., Kanemoto, S., Cui, X., Kaneko, M., Asada, R., Matsuhisa, K., Tanimoto, K., Yoshimoto, Y., Shukunami, C., & Imaizumi, K. (2015). OASIS modulates hypoxia pathway activity to regulate bone angiogenesis. *Scientific Reports*, *5*. https://doi.org/10.1038/srep16455

Cui, X., Cui, M., Asada, R., Kanemoto, S., Saito, A., Matsuhisa, K., Kaneko, M., & Imaizumi, K. (2016). The androgen-induced protein AIbZIP facilitates proliferation of prostate cancer cells through downregulation of p21 expression. *Scientific Reports*, *6*. https://doi.org/10.1038/srep37310

Dandekar, A., Mendez, R., & Zhang, K. (2015). Cross Talk Between ER Stress, Oxidative Stress, and Inflammation in Health and Disease. In C. M. Oslowski (Ed.), *Stress Responses: Methods and Protocols* (pp. 205–214). Springer New York. https://doi.org/10.1007/978-1-4939-2522-3_15

Davis, L. C., Morgan, A. J., Ruas, M., Wong, J. L., Graeff, R. M., Poustka, A. J., Lee, H. C., Wessel, G. M., Parrington, J., & Galione, A. (2008). Ca2+ Signaling Occurs via Second Messenger Release from Intraorganelle Synthesis Sites. *Current Biology*, *18*(20), 1612–1618. https://doi.org/10.1016/J.CUB.2008.09.024

de Marchi, U., Castelbou, C., & Demaurex, N. (2011). Uncoupling protein 3 (UCP3) modulates the activity of sarco/endoplasmic reticulum Ca 2+-ATPase (SERCA) by decreasing mitochondrial ATP Production. *Journal of Biological Chemistry*, *286*(37), 32533–32541. https://doi.org/10.1074/jbc.M110.216044

de Marchi, U., Thevenet, J., Hermant, A., Dioum, E., & Wiederkehr, A. (2014). Calcium co-regulates oxidative metabolism and ATP synthase-dependent respiration in pancreatic beta cells. *Journal of Biological Chemistry*, *289*(13), 9182–9194. https://doi.org/10.1074/jbc.M113.513184

Denboer, L. M., Hardy-Smith, P. W., Hogan, M. R., Cockram, G. P., Audas, T. E., & Lu, R. (2005). Luman is capable of binding and activating transcription from the unfolded protein response element. *Biochemical and Biophysical Research*

Communications, *331*(1), 113–119. https://doi.org/10.1016/J.BBRC.2005.03.141

Dong, Q., Kuefner, M. S., Deng, X., Bridges, D., Park, E. A., Elam, M. B., & Raghow, R. (2018). Sex-specific differences in hepatic steatosis in obese spontaneously hypertensive (SHROB) rats. *Biology of Sex Differences*, *9*(1). https://doi.org/10.1186/s13293-018-0202-x

Duncan, R. E., Ahmadian, M., Jaworski, K., Sarkadi-Nagy, E., & Sul, H. S. (2007). *Regulation of Lipolysis in Adipocytes*. https://doi.org/10.1146/annurev.nutr.27.061406.093734

Eberlé, D., Hegarty, B., Bossard, P., Ferré, P., & Foufelle, F. (2004). SREBP transcription factors: Master regulators of lipid homeostasis. In *Biochimie* (Vol. 86, Issue 11, pp. 839–848). Elsevier B.V. https://doi.org/10.1016/j.biochi.2004.09.018

Elvira, R., Cha, S. J., Noh, G. M., Kim, K., & Han, J. (2020). PERK-mediated eIF2α phosphorylation contributes to the protection of dopaminergic neurons from chronic heat stress in Drosophila. *International Journal of Molecular Sciences*, *21*(3). https://doi.org/10.3390/ijms21030845

Farrukh, M. R., Nissar, U. A., Afnan, Q., Rafiq, R. A., Sharma, L., Amin, S., Kaiser, P., Sharma, P. R., & Tasduq, S. A. (2014). Oxidative stress mediated Ca2+ release manifests endoplasmic reticulum stress leading to unfolded protein response in UV-B irradiated human skin cells. *Journal of Dermatological Science*, *75*(1), 24–35. https://doi.org/10.1016/J.JDERMSCI.2014.03.005

Finck, B. N., & Kelly, D. P. (2006). PGC-1 coactivators: inducible regulators of energy metabolism in health and disease. *The Journal of Clinical Investigation*, *116*. https://doi.org/10.1172/JCI27794

Forostyak, O., Forostyak, S., Kortus, S., Sykova, E., Verkhratsky, A., & Dayanithi, G. (2016). Physiology of Ca2+ signalling in stem cells of different origins and differentiation stages. *Cell Calcium*, *59*(2–3), 57–66. https://doi.org/10.1016/J.CECA.2016.02.001

Gasparotto, J., da Boit Martinello, K., Leandro Silva Oliveira, M., Somensi, N., Eduardo Schnorr, C., & Diéguez, C. (2021). Aerobic Exercise Sensitizes Brown Adipose Tissue and Mobilizes Fat Oxidation in Obese Rats. In *J Nutr Obes* (Vol. 2). www.scholarena.com

Golozoubova, V., Cannon, B., & Nedergaard, J. (2006). *UCP1 is essential for adaptive adrenergic nonshivering thermogenesis*. https://doi.org/10.1152/ajpendo.00387.2005.-Partici

Granatiero, V., Pacifici, M., Raffaello, A., de Stefani, D., & Rizzuto, R. (2019). *Overexpression of Mitochondrial Calcium Uniporter Causes Neuronal Death*. https://doi.org/10.1155/2019/1681254

Greenberg, A. S., Egan, J. J., Wek, S. A., Garty, N. B., Blanchette-Mackie, E. J., & Londos, C. (1991). Perilipin, a major hormonally regulated adipocyte-specific phosphoprotein associated with the periphery of lipid storage droplets. *Journal of Biological Chemistry*, *266*(17), 11341–11346. https://doi.org/10.1016/s0021-9258(18)99168-4

Guillemyn, B., Kayserili, H., Demuynck, L., Sips, P., de Paepe, A., Syx, D., Coucke, P. J., Malfait, F., & Symoens, S. (2019). A homozygous pathogenic missense variant broadens the phenotypic and mutational spectrum of CREB3L1-related osteogenesis imperfecta. *Human Molecular Genetics*, *28*(11), 1801–1809. https://doi.org/10.1093/hmg/ddz017

Guo, C., Chi, Z., Jiang, D., Xu, T., Yu, W., Wang, Z., Chen, S., Zhang, L., Liu, Q., Guo, X., Zhang, X., Li, W., Lu, L., Wu, Y., Song, B. L., & Wang, D. (2018). Cholesterol Homeostatic Regulator SCAP-SREBP2 Integrates NLRP3 Inflammasome Activation and Cholesterol Biosynthetic Signaling in Macrophages. *Immunity*, *49*(5), 842-856.e7. https://doi.org/10.1016/j.immuni.2018.08.021

Guo, L., Li, X., & Tang, Q. Q. (2015). Transcriptional regulation of adipocyte differentiation: A central role for CCAAT/ enhancer-binding protein (C/EBP) β. In *Journal of Biological Chemistry* (Vol. 290, Issue 2, pp. 755–761). American Society for Biochemistry and Molecular Biology Inc. https://doi.org/10.1074/jbc.R114.619957

Guo, R., Gu, J., Zong, S., Wu, M., & Yang, M. (2018). Structure and mechanism of mitochondrial electron transport chain. *Biomedical Journal*, *41*(1), 9–20. https://doi.org/10.1016/J.BJ.2017.12.001

Haar, E. vander, Lee, S. il, Bandhakavi, S., Griffin, T. J., & Kim, D. H. (2007). Insulin signalling to mTOR mediated by the Akt/PKB substrate PRAS40. *Nature Cell Biology*, *9*(3), 316–323. https://doi.org/10.1038/ncb1547

Handschin, C., & Spiegelman, B. M. (2006). Peroxisome proliferator-activated receptor γ coactivator 1 coactivators, energy homeostasis, and metabolism. *Endocrine Reviews*, *27*(7), 728–735. https://doi.org/10.1210/er.2006-0037

Hayashi, Y. (2021). Glucagon regulates lipolysis and fatty acid oxidation through inositol triphosphate receptor 1 in the liver. In *Journal of Diabetes Investigation* (Vol. 12, Issue 1, pp. 32–34). Blackwell Publishing. https://doi.org/10.1111/jdi.13315

He, P. P., Jiang, T., OuYang, X. P., Liang, Y. Q., Zou, J. Q., Wang, Y., Shen, Q. Q., Liao, L., & Zheng, X. L. (2018). Lipoprotein lipase: Biosynthesis, regulatory factors, and its role in atherosclerosis and other diseases. In *Clinica Chimica Acta* (Vol. 480, pp. 126–137). Elsevier B.V. https://doi.org/10.1016/j.cca.2018.02.006

Hino, K., Saito, A., Kido, M., Kanemoto, S., Asada, R., Takai, T., Cui, M., Cui, X., & Imaizumi, K. (2014). Master regulator for chondrogenesis, Sox9, regulates transcriptional activation of the endoplasmic reticulum stress transducer BBF2H7/CREB3L2 in chondrocytes. *Journal of Biological Chemistry*, *289*(20), 13810–13820. https://doi.org/10.1074/jbc.M113.543322

Hofer, A. M., Curci, S., Machen, T. E., & Schulz, I. (1996). ATP regulates calcium leak from agonist-sensitive internal calcium stores. *The FASEB Journal*, *10*(2), 302–308. https://doi.org/https://doi.org/10.1096/fasebj.10.2.8641563

Honma, Y., Kanazawa, K. ya, Mori, T., Tanno, Y., Tojo, M., Kiyosawa, H., Takeda, J., Nikaido, T., Tsukamoto, T., Yokoya, S., & Wanaka, A. (1999). Identification of a novel gene, OASIS, which encodes for a putative CREB/ATF family transcription factor in the long-term cultured astrocytes and gliotic tissue. *Molecular Brain Research*, *69*(1), 93–103. https://doi.org/10.1016/S0169-328X(99)00102-3

Huang, Q., Zhou, H. J., Zhang, H., Huang, Y., Hinojosa-Kirschenbaum, F., Fan, P., Yao, L., Belardinelli, L., Tellides, G., Giordano, F. J., Budas, G. R., & Min, W. (2015). Thioredoxin-2 inhibits mitochondrial reactive oxygen species generation and apoptosis stress kinase-1 activity to maintain cardiac function. *Circulation*, *131*(12), 1082–1097. https://doi.org/10.1161/CIRCULATIONAHA.114.012725

Indiveri, C., Camara, A. K. S., Mammucari, C., Gherardi, G., Monticelli, H., & Rizzuto, R. (2020). *The Mitochondrial Ca 2+ Uptake and the Fine-Tuning of Aerobic Metabolism*. https://doi.org/10.3389/fphys.2020.554904

Jambrina, E., Alonso, R., Alcalde, M., Rodríguez, M. del C., Serrano, A., Martínez-A., C., García-Sancho, J., & Izquierdo, M. (2003). Calcium influx through receptor-operated channel induces mitochondria-triggered paraptotic cell death. *Journal of Biological Chemistry*, *278*(16), 14134–14145. https://doi.org/10.1074/jbc.M211388200

Janah, L., Kjeldsen, S., Galsgaard, K. D., Winther-Sørensen, M., Stojanovska, E., Pedersen, J., Knop, F. K., Holst, J. J., & Albrechtsen, N. J. W. (2019). Molecular Sciences Glucagon Receptor Signaling and Glucagon Resistance. *Int. J. Mol. Sci.*, *20*(13), 3314. https://doi.org/10.3390/ijms20133314

Jin, J. K., Blackwood, E. A., Azizi, K., Thuerauf, D. J., Fahem, A. G., Hofmann, C., Kaufman, R. J., Doroudgar, S., & Glembotski, C. C. (2017). ATF6 Decreases

Myocardial Ischemia/Reperfusion Damage and Links ER Stress and Oxidative Stress Signaling Pathways in the Heart. *Circulation Research*, *120*(5), 862–875. https://doi.org/10.1161/CIRCRESAHA.116.310266

Kammoun, H. L., Chabanon, H., Hainault, I., Luquet, S., Magnan, C., Koike, T., Ferré, P., & Foufelle, F. (2009). GRP78 expression inhibits insulin and ER stress-induced SREBP-1c activation and reduces hepatic steatosis in mice. *Journal of Clinical Investigation*, *119*(5), 1201–1215. https://doi.org/10.1172/JCI37007

Kang, S., Dahl, R., Hsieh, W., Shin, A., Zsebo, K. M., Buettner, C., Hajjar, R. J., & Lebeche, D. (2016). Small molecular allosteric activator of the sarco/endoplasmic reticulum Ca2+-ATPase (SERCA) attenuates diabetes and metabolic disorders. *Journal of Biological Chemistry*, *291*(10), 5185–5198. https://doi.org/10.1074/jbc.M115.705012

Kang, S. U., Kim, H. J., Kim, D. H., Han, C. H., Lee, Y. S., & Kim, C. H. (2018). Nonthermal plasma treated solution inhibits adipocyte differentiation and lipogenesis in 3T3-L1 preadipocytes via ER stress signal suppression. *Scientific Reports*, *8*(1). https://doi.org/10.1038/s41598-018-20768-5

Kim, H., Mendez, R., Zheng, Z., Chang, L., Cai, J., Zhang, R., & Zhang, K. (2014). *Liver-Enriched Transcription Factor CREBH Interacts With Peroxisome Proliferator-Activated Receptor to Regulate Metabolic Hormone FGF21*. https://doi.org/10.1210/en.2013-1490

Kim, J., Park, M. S., Ha, K., Park, C., Lee, J., Mynatt, R. L., & Chang, J. S. (2018). NT-PGC-1 deficiency decreases mitochondrial FA oxidation in brown adipose tissue and alters substrate utilization in vivo. *Journal of Lipid Research*, *59*(9), 1660–1670. https://doi.org/10.1194/jlr.M085647

Kim, T. H., Park, J. M., Kim, M. Y., & Ahn, Y. H. (2017). The role of CREB3L4 in the proliferation of prostate cancer cells. *Scientific Reports*, *7*. https://doi.org/10.1038/srep45300

Kim, T.-H., Jo, S.-H., Choi, H., Park, J.-M., Kim, M.-Y., Nojima, H., Kim, J.-W., & Ahn, Y.-H. (2014). Identification of Creb3l4 as an essential negative regulator of adipogenesis. *Cell Death and Disease*, *5*. https://doi.org/10.1038/cddis.2014.490

Knutti, D., Kaul, A., & Kralli, A. (2000). *A Tissue-Specific Coactivator of Steroid Receptors, Identified in a Functional Genetic Screen* (Vol. 20, Issue 7). http://tto.trends.com]

Kohjima, M., Higuchi, N., Kato, M., Kotoh, K., Yoshimoto, T., Fujino, T., Yada, M., Yada, R., Harada, N., Enjoji, M., Takayanagu, R., & Nakamuta, M. (2008). SREBP-1c, regulated by the insulin and AMPK signaling pathways, plays a

role in nonalcoholic fatty liver disease. *Int J Mol Med*, *21*(4), 507–511. https://doi.org/https://doi.org/10.3892/ijmm.21.4.507

Kondo, S., Saito, A., Hino, S., Murakami, T., Ogata, M., Kanemoto, S., Nara, S., Yamashita, A., Yoshinaga, K., Hara, H., & Imaizumi, K. (2007). BBF2H7, a Novel Transmembrane bZIP Transcription Factor, Is a New Type of Endoplasmic Reticulum Stress Transducer. *Molecular and Cellular Biology*, *27*(5), 1716–1729. https://doi.org/10.1128/mcb.01552-06

Kressler, D., Schreiber, S. N., Knutti, D., & Kralli, A. (2002). The PGC-1-related protein PERC is a selective coactivator of estrogen receptor α. *Journal of Biological Chemistry*, *277*(16), 13918–13925. https://doi.org/10.1074/jbc.M201134200

Kumar, R., Zakharov, M. N., Khan, S. H., Miki, R., Jang, H., Toraldo, G., Singh, R., Bhasin, S., & Jasuja, R. (2011). The Dynamic Structure of the Estrogen Receptor. *Research Journal of Amino Acids*, *2011*. https://doi.org/10.4061/2011/812540

Landolfi, B., Curci, S., Debellis, L., Pozzan, T., & Hofer, A. M. (1998). Ca 2 Homeostasis in the Agonist-sensitive Internal Store: Functional Interactions Between Mitochondria and the ER Measured In Situ in Intact Cells. In *The Journal of Cell Biology* (Vol. 142, Issue 5). http://www.jcb.org

Larrarte, E., Margareto, J., Novo, F. J., Marti, A., & Alfredo Martínez, J. (2002). UCP1 muscle gene transfer and mitochondrial proton leak mediated thermogenesis. *Archives of Biochemistry and Biophysics*, *404*(1), 166–171. https://doi.org/10.1016/S0003-9861(02)00201-1

Lee, A.-H., Scapa, E. F., Cohen, D. E., & Glimcher, L. H. (2008). Regulation of Hepatic Lipogenesis by the Transcription Factor XBP1. *Science*, *320*(5882), 1492–1496. https://doi.org/10.1126/science.1158042

Lee, D., Hokinson, D., Park, S., Elvira, R., Kusuma, F., Lee, J. M., Yun, M., Lee, S. G., & Han, J. (2019). ER stress induces cell cycle arrest at the g2/m phase through eif2α phosphorylation and GADD45α. *International Journal of Molecular Sciences*, *20*(24). https://doi.org/10.3390/ijms20246309

Lee, J. N., & Ye, J. (2004). Proteolytic activation of sterol regulatory element-binding protein induced by cellular stress through depletion of Insig-1. *Journal of Biological Chemistry*, *279*(43), 45257–45265. https://doi.org/10.1074/jbc.M408235200

Lee, J. Y., Hashizaki, H., Goto, T., Sakamoto, T., Takahashi, N., & Kawada, T. (2011). Activation of peroxisome proliferator-activated receptor-α enhances fatty acid oxidation in human adipocytes. *Biochemical and Biophysical*

Research Communications, *407*(4), 818–822. https://doi.org/10.1016/J.BBRC.2011.03.106

Lee, M. W., Chanda, D., Yang, J., Oh, H., Kim, S. S., Yoon, Y. S., Hong, S., Park, K. G., Lee, I. K., Choi, C. S., Hanson, R. W., Choi, H. S., & Koo, S. H. (2010). Regulation of Hepatic Gluconeogenesis by an ER-Bound Transcription Factor, CREBH. *Cell Metabolism*, *11*(4), 331–339. https://doi.org/10.1016/J.CMET.2010.02.016

Li, S., Shui, K., Zhang, Y., Lv, Y., Deng, W., Ullah, S., Zhang, L., & Xue, Y. (2016). CGDB: a database of circadian genes in eukaryotes. *Nucleic Acids Research*, *45*, 397–403. https://doi.org/10.1093/nar/gkw1028

Liang, G., Audas, T. E., Li, Y., Cockram, G. P., Dean, J. D., Martyn, A. C., Kokame, K., & Lu, R. (2006). Luman/CREB3 Induces Transcription of the Endoplasmic Reticulum (ER) Stress Response Protein Herp through an ER Stress Response Element. *Molecular and Cellular Biology*, *26*(21), 7999–8010. https://doi.org/10.1128/mcb.01046-06

Lin, H., Peng, Y., Li, J., Wang, Z., Chen, S., Qing, X., Pu, F., Lei, M., & Shao, Z. (2021). Reactive Oxygen Species Regulate Endoplasmic Reticulum Stress and ER-Mitochondrial Ca2+Crosstalk to Promote Programmed Necrosis of Rat Nucleus Pulposus Cells under Compression. *Oxidative Medicine and Cellular Longevity*, *2021*. https://doi.org/10.1155/2021/8810698

Liu, L., Cai, J., Wang, H., Liang, X., Zhou, Q., Ding, C., Zhu, Y., Fu, T., Guo, Q., Xu, Z., Xiao, L., Liu, J., Yin, Y., Fang, L., Xue, B., Wang, Y., Meng, Z. X., He, A., Li, J. L., … Gan, Z. (2019). Coupling of COPII vesicle trafficking to nutrient availability by the IRE1α-XBP1s axis. *Proceedings of the National Academy of Sciences of the United States of America*, *116*(24), 11776–11785. https://doi.org/10.1073/pnas.1814480116

Liu, Y., Adachi, M., Zhao, S., Hareyama, M., Koong, A. C., Luo, D., Rando, T. A., Imai, K., & Shinomura, Y. (2009). Preventing oxidative stress: a new role for XBP1. *Cell Death and Differentiation*, *16*, 847–857. https://doi.org/10.1038/cdd.2009.14

Lomax, R. B., Camello, C., van Coppenolle, F., Petersen, O. H., & Tepikin, A. v. (2002). Basal and physiological Ca2+ leak from the endoplasmic reticulum of pancreatic acinar cells. Second messenger-activated channels and translocons. *Journal of Biological Chemistry*, *277*(29), 26479–26485. https://doi.org/10.1074/jbc.M201845200

Lowe, C. E., Dennis, R. J., Obi, U., O'Rahilly, S., & Rochford, J. J. (2012). Investigating the involvement of the ATF6α pathway of the unfolded protein response in adipogenesis. *International Journal of Obesity*, *36*(9), 1248–1251. https://doi.org/10.1038/ijo.2011.233

Lu, P. D., Harding, H. P., & Ron, D. (2004). Translation reinitiation at alternative open reading frames regulates gene expression in an integrated stress response. *Journal of Cell Biology*, *167*(1), 27–33. https://doi.org/10.1083/jcb.200408003

Lu, R., Yang, P., O'hare, P., & Misra, V. (1997). Luman, a New Member of the CREB/ATF Family, Binds to Herpes Simplex Virus VP16-Associated Host Cellular Factor. In *MOLECULAR AND CELLULAR BIOLOGY* (Vol. 17, Issue 9). https://journals.asm.org/journal/mcb

Marcelo, K. L., Means, A. R., & York, B. (2016). The Ca2+/Calmodulin/CaMKK2 Axis: Nature's Metabolic CaMshaft. *Trends in Endocrinology & Metabolism*, *27*(10), 706–718. https://doi.org/10.1016/J.TEM.2016.06.001

Martyn, A. C., Choleris, E., Gillis, D. J., Armstrong, J. N., Amor, T. R., McCluggage, A. R. R., Turner, P. v., Liang, G., Cai, K., & Lu, R. (2012). Luman/CREB3 Recruitment Factor Regulates Glucocorticoid Receptor Activity and Is Essential for Prolactin-Mediated Maternal Instinct. *Molecular and Cellular Biology*, *32*(24), 5140–5150. https://doi.org/10.1128/mcb.01142-12

Miller, B. H., Mcdearmon, E. L., Panda, S., Hayes, K. R., Zhang, J., Andrews, J. L., Antoch, M. P., Walker, J. R., Esser, K. A., Hogenesch, J. B., & Takahashi, J. S. (2007). *Circadian and CLOCK-controlled regulation of the mouse transcriptome and cell proliferation*. www.pnas.org/cgi/content/full/

Miller, K. K., Parulekar, M. S., Schoenfeld, E., Anderson, E., Hubbard, J., Klibanski, A., Grinspoon, S. K., & Unit, N. (1998). *Decreased Leptin Levels in Normal Weight Women with Hypothalamic Amenorrhea: The Effects of Body Composition and Nutritional Intake**. https://academic.oup.com/jcem/article/83/7/2309/2865258

Minster, R. L., Hawley, N. L., Su, C. T., Sun, G., Kershaw, E. E., Cheng, H., Buhule, O. D., Lin, J., Reupena, M. S., Viali, S., Tuitele, J., Naseri, T., Urban, Z., Deka, R., Weeks, D. E., & McGarvey, S. T. (2016). A thrifty variant in CREBRF strongly influences body mass index in Samoans. *Nature Genetics*, *48*(9), 1049–1054. https://doi.org/10.1038/ng.3620

Mirabelli, C., Pelletier, I., eoul, F. T., Vidalain, P.-O., Brisac, C., ed eric Tangy, F., Delpeyroux, F., & Blondel, B. (2016). The CREB3-Herp signalling module limits the cytosolic calcium concentration increase and apoptosis induced by poliovirus. *J Gen Virol*, *97*(9), 2194–2200. https://doi.org/10.1099/jgv.0.000544

Moncan, M., Mnich, K., Blomme, A., Almanza, A., Samali, A., & Gorman, A. M. (2021). Regulation of lipid metabolism by the unfolded protein response. In *Journal of Cellular and Molecular Medicine* (Vol. 25, Issue 3, pp. 1359–1370). Blackwell Publishing Inc. https://doi.org/10.1111/jcmm.16255

Moschinger, M., Hilse, K. E., Rupprecht, A., Zeitz, U., Erben, R. G., Rülicke, T., & Pohl, E. E. (2019). Age-related sex differences in the expression of important disease-linked mitochondrial proteins in mice. *Biology of Sex Differences*, *10*(56). https://doi.org/10.1186/s13293-019-0267-1

Murakami, T., Saito, A., Hino, S. I., Kondo, S., Kanemoto, S., Chihara, K., Sekiya, H., Tsumagari, K., Ochiai, K., Yoshinaga, K., Saitoh, M., Nishimura, R., Yoneda, T., Kou, I., Furuichi, T., Ikegawa, S., Ikawa, M., Okabe, M., Wanaka, A., & Imaizumi, K. (2009). Signalling mediated by the endoplasmic reticulum stress transducer OASIS is involved in bone formation. *Nature Cell Biology*, *11*(10), 1205–1211. https://doi.org/10.1038/ncb1963

Murphy, E., & Steenbergen, C. (2021). Regulation of Mitochondrial Ca 2+ Uptake. *Annual Review of Physiology Annu. Rev. Physiol. 2021*, *83*, 107–126. https://doi.org/10.1146/annurev-physiol-031920

Nakagawa, Y., Satoh, A., Tezuka, H., Han, S.-I., Takei, K., Iwasaki, H., Yatoh, S., Yahagi, N., Suzuki, H., Iwasaki, Y., Sone, H., Matsuzaka, T., Yamada, N., & Shimano, H. (2016). *CREB3L3 controls fatty acid oxidation and ketogenesis in synergy with PPARα*. https://doi.org/10.1038/srep39182

Nakagawa, Y., & Shimano, H. (2018). CREBH regulates systemic glucose and lipid metabolism. In *International Journal of Molecular Sciences* (Vol. 19, Issue 5). MDPI AG. https://doi.org/10.3390/ijms19051396

Nakagawa, Y., Wang, Y., Han, S. iee, Okuda, K., Oishi, A., Yagishita, Y., Kumagai, K., Ohno, H., Osaki, Y., Mizunoe, Y., Araki, M., Murayama, Y., Iwasaki, H., Konishi, M., Itoh, N., Matsuzaka, T., Sone, H., Yamada, N., & Shimano, H. (2021). Enterohepatic Transcription Factor CREB3L3 Protects Atherosclerosis via SREBP Competitive Inhibition. *CMGH*, *11*(4), 949–971. https://doi.org/10.1016/j.jcmgh.2020.11.004

Navid, F., & Colbert, R. A. (2017). Causes and consequences of endoplasmic reticulum stress in rheumatic disease. In *Nature Reviews Rheumatology* (Vol. 13, Issue 1, pp. 25–40). Nature Publishing Group. https://doi.org/10.1038/nrrheum.2016.192

Nedergaard, J., Golozoubova, V., Matthias, A., Asadi, A., Jacobsson, A., & Cannon, B. (2001). UCP1: the only protein able to mediate adaptive non-shivering thermogenesis and metabolic inefficiency. *Biochimica et Biophysica Acta (BBA) - Bioenergetics*, *1504*(1), 82–106. https://doi.org/10.1016/S0005-2728(00)00247-4

Omori, Y., Imai, J. ichi, Suzuki, Y., Watanabe, S., Tanigami, A., & Sugano, S. (2002). OASIS is a transcriptional activator of CREB/ATF family with a transmembrane domain. *Biochemical and Biophysical Research*

Communications, *293*(1), 470–477. https://doi.org/10.1016/S0006-291X(02)00253-X

Oyadomari, S., Harding, H. P., Zhang, Y., Oyadomari, M., & Ron, D. (2008). Dephosphorylation of Translation Initiation Factor 2α Enhances Glucose Tolerance and Attenuates Hepatosteatosis in Mice. *Cell Metabolism*, *7*(6), 520–532. https://doi.org/10.1016/j.cmet.2008.04.011

Ozes, O. N., Akca, H., Mayo, L. D., Gustin, J. A., Maehama, T., Dixon, J. E., Donner, D. B., & Kahn, C. R. (2001). *A phosphatidylinositol 3-kinaseAktmTOR pathway mediates and PTEN antagonizes tumor necrosis factor inhibition of insulin signaling through insulin receptor substrate-1*. www.pnas.orgcgidoi10.1073pnas.051042298

Paiva, P., Sousa, S. F., Ramos, M. J., & Fernandes, P. A. (2018). Understanding the Catalytic Machinery and the Reaction Pathway of the Malonyl-Acetyl Transferase Domain of Human Fatty Acid Synthase. *ACS Catalysis*, *8*(6), 4860–4872. https://doi.org/10.1021/acscatal.8b00577

Panagopoulos, I., Möller, E., Dahlén, A., Isaksson, M., Mandahl, N., Vlamis-Gardikas, A., & Mertens, F. (2007). Characterization of the native CREB3L2 transcription factor and the FUS/CREB3L2 chimera. *Genes Chromosomes and Cancer*, *46*(2), 181–191. https://doi.org/10.1002/gcc.20395

Park, S. M., Kang, T. il, & So, J. S. (2021). Roles of XBP1s in transcriptional regulation of target genes. In *Biomedicines* (Vol. 9, Issue 7). MDPI AG. https://doi.org/10.3390/biomedicines9070791

Park, S. W., Zhou, Y., Lee, J., Lee, J., & Ozcan, U. (2010). Sarco(endo)plasmic reticulum Ca2+-ATPase 2b is a major regulator of endoplasmic reticulum stress and glucose homeostasis in obesity. *Proceedings of the National Academy of Sciences of the United States of America*, *107*(45), 19320–19325. https://doi.org/10.1073/pnas.1012044107

Peng, T. I., & Jou, M. J. (2010). Oxidative stress caused by mitochondrial calcium overload. *Annals of the New York Academy of Sciences*, *1201*, 183–188. https://doi.org/10.1111/j.1749-6632.2010.05634.x

Penney, J. (2017). *Characterization of the potential role of Luman as a novel regulator of animal stress responses*. University of Guelph.

Penney, J., Mendell, A., Zeng, M., Tran, K., Lymer, J., Turner, P. v., Choleris, E., MacLusky, N., & Lu, R. (2017). LUMAN/CREB3 is a key regulator of glucocorticoid-mediated stress responses. *Molecular and Cellular Endocrinology*, *439*, 95–104. https://doi.org/10.1016/J.MCE.2016.10.022

Penney, J., Taylor, T., MacLusky, N., & Lu, R. (2018). LUMAN/CREB3 Plays a Dual Role in Stress Responses as a Cofactor of the Glucocorticoid Receptor

and a Regulator of Secretion. *Frontiers in Molecular Neuroscience*, *11*. https://doi.org/10.3389/fnmol.2018.00352

Peoples, J. N., Saraf, A., Ghazal, N., Pham, T. T., & Kwong, J. Q. (2019). Mitochondrial dysfunction and oxidative stress in heart disease. In *Experimental and Molecular Medicine* (Vol. 51, Issue 12). Springer Nature. https://doi.org/10.1038/s12276-019-0355-7

Piperi, C., Adamopoulos, C., & Papavassiliou, A. G. (2016). XBP1: A Pivotal Transcriptional Regulator of Glucose and Lipid Metabolism. In *Trends in Endocrinology and Metabolism* (Vol. 27, Issue 3, pp. 119–122). Elsevier Inc. https://doi.org/10.1016/j.tem.2016.01.001

Porstmann, T., Santos, C. R., Griffiths, B., Cully, M., Wu, M., Leevers, S., Griffiths, J. R., Chung, Y. L., & Schulze, A. (2008). SREBP Activity Is Regulated by mTORC1 and Contributes to Akt-Dependent Cell Growth. *Cell Metabolism*, *8*(3), 224–236. https://doi.org/10.1016/J.CMET.2008.07.007

Pramfalk, C., Pavlides, M., Banerjee, R., McNeil, C. A., Neubauer, S., Karpe, F., & Hodson, L. (2015). Sex-specific differences in hepatic fat oxidation and synthesis may explain the higher propensity for NAFLD in men. *Journal of Clinical Endocrinology and Metabolism*, *100*(12), 4425–4433. https://doi.org/10.1210/JC.2015-2649

Puigserver, P., & Spiegelman, B. M. (2003). *Peroxisome Proliferator-Activated Receptor-Coactivator 1 (PGC-1): Transcriptional Coactivator and Metabolic Regulator*. https://doi.org/10.1210/er.2002-0012

Puigserver, P., Wu, Z., Park, C. W., Graves, R., Wright, M., & Spiegelman, B. M. (1998). A Cold-Inducible Coactivator of Nuclear Receptors Linked to Adaptive Thermogenesis. *Cell*, *92*(6), 829–839. https://doi.org/10.1016/S0092-8674(00)81410-5

Purdom, T., Kravitz, L., Dokladny, K., & Mermier, C. (2018). Understanding the factors that effect maximal fat oxidation. In *Journal of the International Society of Sports Nutrition* (Vol. 15, Issue 1). BioMed Central Ltd. https://doi.org/10.1186/s12970-018-0207-1

Qi, H., Fillion, C., Labrie, Y., Grenier, J., Fournier, A., Berger, L., El-Alfy, M., & Labrie, C. (2002). AIbZIP, a Novel bZIP Gene Located on Chromosome 1q21.3 That Is Highly Expressed in Prostate Tumors and of Which the Expression Is Up-Regulated by Androgens in LNCaP Human Prostate Cancer Cells 1. In *CANCER RESEARCH* (Vol. 62). http://aacrjournals.org/cancerres/article-pdf/62/3/721/2500667/ch0302000721.pdf

Qiu, S., Vazquez, J. T., Boulger, E., Liu, H., Xue, P., Hussain, M. A., & Wolfe, A. (2017). Hepatic estrogen receptor α is critical for regulation of gluconeogenesis and lipid metabolism in males. *Scientific Reports*, *7*(1). https://doi.org/10.1038/s41598-017-01937-4

Raggo, C., Rapin, N., Stirling, J., Gobeil, P., Smith-Windsor, E., O'Hare, P., & Misra, V. (2002). Luman, the Cellular Counterpart of Herpes Simplex Virus VP16, Is Processed by Regulated Intramembrane Proteolysis. *Molecular and Cellular Biology*, *22*(16), 5639–5649. https://doi.org/10.1128/mcb.22.16.5639-5649.2002

Rhee, J., Inoue, Y., Yoon, J. C., Puigserver, P., Fan, M., Gonzalez, F. J., & Spiegelman, B. M. (2003). *Regulation of hepatic fasting response by PPAR coactivator-1 (PGC-1): Requirement for hepatocyte nuclear factor 4 in gluconeogenesis*. www.pnas.orgcgidoi10.1073pnas.0730870100

Rodríguez, A. M., Monjo, M., Roca, P., & Palou, A. (2002). Opposite actions of testosterone and progesterone on UCP1 mRNA expression in cultured brown adipocytes. In *CMLS, Cell. Mol. Life Sci* (Vol. 59).

Rooney, T. A., Renard, D. C., Sass, E. J., & Thomas, A. P. (1991). Oscillatory cytosolic calcium waves independent of stimulated inositol 1,4,5-trisphosphate formation in hepatocytes. *Journal of Biological Chemistry*, *266*(19), 12272–12282. https://doi.org/10.1016/s0021-9258(18)98892-7

Ruan, H. bin, Han, X., Li, M. D., Singh, J. P., Qian, K., Azarhoush, S., Zhao, L., Bennett, A. M., Samuel, V. T., Wu, J., Yates, J. R., & Yang, X. (2012). O-GlcNAc transferase/host cell factor C1 complex regulates gluconeogenesis by modulating PGC-1α stability. *Cell Metabolism*, *16*(2), 226–237. https://doi.org/10.1016/j.cmet.2012.07.006

Sa, A., Yab, S., & Sh, A. (2014). Hepatic CREB3L3 Controls Whole-Body Energy Homeostasis and Improves Obesity and Diabetes. *S Endo.Endojournals.Org Endocrinology*, *155*(12), 4706–4719. https://doi.org/10.1210/en.2014-1113

Sabaratnam, K., Renner, M., Paesen, G., Harlos, K., Nair, V., Owens, R. J., & Grimes, J. M. (2019). Insights from the crystal structure of the chicken CREB3 bZIP suggest that members of the CREB3 subfamily transcription factors may be activated in response to oxidative stress. *Protein Science*, *28*(4), 779–787. https://doi.org/10.1002/pro.3573

Sadowska-Krpa, E., Klapciska, B., Nowara, A., Jagsz, S., Szoltysek-Boldys, I., Chalimoniuk, M., Langfort, J., & Chrapusta, S. J. (2020). High-dose testosterone supplementation disturbs liver pro-oxidant/antioxidant balance and function in adolescent male Wistar rats undergoing moderate-intensity endurance training. *PeerJ*, *8*. https://doi.org/10.7717/peerj.10228

Saito, A., Kanemoto, S., Zhang, Y., Asada, R., Hino, K., & Imaizumi, K. (2014). Chondrocyte Proliferation Regulated by Secreted Luminal Domain of ER Stress Transducer BBF2H7/CREB3L2. *Molecular Cell*, *53*(1), 127–139. https://doi.org/10.1016/J.MOLCEL.2013.11.008

Salway, J. G. (2018). The Krebs Uric Acid Cycle: A Forgotten Krebs Cycle. *Trends in Biochemical Sciences*, *43*(11), 847–849. https://doi.org/10.1016/J.TIBS.2018.04.012

Sampieri, L., di Giusto, P., & Alvarez, C. (2019). CREB3 transcription factors: ER-golgi stress transducers as hubs for cellular homeostasis. In *Frontiers in Cell and Developmental Biology* (Vol. 7). Frontiers Media S.A. https://doi.org/10.3389/fcell.2019.00123

Sanyal, A. J., & Pacana, T. (2015). *A Lipidomic Readout of Disease Progression in A Diet-Induced Mouse Model of Nonalcoholic Fatty Liver Disease. Trans Am Clin Climatol Assoc.*

Satoh, A., Han, S. iee, Araki, M., Nakagawa, Y., Ohno, H., Mizunoe, Y., Kumagai, K., Murayama, Y., Osaki, Y., Iwasaki, H., Sekiya, M., Konishi, M., Itoh, N., Matsuzaka, T., Sone, H., & Shimano, H. (2020). CREBH Improves Diet-Induced Obesity, Insulin Resistance, and Metabolic Disturbances by FGF21-Dependent and FGF21-Independent Mechanisms. *IScience*, *23*(3). https://doi.org/10.1016/j.isci.2020.100930

Scheuner, D., Song, B., McEwen, E., Liu, C., Laybutt, R., Gillespie, P., Saunders, T., Bonner-Weir, S., & Kaufman, R. J. (2001). Translational Control Is Required for the Unfolded Protein Response and In Vivo Glucose Homeostasis. *Molecular Cell*, *7*(6), 1165–1176. https://doi.org/10.1016/S1097-2765(01)00265-9

Schmitt, C. C., Aranias, T., Viel, T., Chateau, D., le Gall, M., Waligora-Dupriet, A.-J., Melchior, C., Rouxel, O., Kapel, N., Gourcerol, G., Tavitian, B., Lehuen, A., Brot-Laroche, E., Leturque, A., Serradas, P., & Grosfeld, A. (2017). Intestinal invalidation of the glucose transporter GLUT2 delays tissue distribution of glucose and reveals an unexpected role in gut homeostasis. *Molecular Metabolism*, *6*(1), 61–72. https://doi.org/10.1016/j.molmet.2016.10.008ï

Scialò, F., Sriram, A., Fernández-Ayala, D., Gubina, N., Lõhmus, M., Nelson, G., Logan, A., Cooper, H. M., Navas, P., Enríquez, J. A., Murphy, M. P., & Sanz, A. (2016). Mitochondrial ROS Produced via Reverse Electron Transport Extend Animal Lifespan. *Cell Metabolism*, *23*(4), 725–734. https://doi.org/10.1016/J.CMET.2016.03.009

Sha, H., He, Y., Chen, H., Wang, C., Zenno, A., Shi, H., Yang, X., Zhang, X., & Qi, L. (2009). The IRE1α-XBP1 Pathway of the Unfolded Protein Response Is

Required for Adipogenesis. *Cell Metabolism*, *9*(6), 556–564. https://doi.org/10.1016/j.cmet.2009.04.009

Shen, Y., Babu Thillaiappan, N., & Taylor, C. W. (2021). The store-operated Ca 2+ entry complex comprises a small cluster of STIM1 associated with one Orai1 channel. *PNAS*, *118*(10). https://doi.org/10.1073/pnas.2010789118/-/DCSupplemental

Spiegelman, B., Puigserver, P., & Wu, Z. (2000). Regulation of adipogenesis and energy balance. In *International Journal of Obesity* (Vol. 24). www.nature.com/ijo

Sriburi, R., Bommiasamy, H., Buldak, G. L., Robbins, G. R., Frank, M., Jackowski, S., & Brewer, J. W. (2007). Coordinate regulation of phospholipid biosynthesis and secretory pathway gene expression in XBP-1(S)-induced endoplasmic reticulum biogenesis. *Journal of Biological Chemistry*, *282*(10), 7024–7034. https://doi.org/10.1074/jbc.M609490200

Tamaru, T., Hattori, M., Ninomiya, Y., Kawamura, G., Varès, G., Honda, K., Mishra, D. P., Wang, B., Benjamin, I., Sassone-Corsi, P., Ozawa, T., & Takamatsu, K. (2013). ROS stress resets circadian clocks to coordinate pro-survival signals. *PLoS ONE*, *8*(12). https://doi.org/10.1371/journal.pone.0082006

Tanis, R. M., Piroli, G. G., Day, S. D., & Frizzell, N. (2015). The effect of glucose concentration and sodium phenylbutyrate treatment on mitochondrial bioenergetics and ER stress in 3T3-L1 adipocytes. *Biochimica et Biophysica Acta (BBA) - Molecular Cell Research*, *1853*(1), 213–221. https://doi.org/10.1016/J.BBAMCR.2014.10.012

Toprak, U., Doğan, C., & Hegedus, D. (2021). A comparative perspective on functionally-related, intracellular calcium channels: The insect Ryanodine and Inositol 1,4,5-trisphosphate receptors. In *Biomolecules* (Vol. 11, Issue 7). MDPI AG. https://doi.org/10.3390/biom11071031

Torrealba, N., Navarro-Marquez, M., Garrido, V., Pedrozo, Z., Romero, D., Eura, Y., Villalobos, E., Roa, J. C., Chiong, M., Kokame, K., & Lavandero, S. (2017). Herpud1 negatively regulates pathological cardiac hypertrophy by inducing IP3 receptor degradation. *Scientific Reports*, *7*(1). https://doi.org/10.1038/s41598-017-13797-z

Trujillo-Viera, J., El-Merahbi, R., Schmidt, V., Karwen, T., Loza-Valdes, A., Strohmeyer, A., Reuter, S., Noh, M., Wit, M., Hawro, I., Mocek, S., Fey, C., Mayer, A. E., Löffler, M. C., Wilhelmi, I., Metzger, M., Ishikawa, E., Yamasaki, S., Rau, M., … Sumara, G. (2021). Protein Kinase D2 drives chylomicron-mediated lipid transport in the intestine and promotes obesity. *EMBO Molecular Medicine*, *13*(5). https://doi.org/10.15252/emmm.202013548

Uht, R. M., Anderson, C. M., Webb, P., & Kushner, P. J. (1997). Transcriptional Activities of Estrogen and Glucocorticoid Receptors Are Functionally Integrated at the AP-1 Response Element*. *Endocrinology*, *138*(7), 2900–2908. https://academic.oup.com/endo/article/138/7/2900/2988309

Usui, M., Yamaguchi, S., Tanji, Y., Tominaga, R., Ishigaki, Y., Fukumoto, M., Katagiri, H., Mori, K., Oka, Y., & Ishihara, H. (2012). Atf6α-null mice are glucose intolerant due to pancreatic β-cell failure on a high-fat diet but partially resistant to diet-induced insulin resistance. *Metabolism: Clinical and Experimental*, *61*(8), 1118–1128. https://doi.org/10.1016/j.metabol.2012.01.004

van der Reest, J., Lilla, S., Zheng, L., Zanivan, S., & Gottlieb, E. (2018). Proteome-wide analysis of cysteine oxidation reveals metabolic sensitivity to redox stress. *Nature Communications*, *9*(1). https://doi.org/10.1038/s41467-018-04003-3

Walter, P., & Ron, D. (2011). *The Unfolded Protein Response: From Stress Pathway to Homeostatic Regulation*. https://www.science.org

Wang, C., Huang, Z., Du, Y., Cheng, Y., Chen, S., & Guo, F. (2010). ATF4 regulates lipid metabolism and thermogenesis. *Cell Research*, *20*(2), 174–184. https://doi.org/10.1038/cr.2010.4

Wang, X., Sato, R., Brown, M. S., Hua, X., & Goldstein, J. L. (1994). SREBP-1, a membrane-bound transcription factor released by sterol-regulated proteolysis. *Cell*, *77*(1), 53–62. https://doi.org/10.1016/0092-8674(94)90234-8

Wible, R. S., Ramanathan, C., Sutter, C. H., Olesen, K. M., Kensler, T. W., Liu, A. C., & Sutter, T. R. (2018). *NRF2 regulates core and stabilizing circadian clock loops, coupling redox and timekeeping in Mus musculus*. https://doi.org/10.7554/eLife.31656.001

Wu, Z., Puigserver, P., Andersson, U., Zhang, C., Adelmant, G., Mootha, V., Troy, A., Cinti, S., Lowell, B., Scarpulla, R. C., & Spiegelman, B. M. (1999). Mechanisms Controlling Mitochondrial Biogenesis and Respiration through the Thermogenic Coactivator PGC-1. *Cell*, *98*(1), 115–124. https://doi.org/10.1016/S0092-8674(00)80611-X

Xiao, W. C., Zhang, J., Chen, S. L., Shi, Y. J., Xiao, F., & An, W. (2018). Alleviation of palmitic acid-induced endoplasmic reticulum stress by augmenter of liver regeneration through IP3R-controlled Ca2+ release. *Journal of Cellular Physiology*, *233*(8), 6148–6157. https://doi.org/10.1002/jcp.26463

Yamamoto, K., Takahara, K., Oyadomari, S., Okada, T., Sato, T., Harada, A., & Mori, K. (2010). Induction of Liver Steatosis and Lipid Droplet Formation in ATF6-Knockout Mice Burdened with Pharmacological Endoplasmic Reticulum

Stress. *Molecular Biology of the Cell*, *21*, 2975–2986. https://doi.org/10.1091/mbc.E09

Yamamoto1, K., Yoshida2, H., Kokame4, K., Kaufman5, R. J., & Mori2, K. (2004). Differential Contributions of ATF6 and XBP1 to the Activation of Endoplasmic Reticulum Stress-Responsive cis-Acting Elements ERSE, UPRE and ERSE-‡U. *J. Biochem*, *136*, 343–350. https://doi.org/10.1093/jb/mvh

Ying, Z., Zhang, R., Verge, V. M. K., & Misra, V. (2015). Cloning and Characterization of Rat Luman/CREB3, A Transcription Factor Highly Expressed in Nervous System Tissue. *Journal of Molecular Neuroscience*, *55*(2), 347–354. https://doi.org/10.1007/s12031-014-0330-7

Yoshida, H., Haze, K., Yanagi, H., Yura, T., & Mori, K. (1998). Identification of the cis-acting endoplasmic reticulum stress response element responsible for transcriptional induction of mammalian glucose- regulated proteins: Involvement of basic leucine zipper transcription factors. *Journal of Biological Chemistry*, *273*(50), 33741–33749. https://doi.org/10.1074/jbc.273.50.33741

Yoshida, H., Matsui, T., Yamamoto, A., Okada, T., & Mori, K. (2001). XBP1 mRNA Is Induced by ATF6 and Spliced by IRE1 in Response to ER Stress to Produce a Highly Active Transcription Factor phorylation, the activated Ire1p specifically cleaves HAC1 precursor mRNA to remove an intron of 252 nucle-otides. The cleaved 5 and 3 halves of mature HAC1 mRNA are ligated by Rlg1p (tRNA ligase). HAC1 mRNA encodes the basic leucine zipper (bZIP). In *Cell* (Vol. 107).

Yoshida, H., Okada, T., Haze, K., Yanagi, H., Yura, T., Negishi, M., & Mori, K. (2000). ATF6 Activated by Proteolysis Binds in the Presence of NF-Y (CBF) Directly to the cis-Acting Element Responsible for the Mammalian Unfolded Protein Response. In *MOLECULAR AND CELLULAR BIOLOGY* (Vol. 20, Issue 18). https://journals.asm.org/journal/mcb

Yoshizawa, T., Hinoi, E., Dae, Y. J., Kajimura, D., Ferron, M., Seo, J., Graff, J. M., Kim, J. K., & Karsenty, G. (2009). The transcription factor ATF4 regulates glucose metabolism in mice through its expression in osteoblasts. *Journal of Clinical Investigation*, *119*(9), 2807–2817. https://doi.org/10.1172/JCI39366

Young, S. G., Fong, L. G., Beigneux, A. P., Allan, C. M., He, C., Jiang, H., Nakajima, K., Meiyappan, M., Birrane, G., & Ploug, M. (2019). GPIHBP1 and Lipoprotein Lipase, Partners in Plasma Triglyceride Metabolism. In *Cell Metabolism* (Vol. 30, Issue 1, pp. 51–65). Cell Press. https://doi.org/10.1016/j.cmet.2019.05.023

Yu, Y., Pierciey, F. J., Maguire, T. G., & Alwine, J. C. (2013). PKR-Like Endoplasmic Reticulum Kinase Is Necessary for Lipogenic Activation during

HCMV Infection. *PLoS Pathog*, *9*(4). https://doi.org/10.1371/journal.ppat.1003266

Yu, Z., Dou, F., Wang, Y., Hou, L., & Chen, H. (2018). Ca2+-dependent endoplasmic reticulum stress correlation with astrogliosis involves upregulation of KCa3.1 and inhibition of AKT/mTOR signaling 11 Medical and Health Sciences 1109 Neurosciences. *Journal of Neuroinflammation*, *15*(1). https://doi.org/10.1186/s12974-018-1351-x

Zeng, L., Lu, M., Mori, K., Luo, S., Lee, A. S., Zhu, Y., & Shyy, J. Y. J. (2004). ATF6 modulates SREBP2-mediated lipogenesis. *EMBO Journal*, *23*(4), 950–958. https://doi.org/10.1038/sj.emboj.7600106

Zha, B. S., & Zhou, H. (2012). ER Stress and Lipid Metabolism in Adipocytes. *Biochemistry Research International*, *2012*. https://doi.org/10.1155/2012/312943

Zhang, C., Wang, G., Zheng, Z., Maddipati, K. R., Zhang, X., Dyson, G., Williams, P., Duncan, S. A., Kaufman, R. J., & Zhang, K. (2012). Endoplasmic reticulum-tethered transcription factor cAMP responsive element-binding protein, hepatocyte specific, regulates hepatic lipogenesis, fatty acid oxidation, and lipolysis upon metabolic stress in mice. *Hepatology*, *55*(4), 1070–1082. https://doi.org/10.1002/hep.24783

Zhang, K., Wang, S., Malhotra, J., Hassler, J. R., Back, S. H., Wang, G., Chang, L., Xu, W., Miao, H., Leonardi, R., Chen, Y. E., Jackowski, S., & Kaufman, R. J. (2011). The unfolded protein response transducer IRE1Î ± prevents ER stress-induced hepatic steatosis. *EMBO Journal*, *30*(7), 1357–1375. https://doi.org/10.1038/emboj.2011.52

Zhang, T., Chen, J., Tang, X., Luo, Q., Xu, D., & Yu, B. (2019). Interaction between adipocytes and high-density lipoprotein:new insights into the mechanism of obesity-induced dyslipidemia and atherosclerosis. In *Lipids in Health and Disease* (Vol. 18, Issue 1). BioMed Central Ltd. https://doi.org/10.1186/s12944-019-1170-9

Zhao, R. Z., Jiang, S., Zhang, L., & Yu, Z. bin. (2019). Mitochondrial electron transport chain, ROS generation and uncoupling (Review). In *International Journal of Molecular Medicine* (Vol. 44, Issue 1, pp. 3–15). Spandidos Publications. https://doi.org/10.3892/ijmm.2019.4188

Zhenqi, Z., M, M. T., G, D. B., Vicent, R., Jonathan, W., Mete, C., Mayuko, S., M, W. D., Frode, N., M, S. M., R, S. A., A, W. K., Ellen, L., R, R. B., Laurent, V., Karen, R., Prashant, R., Peter, T., Jason, L., … L, H. A. (2020). Estrogen receptor α controls metabolism in white and brown adipocytes by regulating Polg1 and mitochondrial remodeling. *Science Translational Medicine*, *12*(555), eaax8096. https://doi.org/10.1126/scitranslmed.aax8096

Zhu, X., Xiong, T., Liu, P., Guo, X., Xiao, L., Zhou, F., Tang, Y., & Yao, P. (2018). Quercetin ameliorates HFD-induced NAFLD by promoting hepatic VLDL assembly and lipophagy via the IRE1a/XBP1s pathway. *Food and Chemical Toxicology*, *114*, 52–60. https://doi.org/10.1016/J.FCT.2018.02.019

Appendix

Gene	Forward (5'-3')	Reverse (5'-3')
Pgc-1a	TGAAAAAGCTTGACTGGCGTC	ACCAGAGCAGCACACTCTATG
Lpl	GGAGAAGCCATCCGTGTGAT	CTCAGGCAGAGCCCTTTCTC
Ppary	TTGCTGTGGGGATGTCTCAC	AACAGCTTCTCCTTCTCGGC
Ppara	CCTCAGGGTACCACTACGGA	TTGCAGCTCCGATCACACTT
Creb3	GGGTGCGGTTTAGAGTGACA	CCACCAGGATCCATTTGGGA
Sqle	AGCTTGGTCCTCAAGTCCAC	AGTCCACGTGCAGTCAAGTC
Apoa4	TACGTATGCTGATGGGGTGC	TCTGCATGTTCTCCCCGAAC
Pepck	TGCGGATCATGACTCGGATG	AGGCCCAGTTGTTGACCAAA
Mtp	CTCTTGGCAGTGCTTTTTCTCT	GAGCTTGTATAGCCGCTCATT
Scd1	TTCTTGCGATACACTCTGGTGC	CGGGATTGAATGTTCTTGTCGT
Dgat2	GCGCTACTTCCGAGACTACTT	GGGCCTTATGCCAGGAAACT
Acox1	TAACTTCCTCACTCGAAGCCA	AGTTCCATGACCCATCTCTGTC
Fasn	GGAGGTGGTGATAGCCGGTAT	TGGGTAATCCATAGAGCCCAG
Cyp3a4	AGGCACCTCCCACGTATGAT	ATCACTGTGACCCTTGGGGA
Hmgcr	AGCTTGCCCGAATTGTATGTG	TCTGTTGTGAACCATGTGACTTC
Gr	CCACTGCAGGAGTCTCACAA	AGCAGTGACACCAGGGTAGG
Gapdh	TACCCCCAATGTGTCCGTCG	CCTGCTTCACCACCTTCTTG
Creb3-genotype	CACAGCATGAGTGGAGAGGGTAG	AAGAGACGAGAGGAGACGGTAG
lacZ-genotype	GGTAAACTGGCTCGGATTAGGG	TTGACTGTAGCGGCTGATGTTG
Chop	GCAGCGACAGAGCCAGAATAA	TTCTGCTTTCAGGTGTGGTGG
Grp78	TTCAGCCAATTATCAGCAAACTCT	TTTTCTGATGTATCCTCTTCACCAGT
Xbp1	CTGGAACAGCAAGTGGTAGA	CTGGGTCCTTCTGGGTAGAC
Xbp1-s	GGCCTTGTAGTTGAGAACCAG	GTCCAAGTTGTCCAGAATGC
Atf6	TCGCCTTTTAGTCCGGTTCTT	GGCTCCATAGGTCTGACTCC
Catalase	TCGAGTGGCCAACTACCAGCGTG	GTACTTGTCCAGAAGAGCCTGGATG
Sod1	AACCAGTTGTGTTGTCAGGAC	CCACCATGTTTCTTAGAGTGAGG
Creb3-qRTPCR	CCCACAAATCTCCGCTTTCC	GGTTCGGAGGTTGGATCTG
Actin	CTTTCTACAATGAGCTGCGT	TCATGAGGTAGTCTGTCAG

Sup Table 1: Primer sequences used for qRTPCR analysis and mouse genotyping. Primer efficiencies were completed for each set of qRTPCR primers and determined to be between 90-110%.

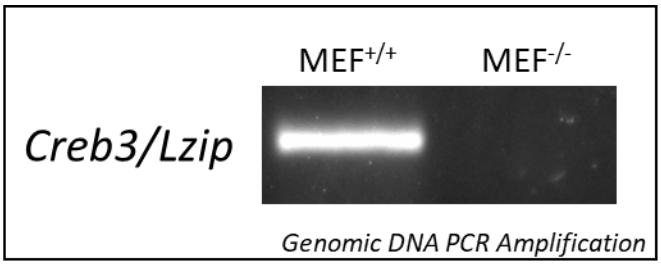

Sup Figure 1: Genomic PCR amplification of *Creb3* in MEF$^{+/+}$ and MEF$^{-/-}$ cells.

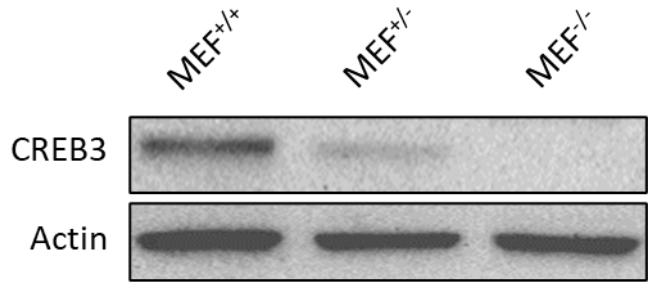

Sup Figure 2: Western blot of CREB3 protein expression in $MEF^{+/+}$, $MEF^{+/-}$, and $MEF^{-/-}$ cells.

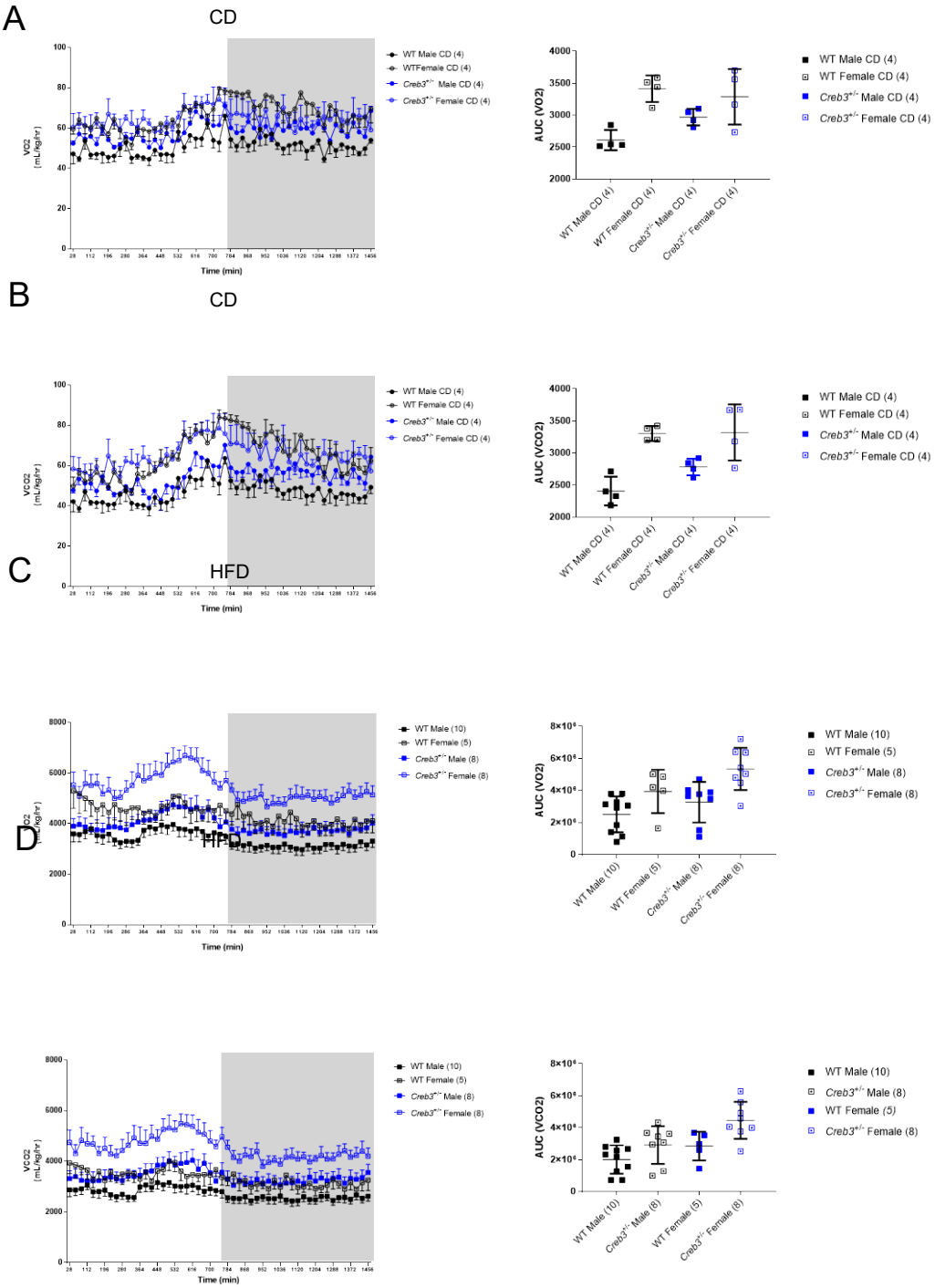

Sup Figure 3: WT and *Creb3*$^{+/-}$ mice VO2 and VCO2 exchange on control and HFD. 16-week-old male and female WT, and *Creb3*$^{+/-}$ mice fed a CD or HFD for 8 weeks. **(A)** VO2 consumption over 24 hours and AUC, n=4 per group (CD WT males: solid black circles, *Creb3*$^{+/-}$ males: solid blue circles, WT females: open black circles, *Creb3*$^{+/-}$ females: open blue circles) **(B)** CD VCO2 exhalation over 24 hours and AUC, n=4 per group. **(C)** HFD VO2 consumption over 24 hours and AUC, n=10 WT males, n=8

Creb3$^{+/-}$ males, n=5 WT females, n=8 *Creb3*$^{+/-}$ females **(D)** HFD VCO2 exhalation over 24 hours and AUC, n=10 WT males, n=8 *Creb3*$^{+/-}$ males, n=5 WT females, n=8 *Creb3*$^{+/-}$ females. Data is represented as the mean ± SEM (line graphs) and the mean ± SD (AUC).

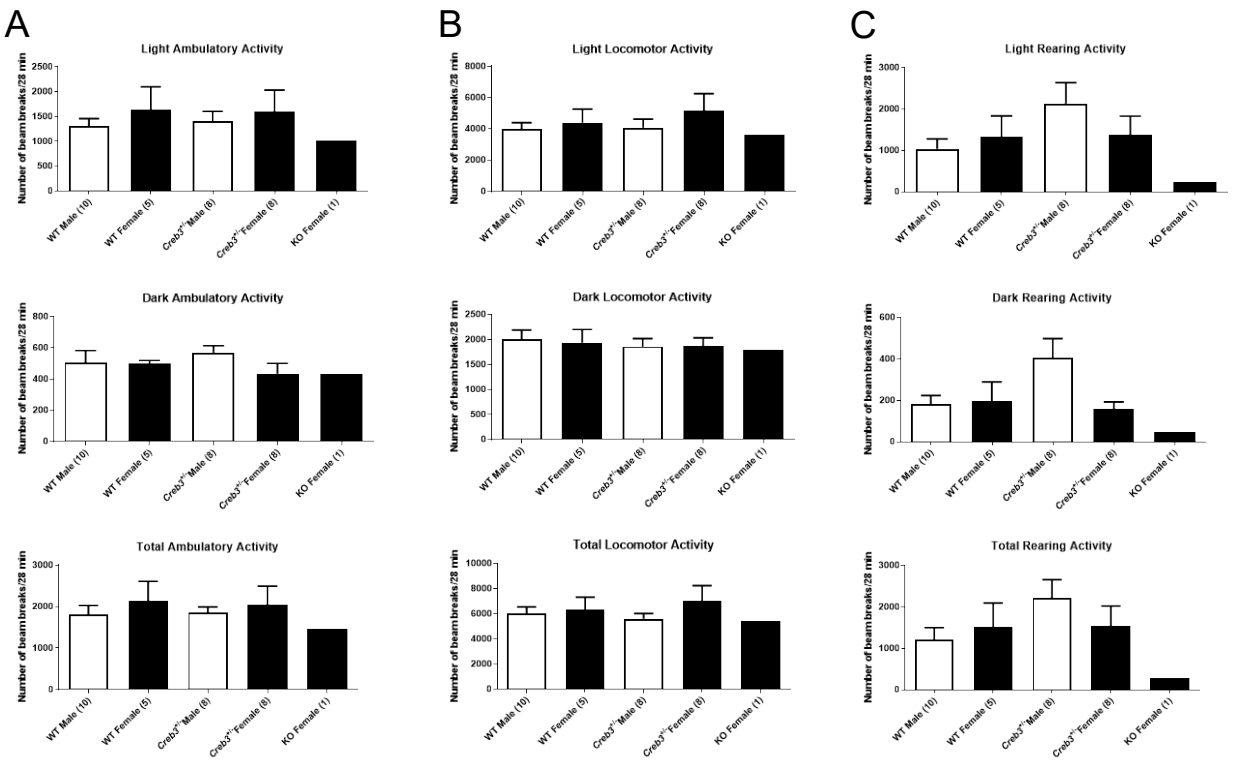

Sup Figure 4: WT and *Creb3*-deficient mice activity after an 8-week HFD. 16-week-old male and female WT, *Creb3*$^{+/-}$, *Creb3*$^{-/-}$ mice fed a HFD for 8 weeks. **(A)** Ambulatory activity in light/dark phases and total over 24 hours **(B)** Locomotor activity in light/dark phases and total over 24 hours **(C)** Rearing activity in light/dark phases and total over 24 hours, n=10 WT males, n=8 *Creb3*$^{+/-}$ males, n=5 WT females, n=8 *Creb3*$^{+/-}$ females, n=1 *Creb3*$^{-/-}$ female. Data is represented as the mean ± SD (AUC).

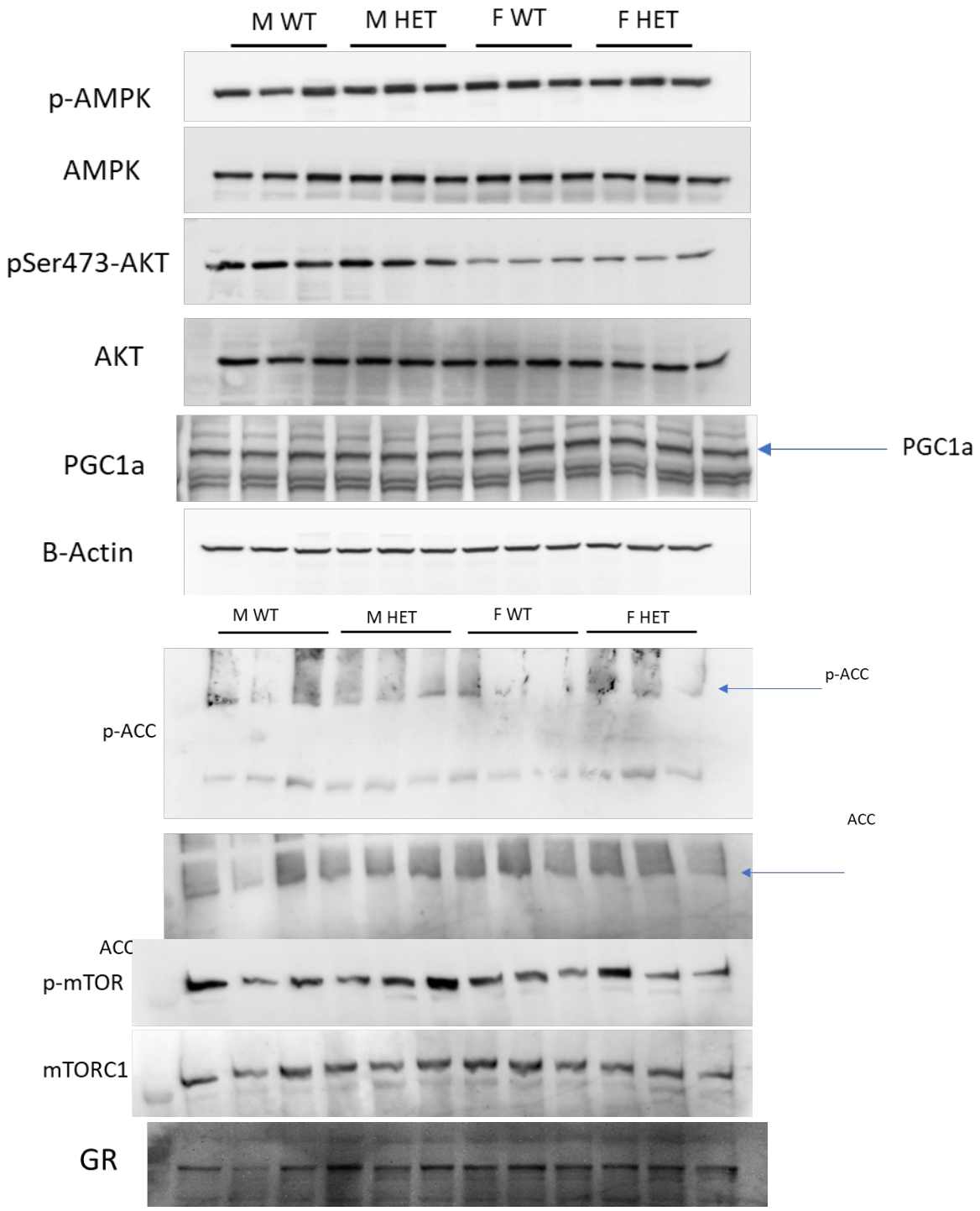

Sup Figure 5: HFD WT and *Creb3*$^{+/-}$ mouse liver western blots. Liver lysate of 16-week-old male and female WT and *Creb3*$^{+/-}$ mice fed a HFD for 8 weeks. Western blots performed by Sophie Grapentine of the Bakovic Lab. n=3 for all groups. Liver tissue was homogenized via PolyTron in RIPA buffer (150mM NaCl, 50mM Tris, 1% (v/v) triton x-100, 0.5% (v/v) sodium deoxycholate, 0.1% (v/v) SDS). Protein lysates were normalized to 1µg/µL using the Bradford Protein Assay (Bio-Rad # 5000002). Proteins were

resolved in a 10% denaturing SDS-PAGE gel and semi-dry transferred to PVDF membranes. Membranes were blocked at room temperature for 2 h in 5% BSA in TBS-T followed by primary antibody incubation; Total AKT, pSer473-AKT, total ACC, p-ACC, total mTORC1, p-mTOR, total AMPK, p-AMPK, β-Actin (Cell signaling, 1:1000 dilutions in 5% BSA); PGC-1a (ProteinTech, 1:7500 in 5% skim milk in PBS-T); GR (Santa Cruz, 1:1000 dilution in 5% BSA/TBS-T) at 4^{o}C overnight. The following day, membranes were washed 3x in TBS-T, then incubated with appropriate horseradish peroxidase conjugated secondary antibody (1:10000 in 5% BSA/TBS-T) for 1 h at room temperature and visualized with chemiluminescent substrate (Sigma). β-Actin was used as a loading control.

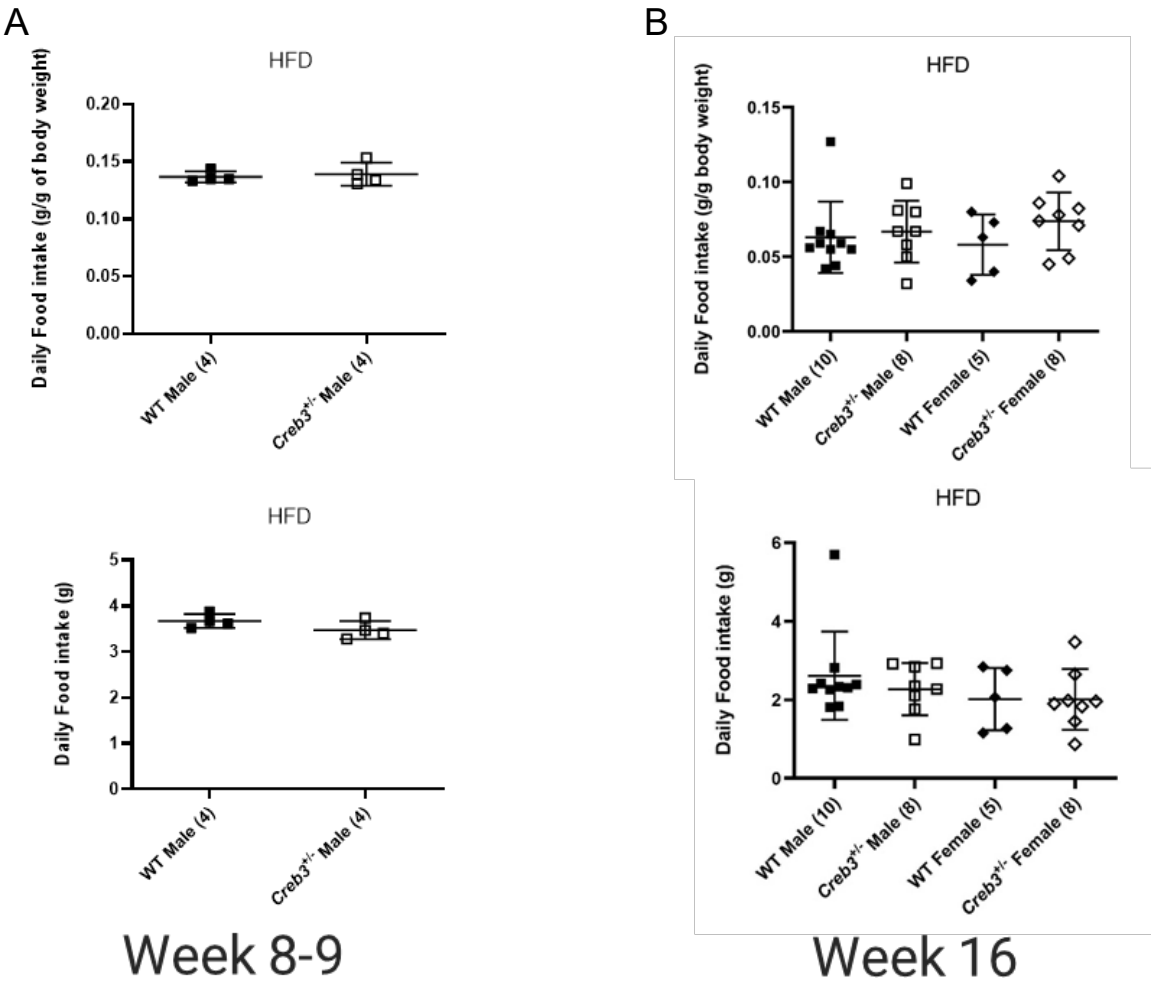

Sup Figure 6: HFD 24h food intake of WT and *Creb3*$^{+/-}$ mice. (A) Average daily HFD absolute and g/g of body weight food intake of WT (n=4) and *Creb3*$^{+/-}$ (n=4) male mice during the first week on HFD. **(B)** Average 24h absolute and g/g of body weight HFD food consumption in metabolic cages (n=10 WT males, n=8 *Creb3*$^{+/-}$ males, n=5 WT females, n=8 *Creb3*$^{+/-}$ females) over 24h. Data is represented as the mean ± SD. Two-way ANOVA with Tukey post hoc.